S1 Appendix reading guide

Stonehenge | Heritage v1.29 | 27 September 2026

The following 87 analytical pages retain the original v1.23 scientific record, printed page numbers and citation labels. Marginal notices introduced in v1.26 remain in place. This guide and S5 define the current interpretation; the original calculations have not been recast as newly executed or prospectively specified tests.

Scope of the retained analyses

Information order. The 26 August 2026 public archive contains the word, operator and 2965.2 BCE clock result in its Calanais subtree. Exact extracts and checksum verification are in S5 section 8.1. The Stonehenge mapping and subsequent diagnostics remain retrospective.

Geometry. The 2.02% prediction RMS uses the outer-only scale. The descriptive all-channel fit in Note 2 is different. The same four residuals partition into 2.05% for sarsen/trilithon and 1.99% for Y/Z.

Stellar comparisons. S4 varies more subsets within regions but retains spatial conditions. S5 uses five brightest stars per region. Fixed words, unrestricted words, integer-compatible words and free temporal scale define distinct tests.

Inventory. The three-closure uniqueness theorem is preserved. The timing word alone leaves an inventory family. Of 512 words, 55 admit any positive integer inventory under the original map; 26 timing passes satisfy this weaker condition.

Chronology. Fixed W and scale rank Cygnus first among 5,280 classes without chronology. S5 section 3.3 separately shows a 5.33-fold minimum-error increase in Stage 2 and preserved first place when fitting within the 68% ditch interval. The original unconstrained optimum still lies outside that narrower interval; free-word alternatives remain in S5 section 3.2. Section 3.4 adds channelwise bounds showing that reweighting alone cannot make Stage 2 outperform the nominated early epoch.

Measurement limits. Notes 20–23, 36–43 and 54 use drawing or hatch-centroid proxies. These are not independent surveys. Updated Figure 1 documents sources and boundaries, without supplying all original settings or a homogeneous measured site plan.

Historical scope. The nominal minimum near 2965 BCE does not date all structures. The complete inventory and calibration span construction phases. An ancient angular convention, intention and transmission remain unestablished.

Source status

Old [26] / main [28] identifies the Daw/Rees click-plan; old [33] / main [45] is the Wessex Archaeology Bulford announcement; old [39] / main [35] is the English Heritage chronology summary. These source types remain explicit. The news report is archaeological context, not a numerical input or independent proof of the model.

S1 retains historical figure, table and citation labels. Main Figures 1–10 and Tables 1–4 keep their identities; Figure 11 and S5 section 3.3 contain the v1.28 temporal diagnostics; section 3.4 adds the v1.29 channelwise comparison. Notes remain 1–54. The 87 analytical pages below are retained as the original record; this guide and S5 state the current interpretation and execution scope.

Reference correspondence

Citation numbers in the retained S1 pages refer to the old main bibliography. Use the correspondence below when consulting the Heritage main manuscript, whose 46 references are numbered by first appearance. All 44 original source entries are retained in that current list; two relevant Heritage articles have been added.

S1 original	Heritage main	S1 original	Heritage main
1	1	23	25
2	4	24	26
3	2	25	27
4	5	26	28
5	6	27	29
6	7	28	30
7	8	29	31
8	9	30	32
9	10	31	33
10	11	32	34
11	12	33	45
12	13	34	20
13	14	35	40
14	15	36	41
15	16	37	44
16	17	38	46
17	18	39	35
18	19	40	3
19	21	41	36
20	22	42	37
21	23	43	38
22	24	44	39

Supporting Information

Stonehenge's exterior predicts its interior:
counts and Cygnus yield an astronomical epoch consistent with its first phase
Lucas Giovani Ribeiro and Marcos André Simonssini

S1 Appendix - Version 1.23 - References follow the main manuscript.
Notes 1-53 retained; Note 54 adds ordered directional channels.

Supplementary Note 1 Information order and dependency map

The paper reports one dependent generative system. Metric, cyclic, register and temporal outputs are not multiplied as independent evidence. The information order is: Stonehenge counts and Station-Aubrey geometry; outer-only scale calibration; held-out plan prediction; four-seed compilation; bounded seed-map census; exact inversion; word census; evaluation in the fully specified Cygnus operator; and archaeological comparison last. The January 2026 book establishes provenance of the Cygnus grammar but supplies no Stonehenge measurement or fitted parameter.

Layer	Input	Output	Evidential status
Cyclic geometry	N=56; ideal model gaps; published Station sides	Approximate 7|21|7|21 and 5:12:13	Dependent geometric construction; exact indexing unresolved
Metric plan	Outer roles 10,24,26	Held-out 4,10,12,16	Out-of-fit scale transfer
Material seed map	Counts 56,30,10,4	Seeds 16,10,34,62	Exact compilation and inversion
Common expansion	Seeds 16,10,34,62	Q=(16,24,28,34,52,62,72,96)	One shared rule
Directional ablation	Exchange typed 34 and 62	Station count 4 becomes 32	Allocation sensitivity
Temporal execution	W=(28,72,16) and fixed Cygnus graph	2965.2 BCE primary	Pre-existing phase; chronology compared afterward

Supplementary Note 2 Complete spatial inputs and outputs

The four unequal Station sides are the centre-to-centre distances in the published Atkinson survey dataset [22, pp. 50-52], reproduced explicitly as Atkinson values in MacKie's appendix [23, p. 107], not measurements taken from the photograph or an ideal rectangle. Positions 91 and 93 retain stones, whereas 92 and 94 are archaeologically located absent-stone settings [24, p. 28]. Because the accessible source record does not resolve a finer socket- or mound-centre convention for both absent settings, none is inferred here. Averages are taken only after all four observations are declared.

Segment	Observed m	Endpoint status	Primary source and convention
91-92	34.17	91 surviving; 92 absent setting	Atkinson [22]; reproduced in [23], p. 107
93-94	32.70	93 surviving; 94 absent setting	Atkinson [22]; reproduced in [23], p. 107
92-93	79.93	92 absent setting; 93 surviving	Atkinson [22]; reproduced in [23], p. 107
91-94	80.26	91 surviving; 94 absent setting	Atkinson [22]; reproduced in [23], p. 107

Every other metric input is a deliberately rounded architectural summary. The table records what boundary is meant, so unlike dimensions are not silently exchanged.

Feature	Input	Boundary or convention	Source and status
Aubrey circuit primary	86.44 m	hole-centre circuit diameter	Thom survey tabulated by MacKie [23], Appendix p. 107
Aubrey sensitivity	86.87 m	alternative hole-centre diameter	Hawkins survey tabulated by MacKie [23], Appendix p. 107
Aubrey sensitivity	87.0 m	rounded hole-centre diameter	Lawson [24], p. 22
Aubrey adverse branch	85.832 m	implied by prose radius 140.8 ft	MacKie [23], p. 99; conflicts with appendix and is not primary
Y-hole circuit	54.0 m	best-fit hole-centre circuit diameter	Cleal et al. [1], p. 260; approximate
Z-hole circuit	39.0 m	best-fit hole-centre circuit diameter	Cleal et al. [1], p. 260; approximate
Sarsen circle	~33.0 m	occupied outer architectural envelope	rounded outer-face reading from Cleal et al. [1], fold-out Plan 1; not a published scalar
Trilithon horseshoe	~13.7 m	transverse outer width of the five-trilithon setting	rounded outer-face reading from Cleal et al. [1], fold-out Plan 1; not a published scalar
Sarsen inner face	97.33 ft	true-circle diameter through dressed inner faces	Petrie [21], p. 23; retained only as a boundary-convention sensitivity check
Derived Sarsen midline	31.333 m	arithmetic midpoint of 29.666 and 33.0 m; not surveyed	derived diagnostic only; no integer closure

Feature	k	Observed m	Predicted m	Residual	Input precision
Trilithon horseshoe span	4	13.700	13.321	-2.767%	approximate
Station mean short side	10	33.435	33.302	-0.397%	reported sides
Sarsen outer envelope	10	33.000	33.302	+0.916%	approximate
Z-hole circuit diameter	12	39.000	39.963	+2.469%	approximate
Y-hole circuit diameter	16	54.000	53.284	-1.327%	approximate
Station mean long side	24	80.095	79.926	-0.212%	reported sides
Aubrey circuit diameter	26	86.440	86.586	+0.169%	survey table

All-channel descriptive fit: u=3.330230193 m and relative RMS=1.539017%. Outer-only fit: u=3.331412722 m and held-out inner RMS=2.019623%.

Aubrey source branch	Diameter m	Held-out RMS	7-step residual	21-step residual
MacKie appendix: Thom tabulated survey	86.440	2.020%	-1.064%	-0.293%
MacKie appendix: Hawkins tabulated survey	86.870	2.022%	-0.572%	+0.203%
Lawson rounded summary	87.000	2.029%	-0.423%	+0.353%

Aubrey source branch	Diameter m	Held-out RMS	7-step residual	21-step residual
MacKie p. 99 prose-implied branch	85.832	2.067%	-1.761%	-0.995%

The p. 99 prose-implied branch is retained because it is the most adverse interpretation of the accessible text, but it is not promoted over the explicitly tabulated survey values. The narrow held-out RMS range shows that the dimensional prediction is not driven by choosing one Aubrey convention.

Supplementary Note 3 Leave-one-feature-out stability

Held-out feature	Refit u m	Prediction m	Error
Trilithon horseshoe span	3.329411	13.318	-2.791%
Station mean short side	3.329480	33.295	-0.419%
Sarsen outer envelope	3.331940	33.319	+0.968%
Z-hole circuit diameter	3.336932	40.043	+2.675%
Y-hole circuit diameter	3.323120	53.170	-1.537%
Station mean long side	3.327082	79.850	-0.306%
Aubrey circuit diameter	3.333414	86.669	+0.265%

Supplementary Note 4 Geometry specificity diagnostics

Among 16 primitive Pythagorean triples with hypotenuse $c \leq 100$, 5:12:13 is the best Station-side fit.

Combining each triple with all admissible cyclic step pairs creates 208 candidates; 5:12:13 at 7:21 ranks first by the equal-block joint RMS. The runner-up is 36:77:85 at 8:20; the observed candidate is 4.27 times tighter and has L1 complexity 30 versus 198.

Independent side perturbation	Metric first	Metric rate	Metric + cyclic first	Joint rate
±1%	200,000 / 200,000	100.0000%	200,000 / 200,000	100.0000%
±2%	200,000 / 200,000	100.0000%	200,000 / 200,000	100.0000%
±5%	193,447 / 200,000	96.7235%	195,251 / 200,000	97.6255%

Each trial independently perturbs all four published Station side lengths and reranks all 16 primitive triples under the unchanged estimator. The ensemble is a bounded synthetic stress test rather than an empirical error model. It tests only convergence of the measured Station rectangle on 5:12:13. The material count compiler, directed 34-longitudinal | 62-latitudinal allocation, exact inverse and W=(28,72,16) are invariant because they contain no length in metres.

With the outer scale fixed, the held-out role assignment (4,10,12,16) ranks 1/7,854 at 2.019623% RMS. The runner-up (4,10,11,16) gives 3.100024%. Because the integer universe was defined after recognition, this is a compression diagnostic rather than a p-value.

Supplementary Note 5 Reversible four-seed map and census

Seed	Typed formula	Stonehenge evaluation
r	A−B−C	56−30−10=16
g	C	10
j	B+D	30+4=34
v	A+C−D	56+10−4=62

The common expansion uses q=j−g and d=v−j, then Q=(r,q,d,j,d+q,v,3q,v+j). The inverse is A=(r+j+v)/2, B=(−r−2g+j+v)/2, C=g and D=(r+2g+j−v)/2. It returns (56,30,10,4) exactly. The seed-map determinant has magnitude 2, so the inverse is integral on the observed parity lattice.

The census enumerates every non-zero signed-subset row over four inputs with coefficients in {−1,0,1}: $3^4-1=80$ possible rows. Four ordered output rows give $80^4=40{,}960{,}000$ maps. Two maps return the ordered tuple (16,10,34,62), and both are invertible. Under coefficients in {−2,−1,0,1,2}, 375 maps return the tuple and 349 are invertible. The further condition that r contain A and exclude D was declared after recognition and is retained only as a descriptive archaeological-role filter. These are function-class counts, not p-values.

Supplementary Note 6 Algebraic notation for cross-site comparison

For the selected frame (a,b,c)=(5,12,13), X=2ac=130, Y=2a=10, Z=b=12 and J=2(a+b)=34 satisfy $XY-Z^2-J^2=1300-144-1156=0$. Thus the register channel J=34 appears as a zero-defect term of the selected frame. This is a compact algebraic description. The form was written after the register was known and J was selected to contain a register value. No uniqueness is claimed: alternative simple forms can yield singleton defects for this and other primitive frames. It receives no independent evidential weight (see also Note 19).

Supplementary Note 7 Provenance and self-contained Cygnus specification

The core grammar 16,28,34,62, the directional typing of 34 as longitudinal and 62 as latitudinal, and the 96 closure appeared in O Código Oculto de Cygnus in January 2026, before the present Stonehenge analysis [20]. Its QR-indexed public archive recorded the two-state register and W=(28,72,16) by 26 August 2026 (Zenodo 22103786) and the five-star temporal operator by 10 September 2026 (Zenodo 22691368). The tables, inputs and code reproduce the historical radial figure, carrier-area context and named stellar roles without requiring another manuscript as numerical input.

Route	Quantity	Observed value	Typed output	Status
All-88 area-rank	$\lvert A/(\pi n_A^2)-1\rvert$	0.032915%; 12.189537%	Cygnus first; Taurus second	Principal modern screen
All-88 planar	Cygnus distance; Taurus second	0.002633; 1.069770	Cygnus sole survivor	Dependent area-rank variant
All-88 spherical	Cygnus distance; Taurus second	0.049790; 1.018007	Cygnus sole survivor	Dependent area-rank variant
All-88 interior	Cygnus; Taurus epsilon	0.030626%; 13.366395%	Cygnus first	Dependent area-rank variant
Primary J2000 positions	Deneb-Albireo Delta lambda	34.077500°	34 lambda	Fixed J2000 ecliptic
Primary J2000 positions	mean beta Deneb/Fawaris	62.160110°	62 beta	Fixed J2000 ecliptic

Route	Quantity	Observed value	Typed output	Status
Primary J2000 positions	Deneb-Sadr Delta lambda	10.487650°	10 axial step	Fixed J2000 ecliptic
Albireo J2000 diagnostic	delta; polar distance; difference	27.959674°; 62.040326°; 34.080653°	28; 62; 34	Modern-frame diagnostic only
Ptolemy 17-star figure	minimum-cover radius	15.888333°	16 radial	Historical portability
Ulugh Beg 17-star figure	minimum-cover radius	16.115875°	16 radial	Historical portability
Ulugh Beg named stars	Delta lambda; mean beta	34.35°; 62.10°	34 lambda; 62 beta	Historical portability

The principal all-88 screen is recomputed directly from each constellation’s catalogued area and descending area rank. Cygnus has A=803.983 deg² and n_A=16, giving A/n_A²=3.140558594 and a 0.032915% residual from π; Taurus is second at 12.189537%. The planar, spherical and interior rows are alternative metrics of the same area-rank construction and receive no additional evidential vote. All are modern, non-scored descriptive context: they neither select the internal stellar descriptors nor imply prehistoric knowledge of IAU boundaries.

Recomputed primary J2000 descriptors give v−j=28.082610° and v+g=72.647760°. Note 24 distinguishes these from the archived decimal values retained by the original dependent tangent audits. The rounded register and all primary results are unchanged.

The Albireo quadrantal identity is valid in the modern equatorial frame but changes under precession; it is retained only as a modern diagnostic with zero evidential weight for the proposed ancient phase. Ptolemy gives a 34.666667° longitude span, rounding to 35, and is retained as a near-miss.

Supplementary Note 8 Complete sky register and directional controls

Case	Seed tuple r g j v	Compiled register	Typed inverse
Ulugh Beg directed	16,10,34,62	16,24,28,34,52,62,72,96	56,30,10,4
Ptolemy adverse	16,11,35,62	16,24,27,35,51,62,72,97	56.5,29.5,11,5.5
Seed transposition	16,10,62,34	Allocation exchanged before inversion	56,30,10,32
Register-slot swap	Q4=62; Q6=34	Diagnostic only	Non-target

The exact Ulugh Beg row uses a 16.115875° minimum-cover radius, a 10.30° Deneb-Sadr longitude step, a 34.35° Deneb-Albireo longitude span and a 62.10° Deneb/Fawaris mean latitude. All four decode by one nearest-integer rule. Ptolemy rounds to (16,11,35,62) and yields half-integer non-target counts under the unchanged seed inverse.

The dimensionless plan-role ladder (4,10,12,16,24,26) is an independently declared Stonehenge metric model, not a slot-by-slot derivation from Q. One Stonehenge-derived scale converts those roles to metres.

The perturbation null in Note 9 calibrates its flexibility, and the sky supplies no unit of length.

Supplementary Note 9 Chronology outputs and Stonehenge-native controls

Rank	Epoch	Vector sidereal min	RMS sidereal min	RMS degrees
Primary	2965.2 BCE	27.78483 : 72.65278 : 16.23280	0.418975	0.104744
6D sensitivity	2965.9 BCE	27.78594 : 72.65534 : 16.23411	0.420359	0.105090

Control	Result	Interpretation
Material seed maps	2 exact in {-1,0,1}; 375 exact in {-2,...,2}	Two declared coefficient classes
Stonehenge-native words	W uniquely combines observed RMS and Darvill Stage 1	Conditional on 512-word material library
Arbitrary integer words	179 attain equal or smaller full-window RMS	Raw sky fit is not globally exceptional
Chronological conjunction	Observed W alone reaches Darvill interval and observed RMS	Model-sensitive archaeological concordance
Six-dimensional propagation	Shift of about 0.64 year	Astrometric sensitivity
Ladder perturbation null	72,285/1,000,000 at or below 2.020%	Metric ladder is supporting, not decisive
Darvill Stage 1	3000-2920 cal BCE; optimum inside	Applied only after ranking
Greaney ditch 95%	2980-2720 cal BCE; optimum inside	Applied only after ranking
Greaney ditch 68%	2940-2800 cal BCE; optimum earlier	Reported adverse interval

For the ladder null, the four held-out dimensions (13.7, 33.0, 39.0 and 54.0 m) were independently perturbed by uniform factors from 0.8 to 1.2. Each perturbed dimension was assigned the nearest integer multiple of the frozen outer scale u=3.331412722 m. Across 1,000,000 seeded trials, the median RMS was 4.1226%; 72,285 trials reached or improved on the observed 2.019623% RMS. This simulation calibrates only nearest-integer metric compression under the declared perturbation model.

Supplementary Note 10 Post result solar audit

The ideal cyclic construction has N=56, diameter role 26 and complementary long step 21, giving C21=26 sin(21π/56)=24.020867845. Numerically identifying this dimensionless chord value with an angle in degrees is an explicit additional model convention, not a dimensional identity.

At the previously fixed stellar phase (astronomical year −2964.218492; 2965.2 BCE), the primary propagated obliquity is 24.016307710°, for an absolute residual of 0.004560135°. This comparison is post-result and conditional on the ideal cyclic shape. No latitude, horizon, azimuth or solar cross is used in the temporal calculation. Note 25 reports the effect of changing the shape while retaining diameter role 26.

Inverting the normalized chord over astronomical years −8000 to +2000 gives 3016.7 BCE under the primary Vondrák-Capitaine-Wallace model and 2999.4 BCE under the Laskar long-period obliquity sensitivity model [27], respectively 51.5 and 34.2 years from the previously fixed stellar phase. The primary reading is 16.7 years before the 3000 BCE opening of Darvill et al.’s Stage 1 interval; the sensitivity reading is 0.6 year inside that edge. Across 16 primitive triples, 13 cyclic steps and both arms (416 equal-freedom candidates), only three arms intersect the obliquity range reached in that window: 28:45:53 step 4 short (856.5 CE), the selected diameter-26 step 7 long (3016.7 BCE), and 7:24:25 step 9

short (5535.7 BCE). At the fixed stellar phase, the selected ideal arm ranks first with residual 0.004560135°; the runner-up, 7:24:25 step 9 short, has residual 0.169636645°, 37.2 times larger. The temporal census and conditional rank are descriptive diagnostics, not p-values or evidence of prehistoric intention.

Supplementary Note 11 Input side seed flexibility null

The inverse question is whether arbitrary count inputs make the four target seeds easy to express in the declared signed-subset class. We therefore enumerate exactly all 12,960,000 ordered count quadruples in [1,60]^4. For each quadruple, every non-zero row in {-1,0,1}^4 is evaluated, and a success requires that each of the four fixed targets (16,10,34,62) be expressible by at least one row. Exactly 330,486 quadruples succeed, a rate of 2.550046%. This is an input-side flexibility null for the local formula class, not a probability of prehistoric intention, a site-level null, or a test of the full reversible Stonehenge model.

Supplementary Note 12 Adverse conventions

The three Sarsen boundaries make the convention cost explicit. Petrie's 97.33 ft (29.666 m) inner-face diameter is +1.031% from role 9. The arithmetic midpoint of the inner face and rounded 33.0 m outer face is 31.333 m, or 9.409 fitted units; it misses role 9 by -4.344% and role 10 by +6.285% under the paper's observed-relative residual. Only the occupied outer face enters the declared role-10 ladder. The outer-envelope and Trilithon scalars are explicitly rounded readings from Cleal et al.'s fold-out Plan 1, whereas the midline is a derived diagnostic; none is represented as a new survey observation. The centre-to-Heel-Stone distance is +3.263% from role 24 and fails an exact equality with the Station long side. None of these convention checks enters the primary fit.

Supplementary Note 13 Confirmatory coordinate protocol

1. Acquire or digitise georeferenced primary coordinates with source-level provenance for every included feature.

2. Define the monument centre and principal axis independently of the tested ladder.

3. Fit hole circuits by robust circle and radial-field methods and propagate coordinate uncertainty.

4. Reconstruct surviving and socket-derived Station positions under every defensible source branch.

5. Define Sarsen centre-line, inner-edge and outer-envelope algorithms before reading their results.

6. Repeat the outer-only calibration while keeping every inner channel held out.

7. Compare one-scale, phase-specific-scale and feature-specific-scale models by cross-validation and information criteria.

8. Freeze a bounded census of alternative material compilers before rerunning the chronological comparison.

9. Publish all failed conventions, source branches, code, environment and checksums.

Supplementary Note 14 Claim and falsification ledger

Claim	Present status	Clean falsifier
Primitive outer geometry	Supported in summary data	Primary coordinates remove 5:12:13 lead
Station–Aubrey indexing	Cleal anchored gaps 8|21|7|20; source sensitive	Resolve original centres with independent source-licensed coordinates
Nested one-scale plan	Held-out 2.02% RMS; 2.020-2.067% across Aubrey source branches	Coordinate model favours phase/feature scales
Exact material register	Algebraically verified	Typed archaeological counts or roles are wrong
Complete sky register	Fixed J2000 module retains rounded tuple at both tested epochs; historical routes separate	Independent catalogue recomputation fails
Directional allocation	34λ|62β returns D=4; transpose gives D=32	Transposed roles return the target inventory
Bidirectional reconstruction	Exact within declared compiler	Independent recalculation fails the stated inverse or archaeological typing changes
Celestial phase	2965.2 BCE primary; 6D shift 0.64 year	Changed stellar inputs/operator move or remove the reported optimum
Chronological compatibility	Inside Darvill and Greaney 95%; earlier than Greaney 68%	A revised model excludes the optimum
Intentional prehistoric code	Not claimed	Requires independent archaeological evidence

Supplementary Note 15 Enclosure-ditch centreline compatibility calculation

This outer-earthwork calculation is separate from the whole-plan ladder. It neither supplies a direct survey of the ditch centreline nor enters the scale calibration, nested-plan ladder, register, inverse or stellar chronology.

Convention and decision rule

The primary scale branch is u = 3.331413 m. The reported quantity is a derived centreline diameter assessed against the adjacent integer k = 32 under nearest-integer rounding. Half of the reported ditch width is added on each side to the published internal-lip diameter. The internal-lip boundary is retained as an adverse convention.

Published values and arithmetic

Field and Pearson report an internal-lip diameter close to 102 m, an eastern ditch width of about 4 m, a western width of about 6-6.5 m, and local variation up to 1 m. On the east-west transect the derived centreline diameter is 102 + 4/2 + (6.0-6.5)/2 = 107.0-107.25 m. Dividing by u gives 32.12-32.19; both values round to 32.

Boundary and failure condition

The source reports the internal lip and variable widths, not a directly surveyed centreline. The local variation and north-west flattening cannot exclude every adjacent-integer outcome under extreme boundary combinations. The direct 102 m internal-lip value is approximately 30.62u and does not meet the centreline condition. A coordinate-level direct centreline survey may confirm or overturn this compatibility calculation.

Source: Field, D. & Pearson, T. Stonehenge Landscape: An Archaeological Analysis of the Field Survey. English Heritage Research Department Report Series 109-2010 (2010), p. 13.

Supplementary Note 16 Material seed provenance and notation

The material compiler supplies r = 16 directly: r = A-B-C = 56-30-10. The spatial module in the fixed J2000 ecliptic frame supplies the rounded angular descriptors g = 10, j = 34 and v = 62. It evaluates the materially regenerated word W = (28,72,16); it neither calculates nor supplies r.

The 17-star Ptolemy and Ulugh Beg figures are retained solely as non-scored historical-portability controls for an approximately 16-degree minimum-cover radial scale. Their values do not generate the material seed. The all-88 IAU construction is likewise descriptive catalogue context only. Its descending area-rank variable is nA, not r; it neither supplies r = 16, selects internal stellar descriptors nor implies prehistoric knowledge of IAU boundaries.

The core grammar 16, 28, 34 and 62, the directional typing of 34 and 62, and the 96 closure establish provenance only. They supply no Stonehenge measurement, material count, scale, archaeological date or chronological optimisation input.

Supplementary Note 17 Pythagorean factorisation and continuous outer-inventory angle

This note records deterministic structural descriptions of the selected material system. Its minimum typed core is (16R, 34Δλ, 62β): a material radial realization, a longitudinal stellar span and a latitudinal stellar mean. The remaining register terms are deterministic consequences of the stated grammar and compiler. These descriptions share inputs with the inventory compiler and are not independent probability estimates, construction dates or evidence of prehistoric intention.

Native Pythagorean factorisation

Let A = 56, B = 30, C = 10 and D = 4 denote the observed inventories. Let g = C = 10, q = B+D-C = 24, and p = 26 be the selected Aubrey-diameter coefficient. Then $g^2 + q^2 = p^2$, or $10^2 + 24^2 = 26^2$. This is the doubled 5:12:13 relation of the selected Station-Aubrey frame. With R=A/2=28, Q=(p-g,q,R,g+q,2p,R+g+q,3q,4q)=(16,24,28,34,52,62,72,96). It is one factorisation of an already specified system, not a second independent route.

Complementary tangent theorem

The outer inventories obey B/A = 30/56 = 15/28. Let θ=arctan(15/28)=28.178590110 degrees. The positive complementary acute angle is 90 degrees-θ=arctan(28/15)=61.821409890 degrees. Thus θ+(90 degrees-θ)=90 degrees. The relation is exact for the dimensionless ratio; degrees are used only because the compared stellar descriptor is expressed in degrees.

Continuous stellar comparison

Using the retained archival j and v decimals, the non-rounded difference descriptor is d*=62.160117 degrees-34.077511 degrees=28.082606 degrees. The absolute difference |θ-d*| is 0.095984110 degrees. Across the six unordered pairs of A, B, C and D under the single unrounded function arctan(min(x,y)/max(x,y)), A,B ranks first; no complement, rounding, derived count or alternative function is included. This is an exploratory descriptive screen, not a sampling distribution or p-value.

Count pair	Acute angle (°)	Residual to d* (°)
AB	28.178590	0.095984
CD	21.801409	6.281197
BC	18.434949	9.647657
AC	10.124672	17.957934
BD	7.594643	20.487963
AD	4.085617	23.996989

Modern boundary context

For descriptive context only, the IAU/Delporte polygon has declination extrema 27.73 degrees and 61.36 degrees. These boundaries are modern catalogue partitions, not physical stellar edges or historical inputs. The northern tangent value is algebraically fixed by the complementary southern value, so this display has one degree of freedom. The solar calculation is a distinct, model-conditioned relation and is not merged with the tangent theorem.

Supplementary Note 18 Outer-frame theorem and conditional graph resolution

This note records dependent structural observations. They are not independent tests, construction dates or evidence of prehistoric intention; they are excluded from the abstract and primary rankings.

Outer-frame material theorem

With A=56 Aubrey positions and B=30 outer sarsens, the selected 5:12:13 frame supplies c=13 in scale units (diameter 26). Two primitive identities hold: A-B=26=2c and B-2c=4. Together, A−B=2c and B−2c=D=4 imply B/2+c=A/2=28 and $(B/2)^2-c^2=AD/4=56$. Both identities are required for the latter equality. They are compact consequences, not separately scored results. Every disclosed Aubrey branch rounds to radial role 13; the closure remains dependent because the scale and selected frame include the Station-Aubrey relation.

Within-carrier directional specificity

Holding fixed the J2000 ecliptic convention, Deneb anchor and typed targets (10,34,62), every injective allocation of the other three roles among each historical 17-star Cygnus carrier was enumerated: 16x15x14=3,360 allocations. Four allocations (0.119%) reproduce the rounded tuple in each catalogue. Sadr is the sole 10-degree candidate and Albireo the sole 34-degree candidate; four candidates yield rounded 62. The continuous 62.160117-degree value is the Deneb-Fawaris mean latitude, hence Fawaris matches it by construction and it is not an additional selection result.

Residual-partner resolution

The archived comparison keeps primary inputs for the four fixed stars and uses Hipparcos inputs for each alternative partner. The updated script searches -8000 to +2000; the earlier search was local. Fawaris ranks first, with RMS 0.4180 at 2964.8 BCE versus 0.5964 for HIP 99848. At the primary phase, the values are 0.4180 and 0.7499. These mixed-input scores do not replace the primary 2965.2 BCE and 0.4190-minute result. A homogeneous Hipparcos check also selects Fawaris (Note 33). This is dependent role resolution, not another chronology.

Supplementary Note 19. Complete tangent comparator and quadratic Gram notation

Status. This note records post-result dependent descriptions of the selected material system. They share inputs with the primary frame and compiler, are not counted as independent evidence, and supply neither a probability nor a construction date.

Quadratic Gram notation. For the selected primitive frame (a,b,c)=(5,12,13), define X=2ac=130, Y=2a=10, Z=b=12 and J=2(a+b)=34. Then $XY-Z^2-J^2=1300-144-1156=0$. The identity is a compact quadratic reexpression of the already selected frame and register channel J=34. It was written after the register was known; no uniqueness, independent evidential weight or prehistoric construction meaning is claimed. The executable audit records the same calculation as native_Gram.

Complete tangent comparator. For every unordered pair drawn from the documented material counts A=56, B=30, C=10 and D=4, the table reports both the acute angle arctan(min/max) and its 90° complement. Each branch is compared with every declared archival angular target: material radial label

r=16°, stellar difference d*=28.082606°, longitudinal j=34.077511° and latitudinal v=62.160117°. The table deliberately reports all 12 branches and all 48 residuals; it does not select only the closest relation. The source-of-truth machine-readable version is expected_tangent_matrix_results.json in S2.

Pair	Branch	Angle (°)	|−r|	|−d*|	|−j|	|−v|
AB	acute	28.178590	12.178590	0.095984	5.898921	33.981527
AB	complement	61.821410	45.821410	33.738804	27.743899	0.338707
AC	acute	10.124672	5.875328	17.957934	23.952839	52.035445
AC	complement	79.875328	63.875328	51.792722	45.797817	17.715211
AD	acute	4.085617	11.914383	23.996989	29.991894	58.074500
AD	complement	85.914383	69.914383	57.831777	51.836872	23.754266
BC	acute	18.434949	2.434949	9.647657	15.642562	43.725168
BC	complement	71.565051	55.565051	43.482445	37.487540	9.404934
BD	acute	7.594643	8.405357	20.487963	26.482868	54.565474
BD	complement	82.405357	66.405357	54.322751	48.327846	20.245240
CD	acute	21.801409	5.801409	6.281197	12.276102	40.358708
CD	complement	68.198591	52.198591	40.115985	34.121080	6.038474

The AB acute branch, arctan(30/56)=28.178590°, has residual 0.095984° to d*. Its complement is algebraically fixed once that acute branch is specified. The Delporte boundary display remains a modern, non-scored contextual comparison and is not included as an additional target in this matrix.

Supplementary Note 20 Plan proxies, continuous gaps and anchored indices

These are retrospective diagnostics of archived drawing proxies, not a new survey, preregistration or independent confirmation. Cleal et al.’s Plan 1 provides 56 numbered Aubrey symbols and four Station proxies; the source-identification audit used Fig. 13 and Figs. 161, 164 and 165 (printed pp. 272–278). The scale comes from the printed 20 m bar, not a fitted target diameter. The projected surviving stone 91 is inclined, and the source record does not supply its original socket centre. The Rees 1989 click-plan (sheet MP/STO0861, Tim Daw) supplies a clearly indicative 91 alternative. Raw numerical extractions and hashes of the supplied source files are preserved in S2 Code.

The Aubrey-only algebraic circle has diameter 85.81 m and radial RMS 0.24 m. A printed-grid calibration gives 86.17 m; these are source-convention readings, not uncertainty limits. Field and Pearson’s support stations Z1, Z2 and Z4 are modern surveying controls, not prehistoric Station Stones or Z Holes. Their report records 26 visible Aubrey markers and does not resolve all original hole centres. Its use of Rees for central stones also means that the click-plan is not an independent replication.

The angular origin of the ideal 56-position grid is estimated only from the numbered Aubrey symbols. Continuous gaps are evaluated in Station order 91,92,93,94. Rounding each gap is different from assigning each Station to the nearest anchored-grid index and then subtracting indices. The latter retains absolute angular phase.

Source convention	Continuous gaps (steps)	Rounded gaps	Anchored indices	Index gaps
Cleal proxies	7.178 | 21.064 | 7.127 | 20.631	7 | 21 | 7 | 21	10; 18; 39; 46	8 | 21 | 7 | 20
Indicative 91 only	6.996 | 21.064 | 7.127 | 20.813	7 | 21 | 7 | 21	11; 18; 39; 46	7 | 21 | 7 | 21

Source convention	Continuous gaps (steps)	Rounded gaps	Anchored indices	Index gaps
Registered click-plan	6.881 | 21.179 | 7.485 | 20.455	7 | 21 | 7 | 20	11; 18; 39; 46	7 | 21 | 7 | 21

The primary 91 proxy is 0.240° from the nearest index boundary, corresponding to 0.180 m of arc at the fitted Aubrey radius. This is a classification-boundary distance, not an instrumental error or archaeological confidence limit. The two-point registration between drawings uses stones 91 and 93; it has no redundant control. Neither the passing alternative nor the primary classification establishes original socket positions.

Against actual drawn Aubrey directions, the primary Station angular RMS is 2.289°. In 1,000,000 uniform rotations of the same configuration, 78.08% are at least as close. This is a conditional descriptive comparison, not a probability of intention. The indicative-91 variant has zero-phase RMS 2.540°; satisfying the index word does not establish zero phase.

The archived discrete script returns FAIL for the primary proxies and PASS for both alternatives. These are arithmetic outputs only: the archived source manifest remains AWAITING_SOURCE_LOCK, and source eligibility is not met. Nearest-index rounding already ensures an absolute residual of at most half a step, so the archived one-step tolerance cannot test fine positional coincidence. The coordinate-centre protocol excludes image proxies and requires the missing sarsen coordinate class; it has not been executed. Neither protocol nor its manifest has been retrospectively rewritten.

Supplementary Note 21 Free Station circles and all four omissions

An algebraic least-squares circle is fitted to all four Station proxies without fixing the Aubrey centre or radius, the 5:12:13 aspect ratio, the 7|21 partition, the material unit, a stellar descriptor or a date. We report the radial RMS of the 56 Aubrey proxies about that Station-derived circle. The diagonal-midpoint discrepancy is a separate diagnostic of departure from a parallelogram. These residuals are correlated descriptions of one geometry, not independent successes.

Source branch	Station diameter m	Centre separation m	Aubrey radial RMS m	Diagonal midpoint gap m
Cleal proxies	86.493	0.684	0.634	0.436
Indicative 91 only	85.628	0.618	0.504	0.749
Registered click-plan	84.716	1.278	1.087	1.858

Omitted Station	Circle diameter m	Centre separation m	Aubrey radial RMS m	Omitted signed radial residual m
91	86.071	0.208	0.307	0.853
92	86.931	0.673	0.770	-0.863
93	86.081	1.244	0.915	0.833
94	86.916	1.077	0.966	-0.840

Omitting 91 is the best case among four identified retrospectively: the remaining three points give a diameter about 86.07 m, a centre about 0.21 m from the Aubrey centre and Aubrey radial RMS about 0.31 m. Three non-collinear points necessarily define a circle, but proximity of that centre and the other 56 points is not guaranteed. The omitted footprint is about 0.85 m outside the circle; the indicative socket is about 0.92 m inside it. The circle fit does not recover the omitted azimuth or full socket position.

Four synthetic scenarios independently perturb each coordinate by uniform half-widths 0.10, 0.25, 0.50 and 1.00 m, with 50,000 draws per scenario and deterministic seed 20260919. The two plans, circle fits and cross-plan registration are recomputed. For the circle omitting 91 at ±0.25 m, the central 95% sensitivity range for Aubrey radial RMS is 0.29–0.57 m. These are assumed perturbation percentiles, not measured archaeological confidence limits. Systematic source distortion or original socket restitution is not quantified. Registered omissions can retain the omitted point indirectly through the 91/93 registration controls; they are not independent holdouts.

A separate fixed-Aubrey-circle sensitivity analysis predicts each Station from the other three, for both templates and all branches. Primary 7|21 leave-one-out distances are 1.731, 0.354, 0.291 and 1.103 m for Stations 91–94; the continuous 5:12:13 values are 1.643, 0.412, 0.410 and 0.983 m. The indicative-91 target is 0.722 m from the 7|21 prediction. In particular, 1.73 m is model-to-proxy discrepancy, not a measured error bar. Full source branches, coordinate perturbations and quantiles are archived in plan_audits/sensitivity. A 0.12 m separation between the two model predictions for Station 91 does not resolve their archaeological interpretation.

Supplementary Note 22 Fixed shape with one common spatial rotation

Hold the Aubrey centre fixed and express the four Station polar angles in order 91,92,93,94. For short arc γ, use offsets (0,−γ,−180°,−180°−γ), where γ=45° for 7|21 and γ=2 arctan(5/12)=45.239730° for the continuous 5:12:13 rectangle. After circular unwrapping, the mean of angle minus offset estimates one common rotation. The angular RMS of the remaining four residuals measures shape deformation. No individual Station is moved.

Rotation is reported modulo one Aubrey step, counterclockwise relative to the ideal word starting at anchored index 11. The original zero-phase test, anchored indices and source limitations remain unchanged. This added spatial parameter is unrelated to the stellar temporal phase.

Source branch	Template	Spatial rotation (°)	Residual angular RMS (°)
Cleal proxies	7|21|7|21	2.186	0.855
Cleal proxies	5:12:13	2.306	0.792
Indicative 91 only	7|21|7|21	1.894	0.496
Indicative 91 only	5:12:13	2.014	0.461
Registered click-plan	7|21|7|21	1.504	1.624
Registered click-plan	5:12:13	1.624	1.585

The Cleal residual is 0.855° for 7|21 and 0.792° for 5:12:13. The common rotation explains part of the discrepancy while leaving residual deformation. The simpler statement supported across the source conventions is approximate compatibility of centre, scale and shape; exact coincidence with individual Aubrey positions and historical transmission remain unresolved. This retrospective fit does not promote 7|21 over its continuous comparator.

Supplementary Note 23 Discrete rectangle census and phase-independent shape

This additional retrospective diagnostic separates a rectangular shape from its absolute registration with the Aubrey grid. For an inscribed rectangle of short side a and long side b, the short central angle is 2 arctan(a/b), hence k=(56/π) arctan(a/b) in 56-fold steps. Its ordered angular gaps are k|(28−k)|k|(28−k). This follows from the rectangular approximation; it does not assume that a Station lies on an individually numbered Aubrey direction.

The selected 5:12:13 shape gives k=7.037291 and 28−k=20.962709. The published mean sides, 33.435 and 80.095 m, give k=7.049061 and 28−k=20.950939. All four short–long pairings also round to k=7, as shown below. This derivation uses the side ratio and the externally supplied count 56, without using the Aubrey diameter, a Station-to-Aubrey index or an adjusted orientation. It is a dependent expression of the recorded geometry. Shape alone does not uniquely identify the count 56 among possible circle subdivisions.

Short side m	Long side m	Short gap k	Complement 28−k
34.17	79.93	7.201184	20.798816
34.17	80.26	7.174676	20.825324
32.70	79.93	6.922179	21.077821
32.70	80.26	6.896479	21.103521

The discrete comparison includes all 14 templates k|(28−k)|k|(28−k), k=1,...,14, including the square. Station order 91,92,93,94 and the short-side assignment are fixed. Each candidate uses the Aubrey centre and one fitted common rotation, exactly as in Note 22. No Station is independently repositioned. The candidate set here is distinct from the 13 unequal-leg step pairs used in the primary metric–cyclic census: the square is included here, and this comparison scores angular plan residuals rather than the joint primary metric–cyclic score.

The full angular RMS table follows. Columns are source conventions, not independent surveys. The k=7 template ranks first in each column; k=8 ranks second. These ranks condition on the declared discrete family and retrospective adjustment and are not p-values.

Template k|(28−k)|k|(28−k)	Cleal RMS °	Indicative 91 RMS °	Click-plan RMS °
1 | 27 | 1 | 27	19.788270	19.488972	19.931438
2 | 26 | 2 | 26	16.576389	16.275733	16.728220
3 | 25 | 3 | 25	13.365663	13.063009	13.530252
4 | 24 | 4 | 24	10.157189	9.851305	10.342407
5 | 23 | 5 | 23	6.954085	6.642098	7.178183
6 | 22 | 6 | 22	3.770063	3.442380	4.092736
7 | 21 | 7 | 21	0.854820	0.495753	1.624175
8 | 20 | 8 | 20	2.812708	3.050381	3.031280
9 | 19 | 9 | 19	5.979565	6.247171	6.033460
10 | 18 | 10 | 18	9.179452	9.455830	9.180408
11 | 17 | 11 | 17	12.386797	12.667343	12.362055
12 | 16 | 12 | 16	15.597000	15.879978	15.557126
13 | 15 | 13 | 15	18.808598	19.093168	18.758764
14 | 14 | 14 | 14	22.020980	22.306674	21.964096

The continuous 5:12:13 comparator receives the same one-rotation fit. A freely proportioned rectangle estimates two parameters, rotation and short arc, and therefore has greater flexibility. Both are retained below; 7|21 is not the optimum over all continuous shapes.

Comparator	Fitted parameters	Cleal RMS °	Indicative 91 RMS °	Click-plan RMS °
Continuous 5:12:13	1	0.792199	0.461175	1.584713
Free rectangle	2	0.700329	0.454515	1.513946

Source branch	Free short arc °	Free k
Cleal	45.980319	7.152494
Indicative 91	45.395914	7.061587
Registered click-plan	46.176285	7.182978

At the digitized Aubrey radius 42.904486 m, the vertices predicted by the separately rotation-fitted 7|21 and 5:12:13 shapes differ by 0.089758 m. This is a mathematical model separation, not measured archaeological uncertainty or evidence of statistical equivalence. The approximately 0.119677 m separation in Note 21 concerns a different operation: predicting each Station from the other three.

Position rounding and interval rounding are different operations. If x is the continuous angular index, q its nearest integer and e=q−x, then the integer gap minus the continuous gap equals e at the next Station minus e at the current Station, with cyclic closure. For Cleal, x=(10.462628,17.640790,38.704659,45.831485), whereas q=(10,18,39,46). Thus interval rounding gives 7|21|7|21 while subtracting rounded positions gives 8|21|7|20. This identity explains the differing classifications but does not justify changing the anchored phase.

For completeness, the exact interval decomposition over a hypothetical one-step grid rotation is archived in S2. The 7|21 word occupies 0.631143 of that step; the actual Aubrey-anchored phase remains outside that interval. This is a geometric phase-coverage fraction, not a null probability or a reason to select a passing grid orientation.

The earlier 50,000-draw simulations at uniform ±0.25 m per coordinate give the following distinct frequencies. The 99.99% result concerns rounded Cleal gaps only. All four perturbation half-widths and all source branches are retained in S2. The frequencies describe numerical stability under the chosen independent uniform perturbations; they are not archaeological confidence or confirmation probabilities.

Source branch	Rounded 7|21 gaps %	Anchored 7|21 gaps %
Cleal	99.990	11.956
Indicative 91	100.000	99.878
Registered click-plan	22.718	68.244

Changing Station 91 from index 10 to 11 restores the integer word but does not establish exact angular or radial coincidence of all four Stations with Aubrey holes. In the indicative-91 branch the residuals against the anchored regular grid still range from 1.08° to 2.31°. Source-identified original features, common coordinates and documented uncertainties remain necessary to test positional registration. The discrete shape result and the original zero-phase test therefore retain separate interpretations.

Supplementary Note 24 Fixed-reference module and descriptor provenance

The spatial module is defined in a fixed mean J2000 ecliptic frame. Stellar proper motion is propagated to each evaluation epoch while the ecliptic plane and longitude origin remain fixed. The temporal operator is different: it evaluates equatorial right-ascension intervals in the equator and equinox of date against the count-derived, frozen W=(28,72,16). The ecliptic-of-date branch below is a reference-frame sensitivity comparison; it does not replace the spatial definition or change W during temporal optimisation. This two-epoch audit was added retrospectively.

For frame epoch f, let z(f) be the long-term ecliptic pole and x(f) the normalized cross product of the equatorial pole with z(f). The rotation has rows x(f), z(f)×x(f), z(f). Apply it to the stellar vector propagated in J2000 coordinates to epoch t. The fixed-frame branch uses f=2000 for every t; the of-date branch uses f=t. Longitude differences use the same wrapped shorter-arc convention, and v is the mean of the two latitudes. Individual descriptors are rounded before subtraction. The material seed r=16 is supplied separately throughout.

Input / stellar epoch	Ecliptic frame	g (degrees)	j (degrees)	v (degrees)	Rounded g,j,v
Primary / 2000 CE	J2000 fixed	10.487650	34.077500	62.160110	10, 34, 62
Primary / 2965.2 BCE	Of date	10.699767	34.745408	62.570553	11, 35, 63
Primary / 2965.2 BCE	J2000 fixed	10.484801	34.074723	62.141400	10, 34, 62
6D / 2000 CE	J2000 fixed	10.487712	34.077603	62.160094	10, 34, 62
6D / 2965.2 BCE	Of date	10.699829	34.745507	62.570578	11, 35, 63
6D / 2965.2 BCE	J2000 fixed	10.484864	34.074821	62.141427	10, 34, 62

In the fixed frame, (10,34,62), material r=16, Q and the exact inverse (56,30,10,4) are retained for both input variants at both tested epochs. In the ancient ecliptic of date, (11,35,63) produces inverse (57,30,11,5); q=24 and d=28 nevertheless survive. The unrounded values change, and neither universal epoch invariance nor prehistoric adoption of the J2000 reference plane is inferred. Only the temporal execution uses precession to infer a phase.

A second local construction rotates equatorial coordinates of date by the corresponding obliquity and agrees to 5.69×10^{-14} degrees. Comparison with the unchanged official SOFA C routine iauLteqec, release 2023-10-11, gives maximum descriptor difference 0.0137 arcsecond and identical rounded tuples. Small frame-bias terms omitted by the local engine explain this implementation difference. Both implementations use the same propagated input vectors; this is not independent astrometric validation. The optional driver, source provenance and original SOFA copyright and licence notices are included in S2 (https://www.iausofa.org/2023-10-11c).

Descriptor	Archived decimal (degrees)	Recomputed primary J2000 (degrees)
g	10.471553	10.487649629
j	34.077511	34.077500003
v	62.160117	62.160110108

The archived g differs by 57.947864 arcseconds from the specified primary-coordinate computation. The separate bundled Hipparcos position convention gives g=10.487709737°, and the SOFA check gives primary g=10.487649205°. The provenance of the archived g decimal is not established by these inputs. It is therefore corrected in the current descriptor presentation while FROZEN_CYGNUS_ECLIPTIC_DESCRIPTORS.csv is preserved unchanged as an archival record. Every version rounds g to 10; the compiler, inverse, W, metric holdout and chronology are unaffected. The original carrier audit reads the frozen table and is not a fresh derivation of that decimal.

For continuity with the previous dependent tangent audits, Notes 17 and 19 explicitly retain their archived j and v decimal targets. The current homogeneous primary computation gives d*=28.082610104°, arctan(30/56)=28.178590110° and residual 0.095980006°, compared with archived residual 0.095984110°. The same inventory pair remains first. The non-scored v+g diagnostic is now 72.647759737° rather than archived 72.631670°; neither number defines the temporal target 3q=72.

Supplementary Note 25 Solar shape sensitivity

This counterfactual audit retains diameter role 26, the degree-based identification and the primary obliquity model, changing only the shape used to obtain the normalized long chord. The exact 5:12:13 long side is 24. For published mean sides the normalized value is $26\times80.095/\sqrt{(33.435^2+80.095^2)}$. For a fitted short arc k in 56-fold steps it is $26\cos(\pi k/56)$. These alternatives do not alter the primary metric fit, word or stellar phase.

Shape	Normalized long chord	Solar reading	Offset from stellar phase (years)
Ideal 7|21	24.020867845	3016.7 BCE	-51.5
Exact 5:12:13	24.000000000	2784.8 BCE	+180.4
Published mean-side ratio	23.993392004	2713.2 BCE	+252.0
Free Cleal rectangle	23.934870643	2111.9 BCE	+853.3
Free indicative-91 rectangle	23.986348120	2637.9 BCE	+327.3
Free registered click-plan rectangle	23.917469501	1942.6 BCE	+1022.7

Positive offsets mean later astronomical years. These central readings are mathematical outputs under the stated identification, not archaeological dates or uncertainty bounds. The exact 5:12:13 comparator shifts the ideal-cyclic reading by about 232 years; the published mean-side ratio shifts it by about 303 years. The cyclic and continuous shapes differ by about 9 cm per vertex after their separate common rotations, showing that close shape agreement does not guarantee solar-date agreement. The free rectangles have an additional aspect-ratio parameter and are shown for sensitivity rather than equal-complexity ranking. The 416-arm census in Note 10 remains restricted to its declared ideal cyclic class.

Supplementary Note 26 Temporal dependence and score width

The primary operator and W remain unchanged. Channel 1 is Deneb–Sadr, channel 2 Sadr–Albireo, and channel 3 Aljanah–Fawaris, in the original role order. Each channel omission is minimised over the full astronomical-year window −8000 to +2000 using the same astrometry and local-minimum refinement. RMS values below refer only to the retained channels and are not comparable as likelihoods with differing dimensionality.

Retained channels	Best phase	RMS (sidereal minutes)
1,2,3	2965.2 BCE	0.418975
1,2	2838.0 BCE	0.311489
1,3	2993.0 BCE	0.123901
2,3	2962.0 BCE	0.489530

The closest individual-channel roots to the primary phase are approximately 3107.5, 2795.9 and 2990.0 BCE for channels 1–3; channel 3 also has a root near 6246.2 BCE. Complete local minima and endpoints are recorded in S2. The three channels therefore do not independently return the same date.

A separate deterministic screen assigns each squared channel residual one weight from {0.5,1,2}, normalises by the sum of weights and repeats the full-window search for all 27 choices. The resulting optimum range is 2985.2–2914.7 BCE. These weights are hypothetical; no measurement covariance or

empirical noise distribution is inferred. The primary equal-weight solution remains 2965.2 BCE.

Local score threshold	BCE interval about the primary minimum	Width (years)
1.1 × minimum RMS	2997.7 BCE to 2932.8 BCE	64.891
2.0 × minimum RMS	3087.7 BCE to 2842.5 BCE	245.261

These local score widths are not confidence intervals. The squared local derivatives, normalised to sum to one, are 2.20%, 14.08% and 83.73%; they describe local sensitivity to year, not independent evidence or Fisher-information fractions under a fitted noise model. The 0.64-year primary-to-6D shift tests one astrometric specification and does not represent total temporal uncertainty. Reporting the numerical optimum to one decimal place should not be read as archaeological precision.

Supplementary Note 27 Conditional algebra and two-epoch role comparisons

For the stated compiler, W=(A−B+C−2D, 3B−3C+3D, A−B−C). Its matrix has rank three and null direction (1,0,1,1). All positive-integer inventories yielding W=(28,72,16) have the form (56+t,30,10+t,4+t), integer t≥−3. W alone therefore does not recover the full inventory. If the additional material conditions p=r+g and $p^2=g^2+q^2$ are imposed, then g=$(q^2-r^2)/(2r)$=10, j=g+q=34 and v=j+d=62. The Pythagorean residual along the family is 32t, selecting t=0. The assumptions come from the same material counts and selected frame: this is dependent consistency, not a blind reconstruction or an extra astronomical observation.

All six role permutations were retained for both source tuples (10,34,62) and (11,35,63). Under this additional closure-based reconstruction, only the original assignment in each tuple gives a positive-integer target inventory. The table uses the first tuple; full outputs for both are in S2. This diagnostic does not replace the original unchanged-inverse j–v transposition, whose Station result remains 4→32.

Input g,j,v	Closure-derived g,j,v	Recovered A,B,C,D
10, 34, 62	10, 34, 62	56, 30, 10, 4
10, 62, 34	76.5, 128.5, 100.5	122.5, 30, 76.5, 98.5
34, 10, 62	10, -14, 38	20, -6, 10, -8
34, 62, 10	16.5, 44.5, -7.5	26.5, -6, 16.5, 50.5
62, 10, 34	76.5, 24.5, 48.5	44.5, -48, 76.5, 72.5
62, 34, 10	16.5, -11.5, -35.5	-15.5, -48, 16.5, 36.5

The membership census fixes Deneb and assigns the other 16 entries injectively to g,j,v, giving 16×15×14=3,360 assignments per 17-entry list. The Ptolemaic and Ulugh Beg lists supply membership only. A single bundled Hipparcos position/proper-motion convention is propagated for all candidates and transformed into the ecliptic of each date. This homogeneous comparison input is distinct from the primary chronology input. Historical measured coordinates used in Notes 7–8 are a separate analysis. Target roles are Sadr, Albireo and Fawaris, HIP 100453, 95947 and 97165; Deneb is HIP 102098.

Membership list	Absolute tuple at J2000	Absolute tuple ancient	Differences at J2000	Differences ancient	Joint differences
Ptolemaios	4	0	6	3	1
Ulugh Beg	4	0	7	3	1

The absolute target is (10,34,62); the difference target is (24,28), calculated after separately rounding g,j,v as in the original rule. Only Sadr–Albireo–Fawaris passes the difference criterion at both epochs in both lists. The same assignment alone passes at J2000 and at every one of the 81 sampled integer years in Stage 1 (3000–2920 BCE). Generic proper-motion-time offsets of −8.75, 0 and +8.75 years retain the same joint outcome; these offsets are sensitivity scenarios, not a correction of the source epoch or an uncertainty estimate. Rounding raw differences instead admits three joint assignments per list. The order of rounding is consequential and the alternative is retained.

A continuous comparator uses no rounding: it scores q−24 and d−28 in degrees, either at the fixed ancient phase or jointly with J2000 using equal RMS of four residuals. It fits no additional parameter and does not optimise a second ancient phase.

Criterion	Target score (degrees)	Target rank	Next / tied score	Scope
Ancient RMS	0.110553	1 in both lists	0.149591	Two residuals
Joint two-epoch RMS	0.223328	1 in both lists	0.242591	Four residuals
Joint maximum error	0.410177	Tied first (2)	0.410177	Same four residuals
J2000 RMS	0.295853	2 Ptolemy / 4 Ulugh Beg	See full rankings in S2	Two residuals

The joint-RMS runner-up replaces Fawaris with HIP 99848; its margin from the target is only 0.0193°. The ancient-only runner-up has roles HIP 99675, 96683, 100453. The target remains first in ancient and joint RMS for all 81 Stage-1 sampled years. Its four residuals (q,d at J2000, then q,d at the ancient phase) are −0.410177°, +0.082542°, +0.023579°, −0.154557°. Both lists share many stars and the same coordinates, so their agreement is not two independent replications. The criterion and ancient epoch are conditioned on the existing model; no p-value, uncertainty-calibrated significance or independent dating claim follows.

For the named primary graph in the ecliptic of date, the full declared window contains the following open-cell behaviours; values at exact half-integer boundaries use the script’s nearest-even tie rule. This check prevents extrapolating the two-epoch agreement into universal invariance.

Astronomical-year interval	Rounded g,j,v	Derived W
-8000.0000 to -2274.1959	11, 35, 63	28, 72, 16
-2274.1959 to -1225.4862	11, 35, 62	27, 72, 16
-1225.4862 to 1668.6407	11, 34, 62	28, 69, 16
1668.6407 to 2000.0000	10, 34, 62	28, 72, 16

At 321 quarter-year samples across Stage 1 the primary descriptors give (11,35,63), with minimum distance 0.065805° from a half-integer boundary. This is distance from a classification boundary, not astrometric uncertainty. None of these of-date diagnostics changes the fixed-reference spatial definition, primary phase search, original anchored Station result or solar shape sensitivity.

Supplementary Note 28 Reconstruction from stellar contrasts with a Station anchor

This retrospective analysis uses the already declared compiler r=A−B−C, g=C, j=B+D and v=A+C−D. Its contrasts q=j−g and d=v−j give A=q+d+D and B−C=q−D. With D=4 and (q,d)=(24,28), A=56 and B−C=20 follow without an absolute stellar seed or a Pythagorean condition. Separating B and C requires an additional condition: the existing material closure r=D²=16 gives B+C=A−r=40, hence B=30 and C=10. The general conditional inverse is A=q+d+D, B=q+(d−r)/2, C=D+(d−r)/2, with D retained as an observed input.

The closure r=D² is a model relation recognised with the counts available; four observed settings alone do not establish that relation. Without it, infinitely many B/C pairs remain possible. At A=56 and D=4, the pairs (B,C)=(28,8), (30,10) and (32,12) all give the same contrasts, with r=20,16 and 12 respectively. The inventory family in Note 27 already implied that fixing D resolves its free parameter; the present derivation makes that conditioning explicit.

Input convention	Rounded g,j,v	Original absolute inverse with r=16	Conditional inverse with D=4 and r=D²
J2000 positions in fixed J2000 ecliptic	10,34,62	56,30,10,4	56,30,10,4
Ancient positions in ecliptic of date	11,35,63	57,30,11,5	56,30,10,4
Ancient positions in fixed J2000 ecliptic	10,34,62	56,30,10,4	56,30,10,4
Ulugh Beg catalogue	10,34,62	56,30,10,4	56,30,10,4
Ptolemy catalogue adverse control	11,35,62	56.5,29.5,11,5.5	55,29.5,9.5,4

All eight archived configurations in Note 24, combining primary or six-dimensional inputs, two epochs and two reference conventions, retain (q,d)=(24,28) after seed-first rounding. The conditional inverse therefore returns the target inventory in each. These configurations share observations and are not eight independent confirmations. Common integer shifts of the three seeds preserve their contrasts algebraically; changing the physical reference frame is not generally a common shift of continuous coordinates. The full-window adverse cells in Note 27 remain unchanged.

Without rounding the descriptors, the primary modern input returns approximately (55.6725,29.6312,10.0413,4), and the primary ancient-of-date input returns (55.8708,29.9582,9.9126,4). Exact inventory recovery therefore depends on the declared discrete rule. Direct-difference rounding also gives the target in the eight configurations, but is archived as a separate alternative rule. Exchanging j and v while retaining D=4 gives (28,30,−18,4); this is distinct from the original absolute-inverse transposition, which returns 32 Stations.

Changing the retained anchor also changes the reconstruction: D=2 gives (54,36,14,2), and D=6 gives (58,20,2,6). These are positive integer inventories under r=D². Thus D=4 is supplied by the material record rather than chosen from the algebra to produce the preferred inventory. Code checks comprise 1,000 exact round trips with free r, 201 common integer seed shifts and five independent rational Gaussian-elimination cases. These verify implementation, not historical intention. Source outputs, all permutations, anchor alternatives and continuous diagnostics are in S2 Code/added_audits/station_anchor.

v1.26: Conditional uniqueness preserved; 55 library words satisfy weaker integer feasibility. See S5 section 3.1.

Supplementary Note 29 Conditional uniqueness of the material inventory

Proposition. In the fixed primary compiler, let A, B, C and D range over all strictly positive integers. Define r=A−B−C, g=C, q=B+D−C, d=A+C−B−2D and p=A−B. The three conditions r=D², d=A/2 and p²=g²+q² have exactly one solution: (A,B,C,D)=(56,30,10,4). There is no upper bound on inventory size in this statement. The equations and role assignments were recognised with the archaeological counts available; this is retrospective conditional algebra, not a blind prediction or a probability calculation.

Condition	Equation in the inventories	Existing role
R	A−B−C=D²	Third word component equals squared Station count
H	A+C−B−2D=A/2	First word component equals half the Aubrey count
P	(A−B)²=C²+(B+D−C)²	Pythagorean closure of the material channels

Proof. H gives q=A/2−D, hence A=2(q+D). With R, C=(q+3D−D²)/2 and p=C+D². Substitution into P gives q²=D⁴+2D²C=D²q+3D³, or q²−D²q−3D³=0. For integer q and D, k=|2q−D²|/D is rational and k²=D(D+12) is integer; a rational number with integer square must be integer. Therefore (D+6−k)(D+6+k)=36. For D>0 both factors are positive integers with the same parity. The only such factor pairs are (2,18) and (6,6). The latter yields the inadmissible D=0; the former gives D=4 and k=8.

Positivity selects the remaining branch. R implies A=B+C+D²≥D²+2, so q=A/2−D≥((D−1)²+1)/2>0. Thus q=D(D+k)/2=24, A=2(q+D)=56, C=(q+3D−D²)/2=10 and B=A−C−D²=30. Direct substitution verifies all three conditions. The other branch at D=4 gives (−8,−18,−6,4), which violates positivity. This proves existence and uniqueness over the full stated domain.

The solution gives (g,q,p)=(10,24,26), the primitive shape 5:12:13 and W=(d,3q,r)=(28,72,16). The outer identity 2B−A=D follows without being imposed as a fourth condition. On a 56-position circuit, the shape gives 7.037291|20.962709|7.037291|20.962709 and therefore the nearest discrete form 7|21|7|21. These are consequences of the same solution. No positional index, metre scale or celestial epoch is derived by the proof.

Condition-removal controls. Each condition is needed for uniqueness in the stated positive-integer problem. The following non-target examples satisfy both retained equations exactly; the listed residual belongs to the omitted equation. R uses r−D², H uses 2d−A and P uses p²−g²−q².

Condition omitted	Positive integer example A,B,C,D	Residual of omitted equation
R	28,15,5,2	4
H	22,12,6,2	2
P	20,11,5,2	−8

Integrality and compiler controls. Allowing positive real counts leaves the continuous family q=D(D+sqrt(D(D+12)))/2, with A, B and C as in the proof. The other exact radial row in the reported {−1,0,1} census is r′=B−C−D. Substituting r′=D² while retaining H, P and p=A−B yields 2C=6D−9+45/(D+5), so divisors of 45 enumerate three positive integer solutions: (56,30,10,4), (260,137,27,10) and (3440,1756,116,40). Uniqueness is therefore specific to the primary compiler and does not extend automatically to alternative maps or retrospectively selectable closure sets.

Inverse reading of the existing word closures. With N=56 and s=4, N=2s(b−a) and N+s²=s(c+a) give b−a=7 and c+a=18. A positive Pythagorean frame then obeys a²+(a+7)²=(18−a)², or a²+50a−275=0. The roots a=5 and a=−55 leave the unique positive frame (5,12,13). Side measurements do not enter this execution, but the identities were identified with the geometry and counts known; it is another dependent expression of the same material closure.

The audit enumerates factor pairs using exact rational arithmetic. A separate implementation scanned D=1..100 and C=1..10,000, eliminated A and B through R and H, and checked P directly, returning only the target inventory. That bounded computation checks implementation; the unbounded result rests on the factorisation proof. Source manuscript passages and hashes, proof outputs, controls and code are in S2 Code/added_audits/material_uniqueness. The source passages document provenance and are not a preregistration.

Supplementary Note 30 Specified construction procedures and inherited irregularity diagnostics

Scope. This retrospective diagnostic asks whether 56 printed Aubrey symbol-centre proxies support a specified eight-sector construction procedure or a residual pattern repeating every seven holes. They are diagram coordinates, not primary survey hole centres. The input extraction, scale conventions and source hashes are supplied. The test does not cover every possible eight-sector construction history and does not modify the Station shape or its anchored indexing result.

Physical templates divide each side of a regular p-gon into m=56/p equal linear segments and project the resulting points radially onto its circumcircle. The non-degenerate distinct candidates p=4,7,8,14 are compared with a regular 56-position circle; p=28 and p=56 are exact regular-circle aliases, and p=2 is degenerate. Every template receives the same four continuous parameters: two centre coordinates, rotation and scale. Each polygon also has m candidate index origins. Origin choice is optimised only on the training observations in each validation fold.

The contiguous-block validation has 56 folds: eight blocks of seven positions at each of seven partition starts. Each fit uses 49 observations and predicts the withheld seven, so each point is withheld seven times. All points were already known when the diagnostic was designed; this is internal cross-validation, not a prospective archaeological holdout. Positional errors use the declared isotropic printed-scale conversion.

Template	Full-fit positional RMS m	Blocked validation RMS m
Regular 56 positions	0.534841	0.613657
Four sectors	2.186221	3.029685
Seven sectors	0.583839	0.695961
Eight sectors	0.583072	0.733259
Fourteen sectors	0.533292	0.616982

The eight-sector model is 19.49% worse in blocked validation than the regular circle. Separate printed-grid scales give the same ordering: 0.598376 m for the regular circle and 0.718783 m for eight sectors. A flexible angular-residual model with repetition every seven holes gives 0.753254° cross-validated RMS, compared with 0.712489° for the constant baseline, a 5.72% deterioration. None of the tested periods 2,4,7,8,14,28 improves blocked validation. These results do not support the specified equal-linear-division or periodic-residual procedures.

Synthetic coordinate perturbations used 2,000 trials at each of ±1, ±2 and ±4 pixels per coordinate, approximately ±0.056, ±0.112 and ±0.224 m. The eight-sector template never beat the regular circle in full-fit RMS in those 6,000 trials. These are assumed perturbation envelopes, not archaeological error estimates or a significance probability. Exact synthetic recovery, regular-circle aliases and an independent real least-squares formulation validate the implementation. Equal-arc subdivision into eight groups of seven produces the regular 56-position template exactly; coordinates alone therefore cannot distinguish that construction history.

Inherited irregularities across circuits were not tested. The available Y-hole, Z-hole and sarsen inputs do not provide a homogeneous set of survey-grade centres; Rees click-plan labels are not interchangeable

with physical stone or socket centres. The archive records this analysis as not executable with the current coordinate inputs and specifies the needed survey data. It does not claim transmission, absence of transmission or a passed external survey test.

An ancillary meridian calculation retained the existing primary stellar input, operator, phase and a latitude of 51.18°. The five model stars culminate geometrically above the horizon at that phase, with upper-transit altitudes approximately 64.8–80.6°. This does not test darkness, extinction, refraction, ancient observing precision or historical use, and is not an independent chronology. It is retained in the executable archive without additional historical weight. Full construction and periodic tables, perturbation outputs, protocols, input files and the independent verification are in S2 Code/added_audits/construction.

Supplementary Note 31 Constructive interpretation of the dimensional ladder

Scope. The existing inner roles admit a constructive interpretation in terms of a right rectangular frame with short side x, long side y and diagonal z. The operations and associations were recognised after the dimensional ladder and measurements were known. This is a dependent retrospective analysis, not a blind prediction or an additional probability of prehistoric intention. The primary outer calibration and its 2.019623% result remain unchanged.

Architectural role	Geometric operation	For (x,y,z)=(10,24,26)u
Sarsen outer diameter	Copy x	10u
Z-hole diameter	Halve y	12u
Y-hole diameter	Subtract x from z	16u
Trilithon outer span	Inradius (x+y-z)/2	4u

The inradius belongs to the right triangle formed by the rectangle diagonal. Its radius is transferred as a candidate span; no corresponding archaeological incircle has been identified at the Trilithons. The code checks this radius independently as triangle area divided by semiperimeter. Under the concentric model, the long-side lines are tangent to a circle of diameter x; a tangent from a rectangle vertex to that circle has length y/2. The radial clearance between the circles of diameters z and x is (z-x)/2. These are geometric consequences of the same construction.

For the ideal 7|21|7|21 rectangle at the primary Aubrey diameter D=86.44 m, x=D sin(π/8), y=D cos(π/8), and z=D. Applying the same operations gives:

Role	Calculated m	Approximate input m	Signed residual %
Sarsen outer diameter	33.079	33.0	+0.240
Z-hole diameter	39.930	39.0	+2.385
Y-hole diameter	53.361	54.0	-1.184
Trilithon outer span	13.250	13.7	-3.287

The four-channel relative RMS is 2.118465%. At the same fixed diameter, the continuous 5:12:13 comparator gives 2.040002%. Applying the operations to the reported Station side means gives 2.014104%, using a Euclidean diagonal computed from those two means, not a measured diagonal. None of these dependent variants replaces the original three-input outer calibration.

Boundary conventions follow Note 1. The 33.0 m Sarsen input and 13.7 m Trilithon input are rounded outer-face readings from Cleal Plan 1, not published scalar measurements with calibrated uncertainty. Y=54.0 m and Z=39.0 m are approximate hole-centre circuit diameters. Faces, centres and envelopes are not interchangeable. No new survey measurement is introduced.

Supplementary Note 31 continued Complete comparisons and limitations

All 14 discrete rectangles k|(28-k)|k|(28-k), k=1,...,14, receive D=86.44 m and the same four operations. The table lists every candidate, ordered by RMS in each half. This census conditions on the retrospective recipe; it is not a search over all possible construction rules.

k	Gaps	RMS %	k	Gaps	RMS %
7	7|21|7|21	2.118	11	11|17|11|17	33.191
8	8|20|8|20	8.748	12	12|16|12|16	40.443
6	6|22|6|22	10.458	3	3|25|3|25	41.850
9	9|19|9|19	17.311	13	13|15|13|15	47.242
5	5|23|5|23	20.437	2	2|26|2|26	53.192
10	10|18|10|18	25.478	14	14|14|14|14	53.602
4	4|24|4|24	30.922	1	1|27|1|27	64.923

The disclosed Aubrey diameter branches retain k=7 as the best of those 14 candidates. The exact prose-implied value is retained in calculation rather than its rounded display.

Diameter source branch	D m	k=7 RMS %	Best k
Thom	86.44000	2.118	7
Hawkins	86.87000	2.078	7
Lawson rounded summary	87.00000	2.089	7
MacKie p. 99 prose-implied branch	85.83168	2.359	7

The rounded inner inputs do not close every identity exactly. The recipe implies H=Z-Y/2, which gives 12.0 m rather than approximately 13.7 m, a -1.7 m (-12.41%) difference. S+Y=87.0 m is +0.65% from D=86.44 m. Also, $\sqrt{(S^2+(2Z)^2)}$=84.694 m differs from S+Y=87.0 m by -2.65%. Subtraction can amplify relative discrepancies in smaller lengths, but calibrated archaeological uncertainties are unavailable; rounding alone has not been shown to explain the mismatch.

Preliminary positional diagnostic. Using the archived Aubrey proxy centre and an assumed Sarsen radius of 16.5 m, signed clearances to the two long-side lines are:

Proxy branch	Line 92-93 m	Line 94-91 m
Cleal	-0.170	+0.951
Indicative 91	-0.170	+0.200
Registered click-plan	-0.846	+1.067

The Sarsen centre was not measured independently; these proxies do not establish actual tangency. The indicative-91 branch is not adopted because its clearances are smaller. In a purely planar concentric construction, the tangent-ray angle subtended by the inner circle is 2 asin(S/D): 45° for k=7, 44.886° for the rounded source dimensions, and 45.240° for exact 5:12:13. No observing height, terrain, obstruction, visibility or historical optical use was tested.

Supplementary Note 32 Physical model separation and pairwise inverse sensitivity

With a common centre, rectangle-axis orientation and circumdiameter D, put α=atan(5/12) and β=π/8. Corresponding vertices have coordinates (±(D/2)cos α, ±(D/2)sin α) and (±(D/2)cos β, ±(D/2)sin β). Their separation is D sin(|α-β|/2). At D=86.44 m it is 0.090417866 m at every corner; α-β=0.119864948°. Cartesian distances verify the angular expression independently.

Quantity	5:12:13 minus 7|21|7|21
Corresponding vertex position	9.0418 cm separation
Short side / Sarsen role	+16.6998 cm
Long side	-6.9378 cm
Z diameter role	-3.4689 cm
Y diameter role	-16.6998 cm
Trilithon inradius role	+4.8810 cm

Across the four diameter branches, vertex separation is 8.978-9.100 cm. At the archived raster calibration the primary value corresponds to 1.614 pixels. Neither model separation nor pixel size is an archaeological error estimate. The continuous 5:12:13 plan fit remains slightly better in all three archived conventions (Note 23). Historical discrimination requires quantified original-position uncertainty and construction variation; statistical indistinguishability has not been established. This calculation does not resolve anchored indexing or the solar shape sensitivity in Note 25.

Every pair of inner inputs was also inverted under S=x, Z=y/2, Y=z-x, H=(x+y-z)/2 and $z^2=x^2+y^2$. The inputs S=33.0, Z=39.0, Y=54.0 and H=13.7 m retain their approximate boundary conventions. The three external comparison targets are x=33.435, y=80.095 and D=86.44 m. All six pairs are disclosed:

Input pair	Short side m	Long side m	Diagonal m	External RMS %
S,Z	33.000	78.000	84.694	2.051
S,Y	33.000	80.498	87.000	0.888
S,H	33.000	94.432	100.032	13.776
Z,Y	29.333	78.000	83.333	7.533
Z,H	34.819	78.000	85.419	2.908
Y,H	34.351	81.400	88.351	2.240

The favourable S,Y inversion is not promoted alone. The S,H branch has y=2H(S-H)/(S-2H), with denominator 5.6 m and local derivative dy/dH=35.726: a hypothetical 0.1 m change in H produces about 3.57 m in y to first order. This is mathematical sensitivity, not an estimated survey error. These inverse results do not support a general robust recovery claim from arbitrary inner pairs.

Reproduction. S2 Code/added_audits/constructive_lengths contains the inputs, source hashes, expected outputs and full results for Notes 31-32. The standard-library-only scripts reproduce both analyses; run_constructive_audits.py checks regenerated results against the archived JSON and is called by run_all.py. The analyses share the existing measurements and retrospective associations and add no independent historical validation.

Supplementary Note 33 Continuous reconstruction and quantization sensitivity

Scope. This retrospective extension of Note 28 keeps the four-Station anchor and square closure, but compares the continuous stellar contrasts with integer inventories before rounding any individual stellar descriptor. The original fixed-J2000 spatial module, nearest-integer rule, primary temporal operator and headline phase remain separate, unchanged definitions. The added estimator does not demonstrate an ancient coding convention.

The existing compiler gives r=A-B-C, q=B+D-C and d=A-B+C-2D. With D=4 and r=D²=16, it follows that A=B+C+16, q=B+4-C and d=2C+8. Let q_obs=j-g and d_obs=v-j be unrounded ecliptic-of-date measurements. Minimize w_q(B+4-C-q_obs)² + w_d(2C+8-d_obs)² over positive integer B,C, with w_q,w_d>0. A is then fixed by the declared closure.

Input and epoch	q_obs degrees	d_obs degrees	Best inventory	RMS degrees
Primary J2000	23.589850	28.082610	56,30,10,4	0.295844
Primary 2965.2 BCE	24.045641	27.825144	56,30,10,4	0.127784
6D J2000	23.589891	28.082491	56,30,10,4	0.295799
6D 2965.2 BCE	24.045678	27.825071	56,30,10,4	0.127841

Unbounded uniqueness. Every allowed q is an integer and every allowed d is even. In all four cases, 23.5<q_obs<24.5 and 27<d_obs<29. Therefore q=24 and d=28 are individually and uniquely nearest. They are simultaneously feasible, giving C=10, B=30 and A=56. Any other inventory increases at least one absolute residual without reducing the other, proving uniqueness for every positive diagonal squared-error weight. A separate B,C=1..100 enumeration checks the implementation; the proof is not bounded by that enumeration.

At the primary ancient phase, equal-weight RMS is 0.127784 degrees. The runner-up inventory (57,31,10,4) has RMS 0.686067 degrees. The unconstrained continuous inverse is approximately (55.870786,29.958213,9.912572,4). These are model estimates, not new archaeological measurements. The inferred inventory compiles to (r,g,j,v)=(16,10,34,62) and W=(28,72,16). The inferred canonical register is not a literal claim that the ancient angular measurements equal those integers.

Directional allocation. All six permutations of the unrounded g,j,v descriptors receive the same positive-integer fit, with D=4 and r=16 held fixed. Only the declared ordering recovers (56,30,10,4) in the four tabled cases and at the homogeneous-Hipparcos temporal optimum. Exchanging j and v gives q=51.870786 and d=-27.825144 degrees at the primary ancient phase. The optimum becomes (66,49,1,4), with RMS 26.746572 degrees. A bound derived from an incumbent error proves that no excluded larger C improves the fit. This allocation failure belongs to the conditional inverse; it neither tests terrestrial azimuths nor supplies an independent 1/6 chance factor.

The estimator retains material information: D=4 and r=D² were not predicted from the sky. The stellar graph, descriptors, epoch and closure were already known when this diagnostic was formulated. Uniqueness concerns inventories within this conditional model, not all stellar models, historical explanations or reference conventions. The raw contrasts themselves vary with the reference plane. No measurement covariance, likelihood, confidence interval or independent significance is inferred.

Supplementary Note 33 continued Reference and candidate sensitivities

With the J2000 plane held fixed, both archived stellar-motion prescriptions retain rounded (10,34,62) throughout astronomical years -8000 to +2000. Primary continuous ranges in degrees are g=10.481913-10.487649, j=34.071910-34.077500 and v=62.122288-62.160106. Annual samples and stationary-point checks under the archived affine-vector propagation verify the range. The smallest rounding-boundary margin is about 0.01229 degrees in the 6D branch; it is not an uncertainty estimate. This fixed-plane stability does not establish prehistoric use of J2000 or invariance in the moving ecliptic of date.

At the primary ancient phase, the ecliptic-of-date descriptors remain approximately (10.699767,34.745408,62.570553). Nearest-integer quantization gives (11,35,63), whereas the retrospectively proposed floor rule gives (10,34,62). Both give q=24,d=28 after seed-wise quantization. The floor rule recovers the original absolute inverse at the two tested epochs but not throughout the moving-ecliptic 10,000-year window. It changes the quantizer rather than correcting a coordinate error.

Across the earlier 3,360-assignment spatial domains, floor admits two joint-epoch assignments in each membership list: Sadr-Albireo-Fawaris and Sadr-Albireo-HIP 99848. Both also survive the 81 annual archaeological-interval checks. The existing temporal operator distinguishes them after a full-window search:

Input convention	Partner	Minimum RMS minutes	Minimum BCE
Primary fixed base; Hipparcos partner	Fawaris	0.418016	2964.8
Primary fixed base; Hipparcos partner	HIP 99848	0.596437	3043.6
Homogeneous Hipparcos 2D	Fawaris	0.389288	2965.0
Homogeneous Hipparcos 2D	HIP 99848	0.566478	3043.9

These comparison scores do not replace the primary 2965.2 BCE and 0.4190-minute result. Fawaris is the unique lowest-error candidate under both conventions; no new binary acceptance cutoff is introduced. The original residual-partner code used a primary-input fixed base with Hipparcos partners, not homogeneous Hipparcos inputs, and a local epoch search. Note 18 and the updated script now describe the inputs correctly and search the full window.

Omitting the transverse channel from epoch fitting provides a further retrospective diagnostic. Fitting only Deneb-Sadr and Sadr-Albireo gives 2838.0 BCE with the primary fixed base and 2848.4 BCE with homogeneous Hipparcos inputs. At those epochs, the held-out third-arc absolute errors are 1.4197 versus 2.2664 minutes, and 1.3080 versus 2.1570 minutes, for Fawaris and HIP 99848 respectively. Fawaris remains closer, but neither third-arc prediction is exact and the primary phase is not independently recovered. This computational omission does not create a prospective or external validation sample.

Supplementary Note 34 Joint conditional role census

Question. Does an alternative stellar assignment recover the same conditional inventory and match the named graph temporally when allowed its own best epoch? This enumeration runs the spatial and temporal criteria on the same alternatives instead of multiplying marginal control rates. Its protocol was recorded before this new enumeration, after the original results and quantization alternatives were inspected. It is retrospective, not a preregistration.

Deneb (HIP 102098) and Aljanah (HIP 102488) remain fixed as distinct anchors. Each archived 17-entry membership list leaves 15 candidates for the ordered g,j,v partner roles; all five stars must be distinct. Thus each domain contains 15×14×13=2,730 assignments. The 3,360 denominator in Notes 18 and 27 refers to a four-star spatial screen that did not reserve Aljanah as a distinct fifth star. The two domains are not interchangeable. Their union contains 3,276 distinct assignments, which are evaluated once and attributed to their respective lists.

All entries use the same archived Hipparcos positions and proper motions with the declared 2D propagation convention. The memberships supply candidate lists, not historical measured coordinates. W=(28,72,16), the operator, role order and numerical epoch window remain fixed. The g and j observables retain their longitude types and v its mean-latitude type; the census already conditions on this assignment. Each alternative graph receives a two-year grid over astronomical years -8000 through +2000; all grid-bracketed local minima are refined, and the window endpoints are included. Near-benchmark candidates are checked again on an annual grid. Finite role enumeration is exhaustive; continuous epoch minimization is numerical.

At each graph’s own best temporal epoch, its unrounded ecliptic-of-date q and d are computed. The continuous inventory criterion in Note 33 recovers the target uniquely when $23.5<q<24.5$ and $27<d<29$. A temporal pass requires RMS no greater than the observed named graph under these same astrometric inputs. An additional continuous spatial comparison requires RMS of (q-24,d-28) no greater than the named graph. Each criterion and its conjunction are reported separately. No archaeological interval is used to search or select an epoch.

The benchmark graph has homogeneous-input optimum 2965.0489 BCE, temporal RMS 0.389288485 minutes, contrasts (24.023563,27.845448) degrees and contrast RMS 0.110547272 degrees. Its comparison-input values are not substituted for the primary chronology. HIP 99848 is the second-best temporal partner, with full-window RMS 0.566478226 minutes and contrast RMS 0.185512243 degrees at its own optimum of 3043.8636 BCE.

To expose quantizer freedom, the same alternatives are also classified by nearest-integer or floor g,j,v followed by contrast calculation and the same Station-anchored inverse. The union means an assignment may succeed under any of these three declared inventory routes. The continuous route is designated for the main added comparison; no branch is silently selected because it gives the smallest frequency.

Supplementary Note 34 continued Frequencies and interpretation

Criterion at each graph's own optimum	Ptolemaios / 2730	Ulugh Beg / 2730
Continuous target-inventory recovery	6	8
Temporal RMS at least as good as named graph	1	1
Continuous spatial RMS at least as good	1	1
Inventory and temporal conjunction	1	1
Continuous spatial-score and temporal conjunction	1	1
Nearest-seed inventory recovery	3	3
Floor-seed inventory recovery	4	6
Any of the three inventory rules	7	9
Any inventory rule and temporal criterion	1	1
Inventory, temporal and Stage 1 conjunction	1	1

The sole joint assignment in both lists is HIP 100453,95947,97165: Sadr-Albireo-Fawaris. One of 2,730 is 0.0366300% in this finite conditional universe. The temporal benchmark alone already retains one assignment. Consequently, the spatial conjunction and the subsequent Stage 1 comparison supply no additional multiplicative rarity factor. The lists overlap and use the same astrometry; their frequencies must not be multiplied or described as independent replications.

This frequency is not a site-level p-value, a probability that the correspondence arose by chance, or a probability of prehistoric intention. The census conditions on the carrier, anchors, word, compiler, closures, descriptors, astrometric convention and retrospective procedure. It does not resample monument construction, source-boundary choices, metric measurements, formula discovery or creation of the grammar. Such an interpretation would require a defensible generating model or external reference corpus and a fully specified selection procedure.

Existing control retained separately	Result	Question conditioned on
Metric ladder randomization	72,285 / 1,000,000 = 7.2285%	Specified synthetic metric null
Input-side formula flexibility	330,486 / 12,960,000 = 2.550046%	Count box and signed-subset class
Material word census	Named word ranks 1 / 512	Declared scalar library and fixed graph
Arbitrary positive integer words	179 at least as good temporally	Much broader word family

These control families share selections or answer different conditional questions. Their rates are not combined into a global chance estimate. Exact inverse closure and the material uniqueness theorem are model consequences and are not counted as independent random successes. The added census gives a direct joint role comparison while leaving the wider historical selection problem explicit.

Reproduction. S2 Code/added_audits/rounding_pipeline includes the inputs, protocols, provenance, assignment records and expected outputs. run_all.py includes the six verified diagnostics via run_rounding_and_joint_audits.py. The corrected residual-partner audit uses the full window; primary metric, inventory, word and chronology results are retained.

Supplementary Note 35
Relative directions of complete trilithons and the Station frame

The three complete trilithon openings represented in the archived click-plan are directionally closer to the long sides of the Station rectangle than to its short sides. This retrospective diagnostic quantifies a relation between material structures that can inform a common setting-out hypothesis. It does not identify a terrestrial realization of the stellar channels.

Source and selection

The input is the Tim Daw click-plan based on the Rees 1989 sheet MP/STO0861, already archived in S2 Code. Its README places numbered markers at hatch centroids. The east/north grid conversion is retained without a fitted rotation. Pairs 51-52, 53-54 and 57-58 are evaluated; fallen fragments of 55 and 59 are not treated as original socket centres. This covers three of five trilithons, including the restored standing arrangement, and is not a survey of the original complete horseshoe. The indicative alternative for Station 91 is retained as a separate sensitivity branch.

Axial comparison

For every pair, the opening axis is the normal to the line between the two support-centroid proxies. A unit vector u represents an unoriented axis, so u and -u are equivalent. With $P = uu^T$, the projector Gram is $K_{ij} = \mathrm{tr}(P_i P_j) = (u_i \cdot u_j)^2$. Its endpoints are 1 for parallel axes and 0 for perpendicular axes. Each opening is compared with both long sides (92-93 and 94-91) and both short sides (91-92 and 93-94); family scores are their arithmetic means. The normal-versus-lintel convention and both side families are fixed across all pairs.

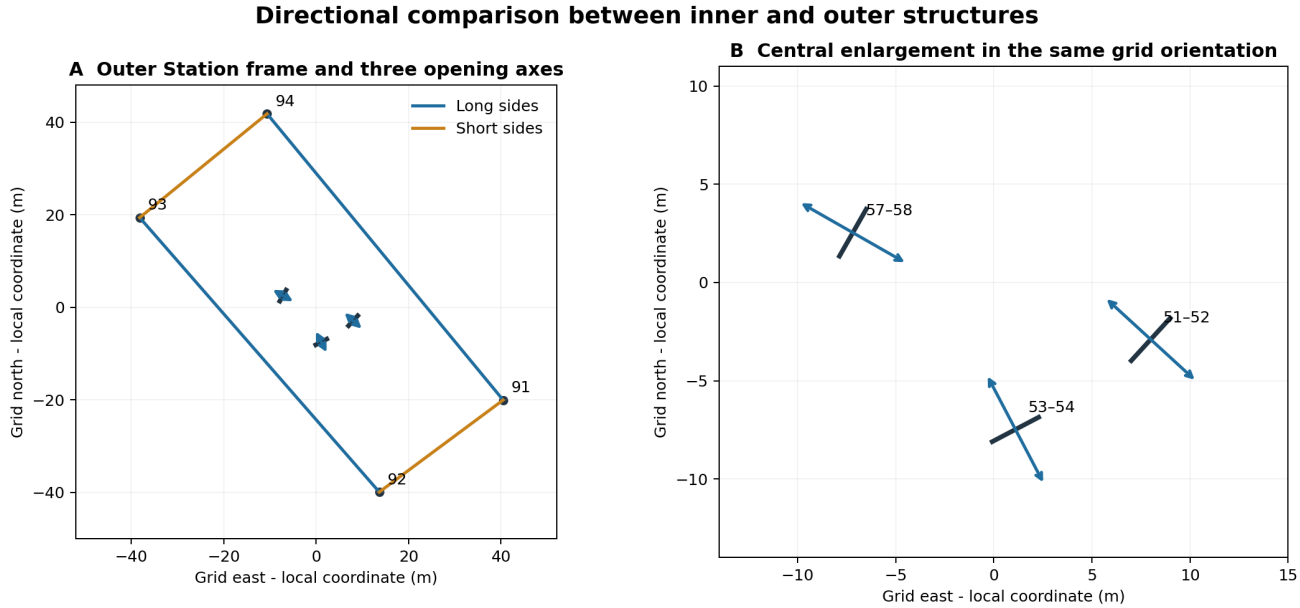
Opening pair	Long-side mean	Short-side mean
51-52	0.984247	0.028716
53-54	0.951820	0.031505
57-58	0.883446	0.146278
Mean over three	0.939838	0.068833

With only Station 91 replaced by its indicative alternative, the overall scores are 0.937926 and 0.064396, and every opening retains the same preference. These are descriptive similarities, not probabilities. Source alternatives share the same plan and do not constitute independent replications.

The internal Gram has off-diagonal values 0.885014, 0.951047 and 0.709656. Thus the geographical H-V-H classification of the three openings does not imply two perpendicular physical families: nearby directions can fall on opposite sides of the categorical boundary. Comparisons with fixed grid east/north axes are retained in the code as a separate diagnostic.

Retained v1.23 reference numbering: use the v1.26 crosswalk and current S5 interpretation.

Physical arrangement and deterministic sensitivity



Mean score: long sides 0.940; short sides 0.069. Scale: 0 = perpendicular; 1 = parallel.
Retrospective drawing-centroid diagnostic; three complete pairs; no fitted rotation.

Supplementary Fig 35.1. Station sides and the three available opening axes in the same grid orientation. Dark segments join support centroids; blue double arrows denote their normals. Panel B enlarges the central area without rotating it. The axes are unoriented. The figure represents drawing proxies, not original socket directions with measured uncertainties.

For an imposed bound ε on each endpoint coordinate, vector perturbations have norm at most $E = 2\sqrt{2}\,\varepsilon$. A vector of nominal length $L > E$ changes direction by at most $\arcsin(E/L)$. Adding the bounds for an opening and a Station side bounds their acute separation. Lower bounds on long-side squared alignment and upper bounds on short-side alignment give a sufficient certificate for long-side preference under every perturbation in the stipulated box. Full equations and values are supplied in the executable protocol.

Coordinate halfwidth	Primary branch	Indicative 91 branch
±0.10 m	3/3 preferences certified	3/3 preferences certified
±0.25 m	3/3 preferences certified	3/3 preferences certified
±0.50 m	1/3 certified; 2 unresolved	1/3 certified; 2 unresolved

These are artificial sensitivity bounds, not archaeological error estimates or confidence intervals. Failure of the sufficient certificate at ±0.50 m does not demonstrate a reversal. Shared endpoints are allowed; the bounds remain conservative.

A joint rigid rotation preserves the relative Gram comparison. Rotating only the opening axes by 90° complements their scores, while geographical anchoring distinguishes a whole-plan rotation. The material relation therefore addresses a possible shared frame of construction; it does not by itself establish cardinal registration, prehistoric transmission or a correspondence with 34 and 62. Existing architectural and astronomical orientation accounts remain to be compared, and original-centre information for the two incomplete pairs is needed before extending this claim to the whole horseshoe.

Reproduction. S2 Code/added_audits/directional_gram provides inputs, complete results and the protocol. run_directional_gram_audit.py, included in run_all.py, verifies the delivered snapshot. This retrospective diagnostic makes no claim of blind prediction, global rarity or a newly discovered architectural alignment.

Supplementary Note 36

The pivot bridge and its primitive constructions

The specified transformation T(s,l,h)=(h−s,(s+l+h)/2,s+l) sends the doubled Station frame (10,24,26) to (16,30,34). These outputs are a difference, a semiperimeter and a sum of lengths. The result is a constructive connection between two primitive families, not an additional survey observation. The original pivot-theorem source extracts and the earlier Calanais texts are preserved in the PIVOT_BRIDGE archive in S3 Code.

For a positive input right triangle put t=l/s. Requiring the transformed sides also to satisfy Pythagoras gives $(t-3)\sqrt{(1+t^2)}+t^2-3t+3=0$. The second term is positive, so $t<3$. Squaring the equivalent positive-sided equality gives $(3-t)^2(1+t^2)-(t^2-3t+3)^2=t(12-5t)=0$. Thus t=12/5 is the sole positive solution, and it satisfies the unsquared equation. The transformation therefore sends (5k,12k,13k) to (8k,15k,17k). An input inradius of 4 fixes k=2. Enumeration of both leg assignments for all primitive triples of hypotenuse at most 1000 checks the proof; it is not a rarity model.

Among integer right triangles with fixed hypotenuse 34, the positive leg pair is 16,30 up to exchange; hypotenuse 62 admits no positive integer legs. This distinguishes algebraic roles under a fixed unit, not terrestrial orientations. Odd/even leg assignments in primitive triples likewise require a declared common basis and are not unique celestial labels. The Gaussian identities $(3+2i)^2=5+12i$ and $(4+i)^2=15+8i$ generate the two families. Their equal-area relation is also exact: the 5-by-12 rectangle and the triangle with legs 8 and 15 both have area 60. A 4:1 auxiliary rectangle provides a physical angular recipe by reflection: $2\arctan(1/4)=\arctan(16/30)=28.072487°$. The complement is 61.927513°, and the difference is 33.855026°. These round to 28, 62 and 34 under the original nearest-integer rule. The length 34 is the hypotenuse, not a third internal angle. The two acute angles and their difference contain one shape parameter.

The pivot triangle has area 240, semiperimeter 40, inradius 6 and exradii 10, 24 and 40 opposite its three sides. The first two exradii recover the original legs. More generally, given positive exradii s,l for the two legs, the right triangle has inradius $\rho=[\sqrt{((s+l)^2+4sl)}-s-l]/2$ and sides $(s+\rho,l+\rho,s+l)$. This inverse exists for arbitrary positive s,l; its agreement with T is special to the declared 5:12:13 case. The circumradii of the two doubled triangles are 13 and 17, whose difference equals the input inradius 4.

Input convention	T normalized to first side 16	Largest internal angle
Exact 5:12:13	16:30:34	90.0000°
Published mean sides with computed diagonal	16:30.03436:34.04295	90.0512°
Ideal 7 and 21 chords	16:29.89148:33.86432	89.8378°

The mean-side calculation uses s=33.435 m, l=80.095 m and $h=\sqrt{(s^2+l^2)}$, not an independent diagonal measurement. Approximate transformed triangles are evaluated by the cosine law without imposing a second right angle. Orthogonal transfer of the first two derived lengths is a separate operator in these approximate cases.

Input	Orthogonal-transfer β / inter-ray angle	Actual triangle β / β−α
Exact 5:12:13	61.927513° / 33.855026°	61.927513° / 33.855026°
Published-side proxy	61.954737° / 33.909475°	61.914830° / 33.880900°
Ideal 7–21–7–21	61.841209° / 33.682417°	61.967347° / 33.772483°

Both operators retain rounded 62/34 in all three cases. Across the 14 declared discrete shapes, only k=7 gives that rounded pair under the examined reading. For orthogonal transfer, the condition is β in [61.75°,62.25°), or b/a in [1.8610905,1.9006874); it is one restriction, not two independent matches. Rotation and reflection preserve these internal relations.

The recovered Calanais technical edition reports lengths 45.734978, 85.404912 and 97.016567 m, normalized as 16:29.878195:33.940436, and an RMS of 0.174406% against 16:30:34. This integration preserves those author-reported values and their source extracts; the Calanais 3D points were not reprocessed here. Applying the exradius reading to the same lengths yields approximately 10:23.83514:25.84790, a dependent reexpression. The comparison supplies context, not an independent Stonehenge validation or a verified historical transmission claim.

Reproduction: PIVOT_BRIDGE, DIRECTION_AND_ARCTAN and REVERSE_LAYOUT in S3 Code preserve the exact rational checks, complete discrete comparisons and source extracts. Scheme Fig. 8 is generated from the same lengths.

Supplementary Note 37

Circular consequences and the completed Y hole test

Each of the four triangles formed by three corners of a rectangle has an incenter. For long side l, short side s and diagonal h, r=(s+l−h)/2 and the four local positions are (±(l/2−r),±(s/2−r)). The 10-by-24 frame gives (±8,±1), with circumdiameter 2√65. At the existing outer-only scale u=3.331412722 m, the predicted diameter is 53.717416 m. Repeating the same outer-scale rule for the discrete chord model gives 53.874819 m. Against the approximate published 54 m Y diameter, their residuals are −0.5233% and −0.2318%, respectively; the corresponding external calibration RMS values are 0.2605% and 0.5142%.

The prediction was extended to each irregular Station quadrilateral without rectangular regularization. For a triangle ABC and opposite side lengths a,b,c, the incenter is (aA+bB+cC)/(a+b+c). All 20 positions from five source conventions are archived. Against a radius-27-m circle centered at the mean of the four Stations, their radial RMS values are 0.4491 m (Cleal), 0.5181 m (indicative 91), 1.2136 m (registered click-plan), 0.7657 m (Rees) and 0.9640 m (Rees indicative). These were radial diagnostics before Y coordinates were read, not matches to individual holes.

The subsequent positional test used all 30 Y symbols on Cleal Plan 1. The supplied book and rendered plan match the earlier archived SHA-256 hashes; no new registration was fitted. Numbering and excavation status were checked against Fig. 151 and Table 19. Y1–Y16 and Y29–Y30 are excavated; the other 12 are indicated unexcavated positions. Coordinates are manually read symbol centres. The preliminary digitization and pre-score visual corrections, including Y9, are preserved. The local protocol predates scoring but postdates knowledge of the geometric hypothesis and approximate diameter.

Every prediction is assigned to a distinct Y symbol by minimum total squared distance. The scale, orientation, Station-derived centre and four predicted points remain fixed. The comparison rotates the complete quartet in 36,000 steps of 0.01°, recomputing distinct assignments at each step.

Convention	Positional RMS	Rotations as good or better
Cleal primary	2.8719 m	97.125%
Indicative 91	2.7116 m	96.467%
Registered click-plan	2.8170 m	96.917%

The primary assignment maps incentres omitting Stations 91,92,93,94 to Y22,Y24,Y8,Y9, with distances 2.4854,2.9981,2.5971,3.3287 m. The first two symbols are unexcavated positions. The original orientation is not favoured by the rotation comparison; the proposed point-to-hole correspondence is unsupported. The rotation fraction is conditional on the fixed quartet and ring, not a probability against prehistoric intention.

A post-test circle fit to all 30 Y symbols gives diameter 53.1631 m and radial RMS 0.6331 m, with local centre approximately (0.294,1.139) m. Against this digitization the continuous and discrete predictions differ by +1.0426% and +1.3387%; the slight preference against the rounded 54 m summary reverses. A two-native-pixel coordinate perturbation of Y alone can reduce primary

positional RMS no lower than about 2.542 m by a triangle-inequality bound. This is digitization sensitivity, not a complete archaeological uncertainty model.

A further exploratory comparison uses the pivot circumdiameter 34u=113.2680 m, or 113.1700 m from the discrete exradius inverse. Field and Pearson’s approximate internal ditch diameter near 102 m and eastern/western widths imply outer edges near 112–112.5 m, placing 113.2680 m about 0.68–1.13% above that derived range. Inner lip, centreline (about 107–107.25 m) and outer edge are retained as different conventions. The outer range is not a directly surveyed diameter or confidence interval and does not establish concentricity.

Reproduction: CIRCLE_CONSEQUENCES and Y_INCENTRES_TEST in S3 Code include all shape rows, coordinates, assignments and rotation scores. The original book is identified by hash and source pages rather than redistributed in full. Main references 1 and 25 provide the archaeological sources.

Supplementary Note 38

Coordinate types radii and the meaning of direction

In the fixed J2000 frame, j=34.077500° is the absolute Deneb–Albireo longitude difference and v=62.160110° is the mean Deneb–Fawaris latitude. Their types matter to the inverse. The latitude difference of Deneb and Fawaris is 4.507895°, the Aljanah–Fawaris latitude difference is 14.991809°, and the five-star latitude span is 15.446371°. Thus v is a coordinate mean, not the vertical length of a celestial arm. Holding the J2000 plane fixed is distinct from using the ecliptic of the ancient date; no rounding rule is changed here.

Promoting g=10 and q=24 to longitude-component vectors gives a rank-one Gram matrix with entries (100,240;240,576), whereas the corresponding perpendicular rectangle legs give (100,0;0,576), of rank two. A single linear map cannot send those collinear components to perpendicular legs. This does not claim that the actual three stellar positions are collinear; their latitude differences are nonzero. It rules out that specific literal component-vector overlay and leaves symbolic constructive mappings as additional hypotheses.

For the three available complete inner pairs, the opening normals are H,V,H in the E/N predominance rule, and the pillar-joining lines are V,H,V. The smallest independent per-coordinate endpoint halfwidth that can reach the H/V boundary is 0.04567 m for 51–52, 0.28065 m for 53–54 and 0.25679 m for 57–58. These are deterministic thresholds, not estimated errors. Two of the six ordered assignments of distinct pairs satisfy a postulated H-for-j/V-for-v allocation; the count map itself specifies none. Rotating the whole configuration 90° swaps these categories while leaving counts and the word unchanged.

The three-normal projector Gram and Station-family comparison already appear in Note 35. Their internal off-diagonal similarities 0.8850,0.9510,0.7097 and mean-projector eigenvalues 0.94668,0.05332 show one collective direction rather than two perpendicular groups. Fixed cardinal comparison changes under rigid rotation; the cross-component Gram does not. This distinction prevents the 4-to-32 numerical swap from being misread as a physical orientation test.

The modern IAU area 803.983 square degrees yields planar equivalent radius $\sqrt{(A/\pi)}=15.997367°$ and spherical-cap equivalent angular radius 16.049790°. Both round to 16 but depend on modern boundaries. The minimum cap covering historical-member stars is a different quantity. Its boundary stars are HIP 95947,94779,104732 in all four rows below; two of these are additional to the j,v descriptor stars, while Albireo is shared.

Input	Minimum covering radius	j cos(v)	Relative difference
Ptolemaic raw coordinates	15.888333°	16.096665°	+1.311225%
Ulugh Beg raw coordinates	16.115875°	16.073389°	−0.263626%
Uniform Hipparcos J2000	15.835952°	15.914308°	+0.494800%
Uniform Hipparcos at fixed ancient phase	15.775224°	15.996341°	+1.401673%

The cap is computed by enumerating one-, two- and three-active-star candidate centres and checking an optimality certificate. The arc j cos(v) is a parallel-circle arc using a mean latitude

from a different pair, not the true Deneb–Albireo separation. Its swapped expression v cos(j) is about 51°. The earlier 0.0355% comparison was against the ideal integer 16 with primary astrometry, not against a measured covering radius. The related projections j cos(v)=15.914274 and j sin(v)=30.133236 with primary J2000 descriptors suggest the pivot proportions only after assigning j a symbolic radial role. None fixes a terrestrial direction.

Reproduction: HV_DIRECTION, GRAM_DIRECTIONAL_EXTENSION, 34_62_PHYSICAL_MAPPING, CYGNUS_RADIUS and the lateral test in ENTRANCE_SELECTOR, S3 Code. Definitions of modern constellation boundaries and parallel-circle arcs are documented by the IAU and PROJ: https://iauarchive.eso.org/public/themes/constellations/ and https://proj.org/en/stable/operations/projections/eqc.html .

Supplementary Note 39

Path inversion and a possible solar realization

Define J=s+l and V=2h+s for a right rectangle with short leg s, long leg l and diagonal h. J is a semiperimeter; V is a path across two diagonals and one short side. Within the existing compiler the second equation additionally uses D=2B−A. Taking J=34,V=62 gives $7s^2-148s+780=0$, hence (s,l,h)=(10,24,26) or (78/7,160/7,178/7). The latter is proportional to 39:80:89 and is a real constructible alternative. Scaling it by seven changes the specified inputs and module, so it cannot silently replace the fixed-unit solution.

With r=h−s, inventory recovery is A=(3h+J)/2, B=(h+J)/2, C=s, D=(J−h)/2. The first branch yields (56,30,10,4), the second (386/7,208/7,78/7,30/7). Both branches receive the same outer-only least-squares scale rule and inner operations s,l/2,h−s,(s+l−h)/2.

Branch	Outer scale m/unit	External relative RMS	Inner relative RMS
10:24:26	3.331413	0.2605%	2.0196%
Rational branch	3.403392	7.9268%	9.5362%

Using continuous primary J2000 descriptors instead gives external RMS 1.6559% and 9.3651%, and inner RMS 2.8118% and 11.1686%. These are separate variants. The integer branch’s ideal 56-step gaps are 7.037291 and 20.962709; the rational branch gives 8.085539 and 19.914461. They round to 7|21|7|21 and 8|20|8|20, respectively.

Among all 14 discrete shapes the path ratio $(2+\sin(k\pi/56))/(\sin(k\pi/56)+\cos(k\pi/56))$ is closest to the continuous target for k=7 (−0.024876%), followed by k=8 (−0.040870%). k=7 also ranks first against 62/34. On irregular plans, J is half the perimeter and V is both diagonals plus the mean of the two short sides. Primary Cleal, indicative 91 and registered click-plan give V/J=1.823231,1.823386,1.822811, with continuous-target relative errors −0.04660%,−0.03811%,−0.06961%.

The ratio is locally flat: with t=s/(s+l), it is $2\sqrt{t^2+(1-t)^2}+t$, minimized at $(1+\sqrt{7})/2\approx1.822876$. Small ratio residuals are therefore not equivalent to equally small coordinate errors. Replacing a calculated diagonal by the published Aubrey diameter also changes the result: mean sides with calculated diagonal give −0.03183%, whereas the primary 86.44 m diameter gives −0.37321%. All diameter conventions are retained.

Endpoint displacement is an explicit first directional convention: the J path between short-side midpoints follows the long axis, while the V path’s displacement follows the short axis. On the Rees grid these give V for J and H for V, opposite the proposed geographic labels. The vectors between endpoints have magnitudes 24 and 10 in the ideal, not 34 and 62. Swapping numerical J,V in the same rectangle recipe yields no real solution because V>J is required; this is recipe asymmetry, not a terrestrial direction measurement.

A separate solar realization uses a vertical rod and horizontal shadow in the inventory ratio 30:56. Their elevation and zenith-distance angles are 28.178590° and 61.821410°, with difference 33.642820°; reversing rod and shadow reverses the two angles. This is a possible realization of a previously defined tangent, not an identified archaeological instrument.

At latitude 51.18° and phase 2965.2 BCE, model obliquity 24.016308° gives summer-solstice noon elevation 62.836308°, zenith distance 27.163692° and difference 35.672616°: nearest integers 63,27,36. Geometric solstice sunrise azimuth is about 49.5152°. The fixed noon-solstice test therefore does not give 62/28/34. An elevation of exactly 62° at culmination instead requires solar longitudes about 75.270° or 104.730°, or can occur about 35.25 apparent solar minutes before/after solstitial noon. These are target-selected occasions without an independent archaeological selector.

Reproduction: BUILDER_AND_SOLAR in S3 Code preserves both branches, all 14 shapes, source conventions, both endpoint mappings and the complete solar event calculations. General solar geometry is documented at https://gml.noaa.gov/grad/solcalc/solareqns.PDF ; its modern seasonal approximation is not used for the ancient epoch.

Supplementary Note 40

Directional decoders and the position of the entrance line

The ideal octagonal division gives 56/8=7 and 7|21|7|21=7(1|3|1|3). Eight cardinal/intercardinal rays select one octagonal orientation; putting side centres on those rays differs by 22.5° from putting vertices there. Combining both types would introduce sixteen rays. In the Rees primary convention the Station angular RMS is 17.504° with octagon vertices on grid compass rays, 5.162° with side centres there, 1.193° with a side-centre ray fixed by the Heel Stone and 1.147° with rotation fitted to the Stations. The corresponding indicative-91 values are 17.215°,5.492°,1.330°,1.304°.

Under the Heel-Stone rule, k=7 ranks first among all 14 discrete shapes; continuous 5:12:13 remains slightly closer at 1.104° primary RMS. A geometric solstice-rise direction with approximate grid convergence gives about 1.32° for k=7 versus 1.24° for 5:12:13. These comparisons use ideal horizon and solar centre, without terrain or refraction. All three fixed octagon orientations give nearest-ray gaps 1|3|1|3, even the poor 17.5° case; coarse classification alone is insufficient. They do not replace the 56-hole anchored index test.

Reading both path symmetries instead of both endpoint displacements swaps the local axes and yields nominal H-for-J/V-for-V. For any orthogonal pair, choosing retrospectively between a direction and its perpendicular can obtain the desired H/V order outside the 45° boundary. The geometric success of one convention cannot select that convention historically. A tangent-vector sensitivity also projected longitude and latitude directions at Deneb at the five stellar culminations, in fixed and date ecliptic frames; all ten cases give longitude E/W and latitude N/S predominance. These are local tangents, not the finite descriptors or a demonstrated sky-to-ground map.

A uniform physical reading uses equal terminal tensions. For path P0,…,Pn, the resultant on the two terminal supports is F=T[unit(P1−P0)+unit(Pn−1−Pn)]. With local x along the long side, the half-perimeter route between short-side midpoints gives FJ=(0,2T); the two-diagonal/short-side route gives FV=(24T/13,0). Their magnitudes have ratio 12/13. All supports together remain in force equilibrium. The formula describes a hypothetical low-friction device, not measured forces on stones.

Rees convention	J axial azimuth	V axial azimuth	Axial separation
Primary	52.151°	140.038°	87.887°
Indicative 91	51.075°	140.336°	89.261°

Both mirrored routes preserve each axis. In the primary drawing the two J routes measure 113.185 and 114.628 m, and the two V routes 208.699 and 206.531 m. A different half-perimeter route, between long-side midpoints, still has length 34 but gives the perpendicular force. Thus length alone does not select attachment points. The rational rectangle branch also retains 34/62 and these direction families, with force ratio 80/89 instead of 12/13. Unequal tension in the stated V path retains N/S predominance for terminal ratio greater than 0.661723 primary or 0.640948 indicative; this is parameter sensitivity, not measured friction.

The documented entrance pair 1–30 supplies a separate physical direction. Its normal is 51.700° from grid north. Fixing this orientation gives Station k=7 RMS 2.023° primary and 1.888°

indicative; the continuous comparator gives 1.972° and 1.853°. Using instead the ray to the entrance midpoint gives 3.378°/2.527° for k=7. All 14 discrete templates are retained, with k=7 first under each rule. The three inner normals have mean squared similarity 0.06665 with the entrance normal; their collective axis is 134.685°, 82.985° away. Its H label is only 0.315° from the boundary and flips after a stipulated 0.4° rotation of each pair, requiring at most 1.024 cm per proxy. Omitting individual pairs gives V,H,V. These are sensitivity constructions, not inferred measurement errors.

For the minimum-path decoder, all 12 open corner-visiting paths modulo reversal have lengths 44,46,58,62,74,76, two of each. Only 62 and 76 cross. The minimum crossed path uses both diagonals and the shortest side; without crossing the minimum is 44, and a closed crossed circuit gives 72. Selecting the perimeter midpoint family by orthogonality then gives total J+V=96 rather than 110. These choices define an operational protocol for any non-square rectangle, not a uniquely Cygnus-specific device. On five correlated plan conventions the selected axes have H/V predominance and 87.887–89.339° separation. V is the minimum here; previous path comparisons use the mean of the two short-side routes.

The entrance can alternatively select families by maximizing J alignment with its normal and V alignment with its perpendicular, without consulting lengths. Primary/indicative similarities are 0.999938/0.999881 for J and 0.999158/0.999433 for V. Mean route lengths are 113.906/207.615 m primary and 112.484/205.037 m indicative. A 90° entrance rotation selects ideal V=76 rather than 62. The selected families persist for reference rotations from −43.33° to +45.80° on the stated grid, demonstrating broad classification stability rather than precision.

The Station-only inverse uses the minimum crossed path, the perpendicular perimeter family and equal-weight axial consensus. It recovers 51.094° primary and 50.705° indicative, respectively 0.606° and 0.995° from the entrance normal. Among 19 available consecutive outer proxy pairs, entrance 30–1 ranks first; next errors are 9.170° for 1–2 and 14.105° for 14–15. J alone is closer, at 0.450°/0.625°; a short-axis PCA comparison gives 2.610°/1.687°. The census is not 19 original entrances and 1/19 is not a p-value. For unit diagonal vectors u,v, crossed-path resultants follow u+v and u−v, whose dot product is zero. Their orthogonality is a construction identity.

Finally, torque $\tau=r1\times f1+r2\times f2$ fixes the equivalent resultant line by $r\times F=\tau$. The J line misses the entrance midpoint by 1.305 m primary or 0.754 m indicative, intersecting the centre-to-centre segment at fractions 0.1241 and 0.2826. The primary line crosses the filled Stone 1 outline under all four raster thresholds; the indicative line clears both outlines, with a conservative drawn-pixel clearance about 0.1626 m. Crossing a centre segment is not crossing a free opening. V’s line passes through the diagonals’ intersection by force concurrence. The directional agreement therefore does not provide source-stable positional recovery.

Reproduction: OCTAGON_DIRECTION, ENTRANCE_AXIS, CORD_TENSION, MINIMUM_CIRCUIT, ENTRANCE_SELECTOR, INVERSE_DIRECTION and DIRECTION_AND_ARCTAN in S3 Code retain every route, reflection, threshold and alternative. Archaeological source: main reference 25, pp.44 and 53. Mechanics: https://openstax.org/books/university-physics-volume-1/pages/5-6-common-forces and https://openstax.org/books/university-physics-volume-1/pages/10-6-torque .

Supplementary Note 41

Pivot rays material axes and original settings

With grid east as x and south as y, pivot rays proportional to (30,16) and (16,30) have azimuths 118.072487° and 151.927513°. Assigning them to the normals of pairs 57–58 and 53–54 yields errors 1.620444° and 0.369838°, RMS 1.175291°. The observed east-to-south angles are 29.692931° and 62.297351°; their opening 32.604420° rounds to 33, not 34. The smaller-inclination ray is near 28°, while 34° is the ideal opening. These quantities cannot be interchanged by labelling the rays horizontal and vertical.

Three references, two reflections and six ordered pair assignments were retained, giving 36 comparisons per model. The favourable reference and assignment were recognized after inspection. With the entrance normal as reference, the best ideal RMS is 31.215890°. Published mean sides give grid-fixed RMS 1.189999°, and k=7 gives 1.131736°, first among the 14 discrete shapes with k=6 next at 2.056378°. A fitted common rotation of 0.995141° would reduce the ideal RMS to 0.625303°; it is diagnostic, not incorporated into the fixed-grid result. Approximate true/grid convergence of 0.135411° changes the ideal RMS to 1.291957°. Neither variant resolves the original-setting precision.

The three inner normals also differ from radial normals at the same midpoints. Using the Station-derived long-axis estimate, observed coherence and alignment are 0.946681 and 0.935549, versus 0.718546 and 0.680125 for radial directions. The 18 other consecutive outer pairs have 0.527370 and 0.525622. Of 816 outer triads, 51 match internal coherence and none match its nominal target alignment; restricting to 616 disjoint triads gives 18 and zero. The best outer alignment, 0.930277, is only 0.005271 lower; a +0.52° target shift removes the advantage. These correlated drawing subsets are not a sampling distribution. Unknown orientations of the two missing pairs allow full-five alignment between 0.561329 and 0.961329. An auxiliary fitted concurrence point is 4.251 m from the Station centroid with 2.374 m perpendicular RMS.

Cleal’s excavation records identify C56 for 53–54 (Figs.99,147,288; printed pp.195,252,562) and C52 for 57–58 (Figs.100,143,285; pp.196,248,559). The former was excavated and straightened in 1964, the latter fell in 1797 and was excavated and re-erected in 1958. The representations are broadly compatible with the categorical directions but do not supply two unambiguous original pillar-axis centres per pair at the precision needed here. Reproductions of the same excavation are not independent surveys.

With proxy separations 2.751 and 2.670 m, the angular discrepancies correspond to transverse offsets 7.78 and 1.72 cm. These are geometric conversions, not measured restoration displacements or errors. The H/V boundaries are much farther away, by 15.307° and 17.297°; vector changes of 0.726 and 0.794 m would reach them. Bounds of less than 0.363 and 0.397 m on each endpoint would preserve class if they covered all errors, but no such archaeological bounds have been measured.

The catalogue of Atkinson drawings identifies groups 301–350 for 1958 and 401–450 for 1964, with used subsets 301–331 and 401–426. These are published archival leads, not verified current custody identifiers. Original sheets, survey notebooks and restoration records are needed to relate cavities, packing, faces and pillar axes. The 1919 Ministry of Works drawings in Cleal Appendix 7 additionally document fallen pieces, with approximate scales and sometimes ambiguous observables; they do not restore original geographic orientation by themselves.

Reproduction: ANCHORED_PIVOT_DIRECTIONS, MATERIAL_AXES and ORIGINAL_SETTINGS_REVIEW in S3 Code, with complete assignments and page index. Main references 1,2,25 supply the material context. The institutional synthesis at https://www.english-heritage.org.uk/visit/places/stonehenge/history-and-stories/understanding-stonehenge/ supports the architectural importance of the solstitial axis, not the 34/62 attribution.

Supplementary Note 42

Placement rules and the complete point triangle comparison

Fixing a pair’s orientation leaves its midpoint and separation undetermined: three planar parameters per pair. The pivot construction supplies directions, not six missing positional parameters for two pairs. Testing a common Station-centroid origin gives perpendicular distances 2.286 m and 3.821 m from that origin to the normals of 57–58 and 53–54. Using the diagonal intersection gives 1.692 m and 3.939 m. The two normals themselves meet at a fitted point 4.194 m from the centroid; this intersection is guaranteed for nonparallel lines, and the third normal misses it by 5.142 m.

A restricted placement test uses the centroid and four previously computed incentres as possible anchors for the two ideal rays. All 25 ordered assignments are retained. Primary best transverse RMS is 3.091 m for one common anchor, 3.476 m if both anchors must be incentres, and 1.975 m over all assignments. The k=7 version gives 2.006 m; indicative-91 best values are 1.728 and 1.758 m. Even zero transverse error would leave along-line position and pillar separation free.

A separate bilateral rule reflects 53 to 58, 54 to 57, 51 to 60 and 52 to the original setting of 59. Reflection uses $p' = O + (2uu^{T} - I)(p - O)$, with O the Station centroid and u the Station-only axis, without fitting to the target pillars. Primary point errors are 1.406,0.917,1.725 m, RMS 1.390 m. Eight previously specified centre/axis/source combinations give RMS 1.390,2.183,3.904,4.455,0.800,1.683,5.110,5.553 m. These are full coordinate errors, unlike the previous transverse distances. The original setting of 59 remains unscored; all eight conditional coordinates are archived, and fallen fragments are not substituted. Reflection does not use 34/62 and could express generic bilateral planning.

The triangle census contains all 220 trios of 12 proxies: four Station-only, 56 internal and 160 mixed. Each is compared with (16,30,34), using one absolute least-squares length scale followed by relative RMS. The best shape is 52–54–60; the best with the prescribed H-long-side/V-short-side predominance is 52–56–58.

Quantity	52–54–60	52–56–58
Side lengths m	8.195 / 15.148 / 17.207	7.704 / 14.005 / 15.553
Scale m/unit	0.506326	0.463757
Shape RMS	0.688824%	2.374650%
Internal angles	28.441 / 61.683 / 89.876°	29.627 / 63.984 / 86.389°
Acute-angle difference	33.241°	34.357°
H long side and V short side	No	Yes

The first trio’s separately rounded acute angles are 28 and 62, but their continuous difference rounds to 33. No trio simultaneously rounds its individual angles to 28,62,90 and its continuous acute-angle difference to 34. Of the 220 trios, 42 satisfy H/V; counts within RMS thresholds 0.5%,1%,2%,5% are 0,1,2,7 overall and 0,0,0,1 with H/V. The full four-Station triangle results and both Station 91 conventions remain in the code. At the external scale, 34u=113.268 m exceeds the largest of the 12-proxy baselines, 87.945 m: these internal fits require separately estimated

scales.

Primitive form	Best trio	RMS	Best H/V trio	H/V RMS
3:4:5	51–57–60	2.490%	51–57–60	2.490%
5:12:13	92–51–56	0.562%	93–54–60	4.403%
8:15:17	52–54–60	0.689%	52–56–58	2.375%
7:24:25	91–56–60	1.602%	91–56–60	1.602%
20:21:29	51–54–57	3.043%	51–57–60	11.136%
12:35:37	51–56–57	1.775%	51–56–57	1.775%
9:40:41	94–51–54	1.638%	91–57–60	4.360%

The seven forms are all primitive triples with hypotenuse at most 50. The two connected primitive families have the two best unconstrained shape fits, but each selects its own best trio among 220. Under H/V, other forms outperform 8:15:17. These are descriptive complete comparisons within the declared family, not joint archaeological probabilities.

Reproduction: REVERSE_LAYOUT, LAYOUT_RULE_TESTS and TRIANGLE_VERIFICATION in S3 Code; geometry.py and all_geometry_comparisons.csv in S4 Code. All original candidate rows and the unscored setting-59 predictions are retained.

Supplementary Note 43

Joint geometry selectivity without multiplying dependent matches

The reference family contains 14 ideal rectangles k|28−k|k|28−k and 18,000 short-axis orientations from 0° to 179.99°, giving 252,000 equally weighted configurations. Each receives one scale from the same outer three dimensions. The reference is k=7 with the Station-only axis 51.094123°, with indicative-91 orientation as a separate sensitivity. This is a specified parameter family, not a frequency model of prehistoric projects.

Six criteria require performance at least as good as the reference: O external relative RMS 0.514169%; I inner RMS 2.087829%; C path-ratio error against 62/34 of 0.005349%; P transformed-triangle right-angle departure 0.162210°; D joint directional loss 0.032282; B H/V predominance of the short/long axes. D=1−[entrance alignment plus mean inner-pair alignment]/2, with equal weights for the two channels and for the three inner pairs. These thresholds were recognized retrospectively and are not uncertainty intervals.

Criteria accumulated	Survivors
None	252,000
O	18,000
O+I	18,000
O+I+C	18,000
O+I+C+P	18,000
Add D	541
Add B	541

O,I,C and P each individually select k=7, excluding exactly the same other shapes. D retains about 3.006% of the orientation grid after that selection; B adds nothing further. All 64 criterion subsets are archived. Removing one of O,I,C,P leaves 541; removing D leaves 8,999; removing B leaves 541. The orientation interval retained on the grid is 45.69°–51.09°. An analytic tensor calculation gives continuous orientation fraction 3.00343%, consistent with the discrete grid.

The primary joint fraction is 541/252,000=0.2147%. Indicative-91 orientation yields 463/252,000=0.1837%; fixing all controls to the reference orientation yields 1/14=7.1429%. Continuous J2000 ratio targets leave 541, while an entrance-only direction score yields 121. The latter is a different, narrower score and does not replace the primary result. The continuous 5:12:13 comparator is better than k=7 in the reported metric and closure scores; the rational branch matches the path ratio but has 7.9268% external and 9.5362% internal RMS and 4.6604° closure departure.

This audit uses operations s,l/2,h−s,(s+l−h)/2 and its own outer-only scale for each shape. Its 2.087829% discrete inner RMS must not be substituted for earlier discrete comparisons under other scale conventions, or for the primary continuous 2.019623%. The archived scripts retain those distinctions. The Y=54 m summary is unchanged in this comparison; the later point-based Y result is not counted as a success.

The fraction conditions on rectangle family, 56-fold circuit, measurement conventions, celestial targets, decoder, orientation score and thresholds. It excludes upstream searches and chronology. It is not a p-value for the historical hypothesis and cannot be converted to 99.7853% probability of intention.

Reproduction: JOINT_CLOSURE in S3 Code includes all 14 forms, 18,000 orientations and 64 subsets, plus a direct-loop verification.

Supplementary Note 44

Releasing the historical catalogue anchor

Each historical 17-member list gives 17×16×15×14=57,120 ordered distinct assignments to anchor,g,j,v. Membership comes from the historical catalogues; positions and motions are propagated Hipparcos values. The audit tests J2000 and the previously fixed ancient phase, rounding each absolute descriptor before taking q=j−g,d=v−j. It does not retest all 81 years of the earlier Stage 1 window.

Membership list	Modern passes	Ancient passes	Same assignment passes both
Ptolemy	10	18	2
Ulugh Beg	17	17	4

The common assignments are HIP (102098,100453,95947,97165), with tuples (10,34,62) modern and (11,35,63) ancient, and (99848,100453,95947,102488), with (5,29,57) in both. Ulugh Beg additionally retains (104060,102177,97165,95947) and (104060,102177,97165,102488), both with (1,25,53). All share contrasts (24,28). Canonical normalization $g=(q^2-r^2)/(2r)$, with r=16, returns (10,34,62) for every one and therefore cannot resolve the anchor ambiguity.

The absolute modern tuple (10,34,62) appears in four assignments per list; the same absolute ancient tuple appears in none. Absolute and contrast-only selection are different questions. The earlier fixed-Deneb result remains valid within its restricted domain, but not as a uniqueness claim after the anchor is released. Both lists already supply Cygnus and overlap substantially.

Reproduction: FREE_ANCHOR in S3 Code preserves all positive rows and scalar checks. The wider search without a supplied constellation is in Notes 45–48.

Supplementary Note 45

A catalogue census with all five stellar identities free

The complete Hipparcos input is filtered for finite position, proper motion and Johnson V data, and grouped uniformly by modern IAU constellation. Five ordered roles a,g,j,t,v must be distinct catalogue entries within one region. No Deneb, Aljanah or Cygnus identity is supplied. The fixed modern spatial rules are rounded $|\Delta\lambda(a,g)|=10$, $|\Delta\lambda(a,j)|=34$ and $[\beta(a)+\beta(v)]/2=62$. The temporal operator is $4(|\Delta RA(a,g)|,|\Delta RA(g,j)|,|\Delta RA(t,v)|)$ in sidereal minutes, compared with $W=(28,72,16)$.

The primary propagation origin is J1991.25, the epoch of the catalogue positions. Coordinate reference frame and position epoch are distinct. A legacy-origin J2000 branch is retained as sensitivity. The principal magnitude cut V≤5 and nested V≤4,V≤6 alternatives use the same nominal benchmark within each branch. Every candidate’s temporal minimum is sought over astronomical years −8000 to +2000 before applying the ancient-contrast and 3000–2920 BCE filters.

Limit	Eligible entries	Regions with at least five	Spatial quartets	Spatial quintets
V≤4	518	42	3	33
V≤5	1,625	77	73	2,990
V≤6	5,041	88	8,635	1,072,375
Limit	Spatial plus temporal	Add contrasts only	Add Stage 1 only	Both added
V≤4	2	1	1	1
V≤5	7	3	2	1
V≤6	903	477	57	6

The two middle diagnostic columns each add their condition separately. Contrasts use individually rounded descriptors in the date ecliptic at each candidate’s own optimum. At V≤4 and V≤5 all temporal survivors belong to Cygnus. At V≤6 they comprise Cygnus 868, Hercules 28, Cepheus 6 and Draco 1. All 57 passing Stage 1 are Cygnus, before the contrast filter. The six joint rows all preserve Deneb and Sadr; they allow a close catalogue alternative for Albireo and three transverse pairs.

HIP roles a/g/j/t/v	Largest V	Minimum BCE	RMS min
102098/100453/95947/98110/96825	5.06	2920.74	0.318835
102098/100453/95947/102488/97165	3.05	2965.43	0.390126
102098/100453/95947/100097/100859	5.76	2937.97	0.381129
102098/100453/95951/98110/96825	5.12	2920.76	0.318260
102098/100453/95951/102488/97165	5.12	2965.40	0.389679
102098/100453/95951/100097/100859	5.76	2937.96	0.380643

HIP 95947 and 95951 are 34.45 arcseconds apart in the catalogue; they remain separate entries, without post-result deduplication or an ancient visual-resolution model. The seven V≤5 temporal survivors, including later Cygnus alternatives, and every evaluated row are retained in the archive. The nominal is the sole joint V≤5 row, not the lowest raw temporal RMS among all survivors.

Uniform primary astrometry gives nominal minimum 2965.425139 BCE and RMS 0.390126064 min. The legacy branch gives 2965.048893 BCE and 0.389288485 min, with 900 temporal and eight joint V≤6 passes. V≤4 and V≤5 headline counts are unchanged. These values do not replace the main paper's primary mixed-input 2965.2185 BCE, RMS 0.418975 min.

The numerical search uses a two-year grid, refinement of local minima and eligible cells adjacent to both boundaries, and the exact endpoints. Groups are discarded only if their optimized lower bound $\sqrt{[(e1^2+e2^2)/3]}$ exceeds the nominal full RMS. The third squared error cannot improve that lower bound. Near-threshold bounds and complete fits are checked at one-year resolution. An initially missed boundary-cell minimum was corrected uniformly and the entire census rerun; the old discrepancy is preserved as diagnostic history, not counted as a final result. The precession engine was compared with ERFA at five epochs. Minima are numerical, not interval-certified.

Modern grouping does not represent a prehistoric constellation map or include asterisms crossing modern boundaries. The grammar, targets, thresholds and interval were known; freeing identities does not remove upstream selection. The census supports conditional identification within this domain, not a historical false-positive rate.

Sources: Hipparcos documentation https://heasarc.gsfc.nasa.gov/W3Browse/star-catalog/hipparcos.html ; Astropy grouping https://docs.astropy.org/en/stable/api/astropy.coordinates.get_constellation.html ; main references 29–31. Reproduction: BROAD_IDENTIFICATION in S4 Code, spatial.py then temporal.py, with full shared input in S2 Code.

v1.26: Keep this magnitude-selected comparison distinct from S5 five-brightest membership.

Supplementary Note 46

Brightness as a property of the retained solutions

This diagnostic was added after the census. The nominal role-ordered magnitude vector is (1.25,2.23,3.05,2.48,2.86). Among the six primary and eight legacy joint survivors, every alternative is no brighter in any role and fainter in at least one. The nominal therefore dominates their catalogue brightness vectors without choosing role weights. This is brightness dominance, not dominance in temporal fit; some alternatives have lower RMS.

The nominal’s faintest entry has V=3.05. The earliest competing joint quintet enters at V=5.06. Because magnitude cuts are nested and the benchmark is unchanged, the nominal is unique for every $3.05 \leq V_{limit} < 5.06$ in the executed census, in both epoch conventions. The upper endpoint is excluded. No candidate was removed by a subsequently fitted visibility score.

Catalogue magnitudes do not establish ancient detectability, component resolution, variability or extinction. The result motivates the possibility of greater visual salience; Note 48 adds a geometric night condition but still does not model all observing conditions. The brightness property and temporal/contrast census reuse the same stars and are not multiplied as independent probabilities.

Reproduction: brightness_diagnostic.py and full role vectors in S4 Code.

Supplementary Note 47

Core ablation and the temporal contribution of each channel

The ablation removes v=62 and both transverse-channel stars, leaving three free identities, modern spatial targets g=10,j=34 and temporal targets (28,72). All ordered triples within modern regions are searched over the same ten-thousand-year interval. RMS now divides by two and is compared with the nominal two-channel minimum, 0.296491836 min. The fixed J2000 spatial convention remains; this is not a reference-free test.

Magnitude	Spatial triples	Temporal passes	Also q=24	Also night feasible
V≤4	4	1	1	1
V≤5	273	5	3	2
V≤6	7,766	131	66	58

The columns are cumulative. At V≤4 the only temporal survivor is Deneb–Sadr–Albireo. Its faintest magnitude is 3.05, while the first competitor enters at 4.59; uniqueness therefore holds throughout 3.05≤Vlimit<4.59 before contrast or horizon filtering. The legacy branch has 7,757 spatial and 130 temporal V≤6 rows, but the same 66 contrast and 58 night-feasible rows and the same bright-cut conclusions.

V≤5 temporal trio HIP	Region	Optimum	RMS min	Ancient q
54751/51849/41037	Carina	2920.5 BCE	0.114505	23
54751/51849/43105	Carina	2377.3 BCE	0.199108	24
102098/100453/95947	Cygnus	2848.4 BCE	0.296492	24
104887/102571/96052	Cygnus	696.9 CE	0.224708	24
75458/80331/82020	Draco	4314.5 BCE	0.202008	26

No q=24 core optimum in the full V≤6 census lies in the Stage 1 interval. The nominal bright core remains identifiable within the stated brightness range, but does not independently reproduce the full-model phase. Removing a temporal channel while keeping the original five stars likewise changes the optimum.

Omitted target	Refit minimum BCE	Omitted-channel prediction	Prediction minus target
28	2962.3131	27.784396	−0.215604 min
72	2991.06796	72.703986	+0.703986 min
16	2848.35971	17.312531	+1.312531 min

These uniform-catalogue numbers remain separate from the earlier primary-input ablations in Note 26. The third channel shifts the nominal two-channel optimum by about 117 years toward the full uniform phase 2965.4251 BCE. The channels form one joint fit, not three independently

concordant clocks. The main search, finer-grid checks and all candidate minima are preserved.

Reproduction: CORE_ABLATION/ablation.py in S4 Code.

Supplementary Note 48

Geometric possibility of simultaneous astronomical night observation

At adopted latitude 51.18° N and a flat astronomical horizon, upper culmination is hmax=90°−|latitude−declination|. The horizon screen was proposed after Carina alternatives were seen and applied uniformly to every temporal survivor at its own optimum and at the nominal common phase. In the two V≤5 Carina triples, HIP 41037 and HIP 43105 have maximum altitudes −10.46° and −6.87° at their own optima, so each triple contains a star that never rises in this model. At the nominal common phase the maxima are −10.43° and −6.27°.

Positive individual culmination is insufficient for simultaneous observation. For each candidate the code examines a common local sidereal-time grid of 0.1°. It then requires a solar position on the epoch’s frozen ecliptic with centre below −18°, the conventional astronomical-twilight threshold. Let Z be the equatorial unit zenith vector and P the equatorial unit ecliptic pole. The unit Sun direction S=−[Z−(Z·P)P]/||Z−(Z·P)P|| gives the lowest possible solar altitude on that ecliptic at the selected sidereal time. Unit norm and plane membership are verified. Season and sidereal time are free: this is an annual geometric witness, not an ephemeris for a specified night or festival.

At uniform nominal phase 2965.4251 BCE, sidereal angle 249.7° supplies the following common configuration.

Object	Geometric altitude
Deneb	69.8905°
Sadr	70.7084°
Albireo	67.3316°
Aljanah	63.0913°
Fawaris	79.0870°
Solar centre	−18.01785°

The minimum stellar altitude exceeds 63°. A separate day-unrestricted maximum-minimum altitude near 64.698° is retained in the JSON and is not labelled a night solution. The night condition leaves 1,2,58 cumulative core survivors at V≤4,5,6 after q=24; multiple constellations remain at the faintest cut. Thus observability is not exclusive to Cygnus.

Terrain, refraction, atmospheric extinction, Moon, weather, instruments, ancient stellar variability and visual resolution are not modeled. The result establishes possibility within the geometric model, and rules out specified non-rising alternatives, without demonstrating actual historical observation.

Source for the −18° convention: US Naval Observatory, https://aa.usno.navy.mil/faq/RST_defs . Reproduction: CORE_ABLATION/horizon.py in S4 Code, including all epoch-specific competitor checks and both source-epoch branches.

Supplementary Note 49

Dependencies and tests that could add historical information

The extended analysis contains several evidential kinds. Conditional theorems establish what follows from a specified compiler or transformation. Geometric operations show what could be constructed. Drawing-proxy comparisons measure compatibility with the available representations. Catalogue censuses measure selection under a fixed grammar. Night geometry checks one physical possibility. None alone establishes that the procedure was used prehistorically.

The main dependency chain is retained: counts and outer dimensions feed the frame and register; these generate the pivot lengths, paths and word. Consequently the pivot angles, exradii, path ratio and inner predictions cannot be treated as independent repetitions. The joint-geometry census explicitly demonstrates redundant exclusions. The star censuses relax named identities while retaining prior targets, modern grouping and retrospective criteria. Brightness and horizon diagnostics add distinct measured properties or physical constraints to the same candidates, with their selection history stated.

The most direct future tests concern information not supplied to the prediction. Original settings and mounting axes can test the declared pair correspondences without changing faces, centres, reflection or north convention after inspection. The archived prediction for Stone 59’s original setting has not been scored against a substitute fallen fragment. The four Y-incentre positions have been scored and failed to receive positional support; they must not be reintroduced as successful predictions solely because a diameter is close. A new survey must distinguish measured uncertainty from stipulated coordinate perturbations.

The geometric model also leaves testable physical specifications: the same unit across specified lengths, the independently measured Sarsen envelope and centre, the line and clearance of the entrance, and positional deviations shared across features under a transformation fixed in advance. A model that predicts only a direction does not yet predict a pillar pair’s midpoint or separation. Correctly predicting those additional quantities would add information; repeatedly expressing the same angle would not.

Historical attribution additionally requires compatible construction phases, support for a reading or construction operation, and discrimination from ordinary rectilinear or bilateral planning. A subsequent frozen application can be confirmatory relative to unseen observations; masking already inspected points does not make the present development retrospectively blind. No acceptance probability, probability of intention, global p-value or Bayes factor is reported.

Supplementary Note 50

Complete integration and reproducibility ledger

Notes 1–35 preserve the primary analysis. Notes 36–49 integrate every subsequent audit package. The following ledger maps all 25 packages to the present text. The original reports, protocols, inputs, full numerical outputs and figures remain available in the associated code group; brief English synthesis here does not delete exploratory branches or unscored predictions.

Archived package	Supplementary notes	Main text destination
34 62 PHYSICAL MAPPING	38	Type and physical direction
ANCHORED PIVOT DIRECTIONS	41	Pivot ray comparison
BROAD IDENTIFICATION	42,45–46	Free stellar identities and brightness
BUILDER AND SOLAR	39	Path inversion and solar test
CIRCLE CONSEQUENCES	36–37	Constructive predictions
CORD TENSION	40	Mechanical realization
CORE ABLATION	47–48	Core identification and night geometry
CYGNUS RADIUS	38	Stellar types and extent
DIRECTION AND ARCTAN	36,40	Angular reading and line position
ENTRANCE AXIS	40	Architectural orientation
ENTRANCE SELECTOR	38,40	Entrance selection
FREE ANCHOR	44	Historical anchor release
GRAM DIRECTIONAL EXTENSION	35,38	Relative material directions
HV DIRECTION	38	Physical direction
INVERSE DIRECTION	40	Station only direction
JOINT CLOSURE	43	Joint geometry restrictions
LAYOUT RULE TESTS	42	Placement and reflection
MATERIAL AXES	41	Directional organization
MINIMUM CIRCUIT	40	Path decoder
OCTAGON DIRECTION	40	Discrete form and direction
ORIGINAL SETTINGS REVIEW	41	Original settings and restoration
PIVOT BRIDGE	36	Two primitive triangles
REVERSE LAYOUT	36,42	Geometric recipe and placement

Archived package	Supplementary notes	Main text destination
TRIANGLE VERIFICATION	42	Complete point triangle search
Y INCENTRES TEST	37	Constructive predictions

The distribution separates the original executable supplement (S2), geometric and material extensions (S3), and expanded stellar diagnostics (S4) so each submission file remains below the journal’s supporting-file size limit. Extract the three archives side by side; the S4 runner restores the full shared catalogue from S2 and checks its hash. The top-level README gives the exact execution commands. Group runners execute in temporary copies and compare numerical snapshots, preserving delivered results. Machine-readable integration_coverage.json identifies each original archive and its SHA-256 hash. Historical reports retain their original version statements as provenance; the present manuscript and Notes 36–50 are the integrated scientific account.

Supplementary Note 51 Expanded methods and analysis definitions

This note retains the extended methodological account accompanying the concise main text. Notes 1–50 and the executable archives contain the original analyses; Notes 51–53 make the detailed definitions, comparisons and dependencies accessible together. No analytical rule, input or computed output is changed by this editorial redistribution. Numerical precision is retained for reproducibility, not as a claim of archaeological accuracy.

Navigation: Note 51 gives methods and comparison universes; Note 52 gives the extended numerical results and source sensitivities; Note 53 gives provenance, dependencies and execution scope. Main-text Tables 1–2 and Figs. 1–9 retain their numbering. Former extended Tables 3–4 are now Supplementary Tables S53.1–S53.2.

Material objects and measurement conventions

Primary material objects are the Aubrey Hole circuit, the four Station positions or sockets, the outer Sarsen envelope, the transverse Trilithon-horseshoe span and the Y- and Z-hole circuits. Hole dimensions are diameters through hole centres. The Sarsen claim concerns the occupied architectural envelope; the published inner-face diameter is retained as an adverse convention [21]. The enclosure ditch is an outer-earthwork compatibility calculation and is excluded from both the scale calibration and the nested-plan ladder. The Heel Stone is axial and excluded from the concentric ladder. Photographic vertices, shadows and modern markers are excluded from the primary metric calibration. Later retrospective point-triangle searches enumerate every eligible trio in a declared 12-proxy set; they use drawing centroids and separate fitted scales, and do not replace the primary survey dimensions.

The four Station-side inputs are the centre-to-centre distances in the published Atkinson survey dataset: 91-92=34.17 m, 93-94=32.70 m, 92-93=79.93 m and 91-94=80.26 m [22, pp. 50-52; 23, Appendix p. 107]. Positions 91 and 93 are surviving stones; 92 and 94 are archaeologically located absent-stone settings, so the calculation uses the numbered Station positions rather than visible stone edges. The primary Aubrey diameter is the 86.44 m Thom survey value tabulated by MacKie [23, Appendix p. 107]. The same table gives 86.87 m for Hawkins, Lawson publishes a rounded 87 m summary [24, p. 22], and MacKie’s p. 99 prose radius implies 85.832 m, internally conflicting with the appendix. All four branches are therefore disclosed as a source-convention sensitivity. The ditch calculation uses the instrumental survey report’s close-to-102 m internal-lip diameter and its reported east-west ditch widths; it derives, rather than measures directly, the corresponding centreline diameter [25]. The remaining inputs are Y-hole diameter 54.0 m, Z-hole diameter 39.0 m, Sarsen occupied outer envelope approximately 33.0 m and Trilithon transverse span approximately 13.7 m [1]. Their boundaries and precision classes are itemised in Supplementary Note 2.

Metric and cyclic estimation

The outer geometry fixes the scale used to predict the inner dimensions. For observed dimensions x_i and fixed roles k_i, the common scale through the origin is $\hat{u}=\Sigma(k_i x_i)/\Sigma(k_i^2)$. The primary estimate uses only k=(10,24,26) for the Station short side, Station long side and Aubrey diameter. Predictions for k=(4,10,12,16) are computed without refitting. Signed metric and relative residuals and relative RMS are reported. Leave-one-feature-out fits test scale stability.

For a circle of diameter Φ divided into N=56 ideal positions, chord k is $c_k=\Phi \sin(\pi k/N)$. Model steps 7 and 21 define the ideal construction; they are not assumed to be measured

Station-to-Aubrey index gaps. Primitive Pythagorean candidates with $c \leq 100$ and all 13 unequal-leg complementary cyclic step pairs were enumerated for the joint geometry diagnostic.

Retrospective plan diagnostics

We analyse the archived digitization of the 56 numbered Aubrey symbols and four Station proxies in Cleal et al.'s Plan 1 [1]. Local metric coordinates use its printed 20 m scale bar. These proxies are distinct from the published Station-side measurements used in the primary metric fit. The projected surviving stone 91 does not establish its original socket centre. A Rees-based click-plan [26] supplies explicitly indicative alternatives; a two-point similarity registration using surviving stones 91 and 93 has no redundant control and does not constitute an independent survey. Field and Pearson's modern survey stations are not prehistoric Station Stones [25].

We distinguish (i) rounding continuous Station-to-Station angular gaps, (ii) assigning Stations to an ideal grid whose phase is estimated only from the 56 numbered Aubrey symbols, and (iii) fitting one common spatial rotation of a fixed shape about the Aubrey centre. The latter adds one parameter and is reported for both 7|21|7|21 and the continuous 5:12:13 rectangle; it does not replace the original zero-phase test. Separately, a free algebraic circle is fitted to all four Stations without imposing the Aubrey centre, radius, aspect ratio or cyclic partition. All four omissions and all source branches are retained. Synthetic coordinate perturbations use declared uniform half-widths and are sensitivity scenarios, not archaeological confidence intervals. These post-inspection diagnostics are not executions of a source-locked confirmatory protocol (Supplementary Notes 20–23).

For the rectangular approximation, short and long sides a and b define a short angular interval of $2 \arctan(a/b)$, or $k=(56/\pi) \arctan(a/b)$ in 56-fold steps; the complementary interval is $28-k$. An additional retrospective census compares every discrete rectangular template $k|(28-k)|k|(28-k)$ for integer $k=1,\ldots,14$, including the square. The Station order and short-side assignment are fixed, the Aubrey centre is held fixed, and one common rotation is fitted for each template. The continuous 5:12:13 shape receives the same one-rotation fit. A freely proportioned rectangle, with both rotation and short arc fitted, is also reported as a two-parameter comparator (Supplementary Note 23).

A supplementary retrospective diagnostic compares construction templates and periodic residuals on the Aubrey printed-symbol proxies. It uses blocked cross-validation, with equal fitting freedom among physical templates (Supplementary Note 30).

A further retrospective analysis gives the existing dimensional ladder a constructive interpretation. For a right rectangular frame with short side x, long side y and diagonal z, we associate the Sarsen outer diameter, Z-hole diameter, Y-hole diameter and Trilithon outer span with x, $y/2$, $z-x$ and $(x+y-z)/2$, respectively. These operations and architectural associations were recognised after inspecting the existing ladder. We apply them without an inner-scale fit to all 14 discrete rectangles and the continuous 5:12:13 comparator. Source sensitivity, model separation at a common diameter, and all six inversions from pairs of inner dimensions are reported in Supplementary Notes 31–32.

Post-result solar audit. The ideal 7|21 cyclic approximation to the selected frame has diameter role 26 and a complementary 21-step long chord, $C21=26 \sin(21\pi/56)=24.020867845$. We compare this continuous material quantity with the obliquity at the previously fixed stellar phase and invert it across astronomical years -8000 to $+2000$ under the primary Vondrák-Capitaine-Wallace model and a Laskar-polynomial sensitivity model [27]. A

temporal-domain census enumerates the same 16 primitive triples, 13 unequal-leg cyclic steps and both arms (416 candidates), recording every candidate whose chord intersects the obliquity range in the declared window. The rank at the fixed stellar phase is reported separately in the Supporting Information. These post-result diagnostics are descriptive. The conversion is a numerical identification of the dimensionless chord value with an angle expressed in degrees; it is an additional model convention, not a dimensional identity. A separate shape-sensitivity audit substitutes the exact 5:12:13 ratio, the published mean-side ratio and the freely fitted plan rectangles while retaining diameter role 26 and the same obliquity model (Supplementary Note 25).

Native Pythagorean factorisation

The selected Station frame has primitive form 5:12:13. Its doubled form is carried directly by three already defined material channels: g=C=10, q=B+D−C=24 and p=26, the Aubrey diameter in the selected unit. Hence $g^2+q^2=p^2$, or $10^2+24^2=26^2$. This factorisation uses no additional fitted coefficient or auxiliary quadratic form: it expresses the selected geometric frame in the same channels that the material compiler already uses.

Measurement stress test and channel separation

To test whether rounded Station dimensions manufacture the 5:12:13 ranking, each of the four published side lengths was independently multiplied by a uniform factor in $[1-\varepsilon,1+\varepsilon]$ for $\varepsilon=0.01$, 0.02 and 0.05. For each level, 200,000 deterministic-seed trials reranked all 16 primitive Pythagorean triples with hypotenuse not exceeding 100 under the unchanged common-scale fit. Metric-only rank and equal-block metric-plus-cyclic rank were recorded separately. This bounded perturbation ensemble is a stress test, not an empirical survey-error distribution and not a p-value.

The separation of metric and discrete inputs locates what each sensitivity test can change. Perturbing side lengths can change which primitive rectangle best represents the Station geometry and the scale of the nested-plan ladder. It cannot change the observed counts (56,30,10,4), their exact seed map, the directed inverse or the count-derived word W=(28,72,16), none of which contains a measurement in metres.

Register compiler and inversion

The four material counts are typed before compilation: A Aubrey positions, B outer sarsen uprights, C trilithon uprights and D Station positions. The seed map is r=A-B-C, g=C, j=B+D and v=A+C-D. Its determinant is 2 and its stated inverse is exact on the corresponding parity lattice. With q=j-g and d=v-j, the common expansion is Q=(r,q,d,j,d+q,v,3q,v+j). The Stonehenge-native word library is defined from material primitives alone: for N=A=56, s=D=4 and each ordered pair (a,b) from the selected frame (5,12,13), it contains $\{N/2, s^2, N-s^2, N+s^2, s(a+b), s|a-b|\}$. After duplicate removal this is {4,16,28,32,40,68,72,100}, which defines the 512 ordered triples evaluated by the temporal census. The library contains no stellar coordinate, archaeological date or fitted temporal output. The map census enumerates all ordered four-row matrices whose non-zero rows use coefficients in {-1,0,1}; exact and role-compatible solutions are counted without symmetry reduction.

Conditional reconstruction and material uniqueness

Two retrospective algebraic analyses make the compiler's dependencies explicit. For the relational reconstruction, $q=j-g$ and $d=v-j$ give $A=q+d+D$ and $B-C=q-D$. Conditioning on the observed D and the declared material closure $r=D^2$ supplies $B+C=A-r$. The calculation uses the contrasts and material conditions rather than the absolute stellar seeds; the original absolute-register inverse is retained unchanged (Supplementary Note 28).

For conditional uniqueness, we solve the existing closures $r=D^2$ and $d=A/2$ jointly with $p^2=g^2+q^2$, using $p=A-B$, $g=C$ and $q=B+D-C$. The domain is all strictly positive integer A, B, C and D, with no upper count bound. A factorisation proof is checked by a separate bounded enumeration, removal of each condition, relaxation of integrality and replacement of the radial row by the other exact row in the reported coefficient census. No new historical prediction or preregistration is asserted (Supplementary Note 29).

Continuous outer inventory angle

The outer circular inventories define an exact scale-free tangent relation. With Aubrey count $A=56$ and outer-sarsen count $B=30$, $\theta_{AB}=\arctan(B/A)=\arctan(15/28)$. Its complementary angle is $\arctan(28/15)$, so $\theta_{AB}+(90-\theta_{AB})=90$ degrees. The non-rounded stellar difference descriptor is $d^*=28.082606$ degrees, computed as the archived mean-latitude descriptor minus the archived longitude-span descriptor. The numerical comparison is explicitly degree-based because d^* is an astronomical angle reported in degrees. For transparency, the same unrounded function $\arctan(\min(x,y)/\max(x,y))$ is evaluated for all six unordered pairs among A, B, C and D. No complement, rounding, derived count or alternative function is included in this comparison.

The tangent relation is a structural reading of the documented inventories. It shares material inputs with the reversible compiler and is therefore interpreted as part of one integrated system, rather than as an independent probability calculation. The existing directed inverse remains a separate algebraic allocation ablation; no register relation beyond the stated angle relation is attributed to the outer ratio.

Outer-frame closure. The previously defined counts $A=56$ and $B=30$ are read with the radial index $c=13$ implied by the selected 5:12:13 frame and diameter role $2c=26$. The two material identities are $A-B=2c$ and $B-2c=D=4$. They imply $B/2+c=A/2=28$ and $(B/2)^2-c^2=AD/4=A$ because $D=4$. These are compact consequences of the two identities, not separately fitted or scored relations. Across the disclosed Aubrey-diameter branches, the selected radial role rounds to 13. This is a dependent closure of the same outer frame and inventories, not a new fit or independent confirmation.

Fixed-reference stellar module and directional ablation

The material compiler supplies the radial seed r=16. The spatial stellar module uses three angular descriptors in a fixed mean J2000 ecliptic reference frame: g is the Deneb-Sadr longitude step, j is the Deneb-Albireo longitude span, and v is the mean latitude of Deneb and Fawaris. The reference plane and longitude origin are held fixed when propagating stellar positions. This spatial definition is distinct from the equatorial frame of date used for temporal execution. The core j|v typing is documented in Ref. [20], and the temporal operator and W in the public archive; the g=10 bridge is recognised here. One nearest-integer rule is applied separately to g, j and v before forming q=j−g and d=v−j. The temporal target W=(28,72,16) remains count-derived and fixed. Historical catalogue measurements are separate portability checks, not the primary astrometric input.

A retrospective reference-frame audit propagates both primary and six-dimensional inputs to J2000 and the primary ancient phase, then compares the fixed J2000 ecliptic frame with the mean ecliptic of date. Two rotation constructions and the official SOFA implementation check the transformation. These checks distinguish frame choice from stellar motion; they do not test prehistoric use of the modern reference plane (Supplementary Note 24).

Directional allocation is tested by exchanging j and v in the seed tuple and applying the unchanged inverse. A non-target count is a failure; formulas are not changed to accommodate the transposition. Modern Albireo declination is retained only in the Supplementary Information as a J2000 diagnostic and has zero chronological or evidential weight because equatorial coordinates precess.

Exploratory within-carrier specificity audit. With Deneb fixed as anchor, the other 16 entries in each published 17-entry Cygnus membership list are exhaustively assigned injectively to the roles g, j and v. J2000 ecliptic coordinates are computed from the bundled Hipparcos positions under one stated obliquity; the target tuple is the already declared rounded tuple (10,34,62). This audit addresses internal role freedom conditional on the declared carrier, anchor, coordinate convention and targets. It is not a test of prehistoric intention, a chronology analysis or an independent vote for the Stonehenge transfer (Supplementary Note 18).

Exploratory residual-partner audit. Each residual spatial candidate is substituted into the existing third temporal arc. Deneb, Sadr, Albireo and Aljanah retain their primary inputs, while every alternative partner uses its archived two-dimensional Hipparcos input. The word (28,72,16), role order and full search window remain fixed. The updated script refines all grid-bracketed minima across astronomical years -8000 to +2000; the earlier implementation searched only a local interval. These mixed-input comparison scores select the residual partner and do not replace the primary phase or RMS. A separate homogeneous Hipparcos comparison is reported in Supplementary Note 33. The comparisons are dependent role-resolution diagnostics, not additional chronologies.

Joint conditional census. Deneb and Aljanah are fixed as distinct anchors. Each 17-entry membership list leaves 15 candidates for the three remaining roles, giving 15×14×13=2,730 five-distinct-star graphs. Every graph receives its own full-window temporal minimization under W=(28,72,16). At its own optimum, continuous ecliptic-of-date contrasts are used in the Station-anchored integer reconstruction. We count inventory recovery, a temporal RMS no greater than the named graph under identical Hipparcos inputs, their conjunction, and subsequent Stage 1 concordance. Nearest-seed and floor-seed alternatives and their union receive the same comparison. These retrospective conditional frequencies do not combine the

metric and formula controls into a site-level probability (Supplementary Note 34).

Further retrospective membership diagnostics retain the same Deneb anchor and 3,360 assignments per list, comparing the differences (q,d)=(24,28) at J2000 and the already determined ancient phase in the ecliptic of each date. Seed-first rounding, direct-difference rounding and continuous RMS are reported separately. The ancient phase is not re-estimated in these screens, and the two membership lists share astrometric data (Supplementary Note 27).

Astronomical propagation and scoring

The fixed graph uses Deneb, Sadr and Albireo on its longitudinal branch and Aljanah, Sadr and Fawaris on its transverse branch. The primary analysis follows the archived proper-motion input and the long-term precession expressions of Vondrák, Capitaine and Wallace, including their corrigendum. A six-dimensional Cartesian space-motion calculation is a declared sensitivity variant. The temporal vector is four times the wrapped role-ordered right-ascension intervals. The unweighted RMS against (28,72,16) is evaluated across astronomical years -8000 through +2000; bounded minimisation refines every local minimum. W is never recomputed from epoch-dependent ecliptic descriptors during this optimisation. Channel omissions, hypothetical weights and local score widths are reported as deterministic sensitivities, not confidence intervals (Supplementary Note 26).

Information order and claim calibration

The calculation order is material extraction, spatial holdout, seed-map census, exact inversion, word census, full-window astronomical evaluation and archaeological comparison last. Frozen before this study were the five-star graph, role order, nearest-integer rule, core typed primitives, W and the temporal operator. Recognised in this study were the g=10 bridge, Stonehenge seed map, metric ladder, material library and their cross-domain connection. Reference [20] and the dated public archive establish provenance but are not treated as independent validation. No archaeological interval is an optimisation prior. Post-result ranks are descriptive, and no result is interpreted as a probability of prehistoric intention. The two-epoch reference-frame audit, relational membership screens, conditional algebraic recovery, joint material uniqueness and construction-procedure diagnostics were added retrospectively; no new preregistration is asserted. Continuous inventory estimation, quantization comparisons and the joint role census are retrospective extensions; they do not change the provenance of the original nearest-integer rule or establish a historical quantizer.

Constructive and physical extensions

The subsequent analyses retain the original nearest-integer rule and primary chronology. For short side s, long side l and diagonal h, the pivot transformation is $T(s,l,h)=(h-s,(s+l+h)/2,s+l)$. Its conditional uniqueness is proved algebraically and checked over primitive triples with hypotenuse at most 1000. Circle consequences, angular readings and inverse constructions are evaluated separately; approximate inputs retain their actual three-sided geometry rather than being forced into a second right triangle (Supplementary Notes 36–37).

Directional analyses use the archived Rees/click-plan hatch-centroid proxies [26]. An opening axis is the normal to a pair of support proxies, and axial similarity is the squared dot product of unit directions. The three complete inner pairs are 51–52, 53–54 and 57–58; fallen fragments do not replace the original settings of 55 or 59. Grid east–north predominance, relative orientation, line position and clearance between drawn stone outlines are different observables. Hypothetical

perimeter and crossed paths are evaluated by endpoint displacement, symmetry, equal-tension terminal resultant and equivalent line of action, with the alternatives retained. These are explicitly retrospective decoder specifications (Supplementary Notes 38–42).

A complete point-triangle census uses 12 proxies, comprising Stations 91–94 and uprights 51, 52, 53, 54, 56, 57, 58 and 60. Every one of the 220 trios is compared with each of the seven primitive Pythagorean forms of hypotenuse at most 50, using the same least-squares length scale and relative RMS. A separate conditional geometry census evaluates all 14 discrete rectangles across 18,000 axial orientations against joint shape and direction criteria. All subsets of its six criteria are enumerated to expose redundant restrictions (Supplementary Notes 42–43).

Expanded stellar identification and observability

The historical-membership diagnostic first releases the previously fixed anchor, yielding 57,120 ordered four-star assignments per 17-member list. The broader diagnostic then releases all five identities across eligible Hipparcos entries in every modern IAU constellation region, rather than supplying Cygnus as input. It retains five distinct catalogue entries, the modern rounded spatial tuple (10,34,62), the temporal word and operator, and one common numerical search over astronomical years −8000 to +2000. The principal magnitude limit is V≤5, with nested V≤4 and V≤6 sensitivities. Every candidate is compared with the nominal graph evaluated using the same uniform astrometry. Hipparcos positions are propagated from their catalogue epoch J1991.25; the legacy epoch-2000 convention is retained separately. Modern IAU membership is a reproducible grouping rule, not an assertion about prehistoric asterisms (Supplementary Notes 44–45).

After obtaining each candidate’s full-window numerical minimum, we report the ancient rounded contrasts (24,28) and membership of the published 3000–2920 BCE Stage 1 interval as separate and joint filters. The interval does not constrain minimization. A lower bound from the first two squared temporal residuals prunes only candidates that cannot reach the full three-channel benchmark. Boundary cells and near-threshold cases are checked on a finer time grid. The later brightness comparison retains all surviving candidates and evaluates their role-by-role magnitude vectors without adding a fitted visibility score (Supplementary Notes 45–46).

A core ablation removes the latitude descriptor and the two stars of the third temporal channel, leaving three free identities, modern spatial targets (10,34) and temporal targets (28,72). Its RMS uses two channels and its own nominal benchmark. A subsequent physical feasibility diagnostic applies the same flat-horizon rule to all temporal survivors at their own optimum. For simultaneous astronomical night, local sidereal time and solar longitude are allowed to vary over an idealized year with the epoch’s ecliptic held fixed; the solar centre must be at or below −18°. This is an existence calculation, not a reconstruction of a ritual date or actual visibility conditions (Supplementary Notes 47–48).

Supplementary Note 52 Extended numerical results and source sensitivities

The following sections preserve the full numerical account, including alternative sources, coefficient classes, stellar assignments and diagnostic outcomes. They expand the main Results without changing the headline specification. Shared geometric or algebraic inputs remain shared; descriptive frequencies are not independent probabilities. References to numbered figures and Tables 1–2 refer to the main manuscript.

The outer circle and Station frame select one primitive geometry

Using the four reported Station side lengths, the 5:12:13 rectangle ranks first among the 16 primitive Pythagorean triples with hypotenuse not exceeding 100. Its common-scale side RMS is 1.568%, compared with 6.643% for the second-ranked 36:77:85 candidate. This ranking identifies the primitive frame used in the reconstruction within the declared Pythagorean class; unrestricted rational rectangles are outside that comparison.

An idealized 56-fold construction closely approximates the same primitive figure. Model gaps of 7, 21, 7 and 21 steps give hypotenuse-normalized chords 13 sin(π/8)=4.974885 and 13 cos(π/8)=12.010434. Against 5 and 12, the cyclic RMS is 0.360%. Across 208 combinations of primitive triples and admissible cyclic steps, 5:12:13 with 7:21 ranks first; the joint metric–cyclic score is 4.27 times better than the runner-up and has substantially lower integer complexity. The joint ranking connects the measured side ratio to the ideal 56-fold construction. Coincidence with numbered Aubrey positions is tested separately.

A 200,000-trial bounded stress test independently perturbed each of the four published Station sides. The 5:12:13 candidate remained first among all 16 primitive Pythagorean triples in 100% of trials at ±1% and ±2%. Even at ±5%, it remained first in 96.7235% of metric-only trials and 97.6255% of equal-block metric-plus-cyclic trials. The separation of inputs is consequential: the count compiler (56,30,10,4)→(16,10,34,62), its directional typing and W=(28,72,16) contain no measured length and therefore remain unchanged. Fig. 1 gives the complete dependency chain; the spatial partition is shown in Fig. 2.

The ideal cyclic construction approximates the Station sides without the fitted scale

Using the 86.44 m Thom diameter explicitly tabulated in MacKie’s survey appendix, the 7-step chord is 33.079 m, -1.064% from the observed mean short side. The 21-step chord is 79.860 m, -0.293% from the mean long side. Across the disclosed 85.832-87.0 m source branches, the short-chord residual ranges from -1.761% to -0.423%, the long-chord residual from -0.995% to +0.353%, and the held-out ladder remains between 2.020% and 2.067% RMS. The circuit diameter and count thus provide a second expression of the same approximate geometry without using the fitted linear unit.

Expressing the selected 5:12:13 rectangle in 56-fold angular steps gives 7.037291|20.962709|7.037291|20.962709. The published mean sides, 33.435 and 80.095 m, give 7.049061|20.950939|7.049061|20.950939 under the rectangular approximation. Both round to 7|21|7|21 without using Station-to-Aubrey positional indices. The digitized Cleal gaps are 7.178, 21.064, 7.127 and 20.631 steps, which also round to that word. These related descriptions identify 7|21|7|21 as the discrete approximation supplied by the side ratio and continuous gaps; they share the underlying geometry (Supplementary Notes 20 and 23).

Across all 14 discrete rectangular templates, 7|21|7|21 ranks first in each archived source convention after fitting a common rotation. Its angular RMS values are 0.855° for Cleal, 0.496° for the indicative-91 branch and 1.624° for the registered click-plan; the next discrete template, 8|20|8|20, gives 2.813°, 3.050° and 3.031°, respectively. The continuous 5:12:13 comparator remains slightly better at 0.792°, 0.461° and 1.585°. The freely proportioned two-parameter rectangle gives 0.700°, 0.455° and 1.514°. Within the tested discrete class, 7|21 gives the closest shape approximation across all three conventions (Supplementary Notes 22–23).

At a common centre, orientation and 86.44 m circumdiameter, corresponding vertices of the ideal 7|21|7|21 and 5:12:13 rectangles are separated by 0.0904 m. This quantifies the physical size of the discrete approximation (Supplementary Note 32).

The outer frame predicts the nested plan

The simplest cross-component comparison is between the mean short Station side, 33.435 m, and the approximate 33.0 m occupied Sarsen outer diameter. Their difference is about 1.3% of the Station mean. In the model both represent 10u: the width of the outer rectangle becomes the diameter of the inner circle (Fig. 3). Calibration on the Station short side, Station long side and Aubrey diameter fixes u=3.331413 m per doubled half-unit, with no inner dimension contributing. Applied without refitting, this scale predicts the Sarsen outer diameter at 33.314 m and all four inner dimensions with 2.019623% relative RMS. Table 2 reports every held-out dimension and signed relative residual.

The shared length makes the dimensional operation explicit: one outer calibration sets the Sarsen envelope and, through the declared multiples 4, 12 and 16, the Trilithon span and Z- and Y-hole diameters. Those multiples also admit the constructive interpretation shown in Fig. 3B and evaluated under Constructive connections and comparative diagnostics. The 1.3% direct comparison uses published summaries, including an approximate outer-envelope boundary. Fitting all seven channels descriptively gives 1.539% relative RMS. Leave-one-feature-out scales range from 3.323120 to 3.336932 m. Fig. 4 reports the four held-out predictions.

One reversible seed map links the material inventory to the complete register

Within the declared model, let N=56 denote Aubrey positions, s=4 Station positions and $(\ell_s,\ell_l,h)=(5,12,13)$ the reduced Station frame. The material system satisfies two closure identities:

$N = 2s(\ell_l-\ell_s) = 56$ and $N+s^2 = s(h+\ell_s) = 72$.

Consequently, two algebraically equivalent readings return the same ordered word:

$s(\ell_l-\ell_s,\ h+\ell_s,\ s) = (N/2,\ N+s^2,\ s^2) = (28,72,16)$.

These equivalent expressions couple the Aubrey count, the four-position figure and the primitive rectangle in one dependent closure. They also permit an inverse reading: with N=56 and s=4, the two identities give $\ell_l-\ell_s=7$ and $h+\ell_s=18$. Imposing a positive Pythagorean frame gives $\ell_s^2+50\ell_s-275=0$, whose unique positive frame is 5:12:13. Measured side lengths do not enter this algebraic execution (Supplementary Note 29).

The reversible form begins with four observed material counts: A=56 Aubrey Holes, B=30 outer sarsen uprights, C=10 uprights in the five trilithons and D=4 Station positions. One shared low-complexity map produces four typed seeds:

r=A-B-C=16; g=C=10; j=B+D=34; v=A+C-D=62.

The same expansion is then applied to the four seeds. With q=j-g=24 and d=v-j=28:

Q=(r,q,d,j,d+q,v,3q,v+j)=(16,24,28,34,52,62,72,96).

The four-seed map is reversible on the parity lattice: A=(r+j+v)/2, B=(-r-2g+j+v)/2, C=g and D=(r+2g+j-v)/2. Substitution returns (56,30,10,4) exactly. One shared seed map and expansion therefore generate the eight-value register while retaining the information needed to recover all four inputs. This establishes exact inventory recovery within the specified map.

In the bounded coefficient class {-1,0,1}, exactly two ordered maps return (16,10,34,62), and both are invertible with determinant magnitude 2. In the wider class {-2,-1,0,1,2}, 375 maps return the tuple and 349 are invertible. The additional filter that r contain the Aubrey count and exclude the Station count was articulated after the result and is reported only as a descriptive role check. These counts calibrate the declared function classes. The reversible material-stellar bridge is summarized in Fig. 5.

Three material closures determine one positive integer inventory

Within the adopted compiler, the three conditions $A-B-C=D^2$, $A+C-B-2D=A/2$ and $(A-B)^2=C^2+(B+D-C)^2$ have exactly one strictly positive integer solution: (A,B,C,D)=(56,30,10,4). This conditional uniqueness is unbounded in inventory size. It fixes the same doubled frame (g,q,p)=(10,24,26), primitive form 5:12:13 and word W=(d,3q,r)=(28,72,16); these are consequences of one solution (Fig. 5B; Supplementary Note 29).

The proof reduces the three conditions to $q^2-D^2q-3D^3=0$. Integrality requires $k^2=D(D+12)$, hence $(D+6-k)(D+6+k)=36$. The only admissible positive same-parity factor pair is (2,18), giving D=4; the pair (6,6) gives the excluded D=0. Positivity then selects q=24, from which A=56, C=10 and B=30 follow. The outer identity 2B−A=D is recovered without being imposed separately.

Stonehenge regenerates a Cygnus grammar documented before the analysis

The January 2026 book documented the Cygnus primitive values 16, 28, 34 and 62, the longitudinal role of 34, the latitudinal role of 62 and their 96 closure before the present Stonehenge analysis [20]. In the present reading these reduce to a three-channel typed core: 16R, realized on the material side, and the stellar channels 34 Δλ and 62 β, with 28=62−34 derived. The remaining register terms are derived, not additional primitive selections. Its QR-indexed public archive recorded the two-state register and W=(28,72,16) by 26 August 2026 and the five-star temporal operator by 10 September 2026 (Zenodo records 22103786 and 22691368). The complete specification and all inputs are reproduced in this Appendix and the code archives, so the test remains self-contained.

The five-star graph uses Deneb-Sadr-Albireo as its longitudinal branch and Aljanah-Sadr-Fawaris as its transverse branch. Recomputing the primary J2000 positions in the fixed J2000 ecliptic frame gives g=10.487650°, j=34.077500° and v=62.160110°, which round to (10,34,62). Propagating the stars to 2965.2 BCE while retaining that reference frame gives 10.484801°, 34.074723° and 62.141400°: the same rounded tuple. The six-dimensional variant retains it as well. Thus the full spatial register and exact inverse remain available in the specified fixed frame at both tested epochs. Supplementary Note 24 documents the correction of the archived g decimal, whose rounded value remains 10. With the J2000 plane held fixed, both archived motion prescriptions retain (10,34,62) throughout the declared 10,000-year window;

continuous-extremum checks accompany the sampled verification (Supplementary Note 33).

Q=(r,j-g,v-j,j,v-g,v,3(j-g),v+j)=(16,24,28,34,52,62,72,96), where r=16 is the material radial seed.

The role of the absolute register can be separated further from that of its contrasts. Within the same compiler, D=4 and (q,d)=(24,28) determine A=q+d+D=56 and B−C=q−D=20. The declared closure r=D²=16 then gives B+C=A−r=40, hence B=30 and C=10. This conditional reconstruction returns the observed inventory for both rounded tuples (10,34,62) and (11,35,63) in the tested conventions (Supplementary Note 28).

The same material conditions permit recovery without first rounding the stellar descriptors. With D=4 and r=D²=16, A=B+C+16, q=B+4−C and d=2C+8. The primary ancient contrasts are q=24.045641° and d=27.825144°. Among positive integer inventories, (56,30,10,4) uniquely minimizes the sum of squared contrast errors for any positive diagonal weights: q=24 and the even value d=28 are individually nearest and jointly feasible. With equal weights, the RMS is 0.127784°, versus 0.686067° for the next inventory. The same optimum holds at J2000 and with the 6D inputs. Among all six allocations of these descriptors, only the declared ordering recovers the target inventory in the tested cases. Exchanging j and v instead yields (66,49,1,4), with primary ancient RMS 26.746572°, under the same constraints (Supplementary Note 33).

Directional allocation determines whether the inverse returns the observed Station count. Exchanging only j=34 and v=62 in the Stonehenge seed tuple and applying the same inverse gives (56,30,10,32): the Aubrey, sarsen and trilithon counts survive, but the Station count changes from 4 to 32. Exact recovery therefore requires the assignment in which the 34.077500° longitude span supplies j and the 62.160110° mean latitude supplies v. The transposition demonstrates what directional typing does within the map: retaining the same four values in exchanged roles fails to recover the complete inventory.

Historical star catalogues provide a separate, non-scored portability check [28]. Their 17-star Cygnus figures retain an approximately 16-degree minimum-cover radial scale; Ulugh Beg also gives angular values rounding to g=10, j=34 and v=62, which with the material r=16 closes the material round trip. Ptolemy gives g=11 and j=35, for which the corresponding inverse yields half-integer, non-target counts (56.5,29.5,11,5.5). Approximate membership in the same constellation tradition is therefore insufficient for exact material reconstruction. Supplementary Table S53.1 distinguishes these routes and their status.

The regenerated word carries a celestial phase

The outer system generates W=(28,72,16) through the equivalent material expressions s(ℓ_l−ℓ_s,h+ℓ_s,s) and (N/2,N+s²,s²). In the fully specified five-star graph, W is evaluated against four times the role-ordered right-ascension separations Deneb-Sadr, Sadr-Albireo and Aljanah-Fawaris. Once W and the operator are fixed, the celestial mapping supplies the phase. The contribution tested at Stonehenge is the material regeneration of the target that this existing operator evaluates.

The primary archived astrometry, propagated across astronomical years -8000 to +2000 with the Vondrák long-term precession model [29–32], gives a global minimum at astronomical year -2964.2185, reported as 2965.2 BCE. The executed vector is (27.7848,72.6528,16.2328) sidereal minutes, with 0.4190 minute RMS (0.1047°). A six-dimensional Cartesian space-motion variant gives 2965.9 BCE and 0.4204 minute RMS, a shift of approximately 0.64 year. Both solutions retain the same archaeological interpretation. Omitting the third arc gives 2838.0 BCE; omitting the second or first gives 2993.0 or 2962.0 BCE. These ablations delimit dependence on the

specified operator rather than replace its primary result (Supplementary Note 26).

Solar comparison for the ideal cyclic construction

The ideal 7|21 construction on the 56-fold frame contains a normalized continuous long chord C21=26 sin(21π/56)=24.020867845. At the previously fixed stellar phase of 2965.2 BCE, the propagated obliquity is 24.016307710°, leaving an absolute residual of 0.004560135°. Inverting C21 as an obliquity under the primary long-term model gives 3016.7 BCE, 51.5 years from the stellar phase and 16.7 years before the 3000 BCE opening of Darvill et al.'s Stage 1 interval; the Laskar long-period obliquity sensitivity model [27] gives 2999.4 BCE, 34.2 years away and 0.6 year inside that boundary.

Across the 416 equal-freedom cyclic arms, only three intersect the obliquity range attained within the declared −8000 to +2000 window, giving solar epochs near 5536 BCE, 3017 BCE and 856 CE. The selected diameter-26, seven-step long arm is the only one near the previously fixed stellar phase. The next temporally nearest solar solution is approximately 2,570 years away. This is a post-result temporal-domain census of the declared construction class. The full-window score and archaeological intervals are shown in Fig. 6.

The Stonehenge-native scalar library {4,16,28,32,40,68,72,100} produces 512 ordered triples with repetition. Under the primary astrometric specification, W=(28,72,16) is the only library word that combines an RMS at or below its observed 0.1047° with a best-fit epoch inside Darvill et al.'s Stage 1 interval. Stonehenge therefore regenerates the ordered target that satisfies both criteria within this declared material library.

The celestial phase meets the archaeological chronology

The 2965.2 BCE celestial phase falls within the published interval for Stonehenge Stage 1, including the earthwork and 56 Aubrey Holes, modelled by Darvill and colleagues at 3000-2920 cal BCE [3]. It also lies within the revised 2980-2720 cal BCE (95%) ditch-construction interval, but earlier than its 2940-2800 cal BCE (68%) range [17]. Neither interval was used to construct the material seed map or optimize the astronomical score. The Stage 1 interval was applied afterward as the reported conjunction in the 512-word census. Their role is an external archaeological comparison for a phase obtained under the specified stellar operator. The word regenerated by Stonehenge already carries that phase; any material system generating the same ordered word under the same operator would inherit it. The contribution is the connection between this monument's material inputs and that conditional temporal reading.

A recently reported solstitial post alignment at Bulford, approximately 5 km from Stonehenge and associated with radiocarbon determinations centred around c. 2950 BCE, indicates that solstitial orientation was already being materially expressed in the Stonehenge landscape during the monument's early phase [33]. Bulford is used only as archaeological context for the plausibility of retained or re-expressed solstitial planning information.

The result does not require all participating layers to be contemporary. The central sarsens are later than the initial earthwork, while the individual Station settings are not securely phased by the present source set; the Y and Z holes are later activity. Under the inheritance interpretation, later builders may have re-expressed a centre, axis, count or scale associated with the early circuit. The model associates its celestial phase with a hypothetical foundation state. The stratigraphic implication is summarized in Fig. 7.

Constructive connections and comparative diagnostics

These checks develop the connections between the selected frame, register and phase. They include reconstruction from stellar contrasts, compatibility calculations, catalogue screens and construction procedures. Supplementary Table S53.2 maps their shared inputs and the information each contributes; Supplementary Notes 18–50 provide the complete calculations.

Free-circle compatibility across plan conventions

Fitting a free circle to all four Cleal Station proxies gives a diameter of 86.49 m and a centre 0.68 m from the separately fitted Aubrey centre; the 56 Aubrey proxies have radial RMS 0.63 m against that Station-derived circle. The Aubrey-only diameter and radial RMS are 85.81 m and 0.24 m. Replacing only Station 91 by its indicative socket gives 85.63 m, 0.62 m and 0.50 m, respectively; the registered click-plan alternatives give 84.72 m, 1.28 m and 1.09 m. Their diagonal-midpoint disagreements are 0.44, 0.75 and 1.86 m, quantifying the departure from exact rectangularity. All four omissions and their conditional sensitivity simulations are reported in Supplementary Note 21.

Constructive interpretation of the dimensional ladder

The four inner roles can be expressed as lengths obtained from the selected rectangle. In the doubled frame (x,y,z)=(10,24,26)u, copying x gives 10u, halving y gives 12u, and subtracting x from z gives 16u. The remaining 4u is the inradius (x+y−z)/2 of the right triangle formed by the diagonal (Fig. 3B). The same frame therefore supplies all four inner model lengths through copying, halving, subtraction and a standard circle construction.

Applying these same operations to the ideal 7|21|7|21 rectangle at D=86.44 m gives inner lengths of 33.079, 39.930, 53.361 and 13.250 m, respectively, with 2.118465% relative RMS. It ranks first among the 14 discrete rectangles under these fixed operations; the runner-up gives 8.748362%. The continuous 5:12:13 frame at the same diameter gives 2.040002%. These calculations use the existing approximate boundary conventions and complement the primary outer-scale result of 2.019623%. Source sensitivities, non-exact internal closures, preliminary tangency proxies and the unstable pairwise inversions are retained in Supplementary Notes 31–32.

Directions of complete trilithons relative to the Station frame

A retrospective comparison of physical directions links the three complete trilithon pairs to the outer frame. For pairs 51–52, 53–54 and 57–58, the axis through the opening is defined as the normal to the line between support-centroid proxies in the archived Rees click-plan. The squared inner product of unit axes, averaged over each pair of opposite Station sides, gives long-side scores of 0.984, 0.952 and 0.883, versus short-side scores of 0.029, 0.032 and 0.146. No rotation is fitted. All three favour the long-side family under both Station 91 conventions and under conservative coordinate-perturbation bounds of ±0.25 m per coordinate (Supplementary Note 35).

The two primitive triangles belong to one specified construction

The pivot transformation links the selected Station frame directly to a second primitive family: T(10,24,26)=(16,30,34), the doubled 8:15:17 triangle. The outputs are the diagonal-minus-short-side difference, the semiperimeter and the sum of the legs. These operations can be executed directly by transferring lengths and halving. Under the stated transformation, requiring both input and output to be right triangles forces l/s=12/5. This conditional theorem joins the two primitive families in one connected construction (Fig. 8; Supplementary Note 36).

The pivot triangle has acute angles 28.072487° and 61.927513°, whose difference is 33.855026°. Nearest-integer rounding gives 28°, 62° and 34° without truncation. The integer 34 also denotes the hypotenuse length, a distinct quantity. For the ideal 7|21|7|21 chord model, the transformed triangle's actual angles give 61.967347° and a difference of 33.772483°; both retain 62/34. The published-side proxy likewise retains this pair.

The construction also has a circle-based inverse: the exradii opposite the 16 and 30 sides of the 16:30:34 triangle are 10 and 24. Its inradius is 6, and its circumradius is 17, compared with 13 for the initial 10:24:26 triangle. The corresponding equal-area relation between the 5-by-12 rectangle and the 8:15:17 triangle, and their Gaussian constructions, are detailed in Supplementary Note 36. The earlier Calanais comparison is retained there as an author-reported contextual application with its source extracts.

Constructive predictions can be tested against individual features

The four incentres of the triangular halves of the ideal Station rectangle lie at (±8,±1) in its local coordinates. Their circumdiameter predicts 53.717 m at the existing outer scale, compared with 53.875 m for the discrete chord model. Both approximate the published Y-ring summary of 54 m. Supplementary Note 37 develops the circle construction, including an exploratory outer-ditch diameter comparison; its point-to-hole test is reported under Source and model sensitivities.

A geometric realization of the ordered pair 34/62 uses J=s+l and V=2h+s: a half-perimeter and an open path consisting of two diagonals and a short side. The equations admit two positive rectangular solutions, (10,24,26) and (78/7,160/7,178/7). Only the first returns integer inventories in the fixed module under the declared compiler; it also fits the external dimensions better, with 0.2605% versus 7.9268% RMS. Across all 14 discrete shapes, 7|21|7|21 is the closest ratio approximation (Supplementary Note 39).

The same paths permit an explicit directional decoder. Their equal-tension terminal resultants follow the short and long axes, respectively. In the Rees convention they have east–west and north–south predominance, with axial azimuths 52.151° and 140.038°; these are oblique directions, not exact cardinal alignments. The entrance normal selects the corresponding path families without consulting the path lengths. Conversely, the specified Station-only construction yields an axis 0.606° from the entrance normal, ranking that pair first among 19 available consecutive drawing-proxy pairs (Supplementary Note 40).

With grid east fixed, the pivot rays approximate the normals of pairs 57–58 and 53–54 at 1.175° angular RMS; the discrete chord construction gives 1.132°. The reference, reflection and pair assignment were selected retrospectively from disclosed alternatives. The observed inter-ray opening is 32.604°. Position tests using existing construction marks and bilateral reflection, together with the restoration history, are retained in Supplementary Notes 41–42.

The complete 220-triangle search finds 52–54–60 closest to 16:30:34 at 0.689% RMS after fitting its own scale. Across the seven primitive comparators, 5:12:13 and 8:15:17 have the smallest best-fit discrepancies, 0.562% and 0.689%, respectively; each selects a different trio and scale. The two connected primitive families therefore also have the smallest shape discrepancies in the complete point census (Supplementary Note 42).

Joint geometry criteria expose which restrictions add information

A retrospective enumeration of 14 discrete forms and 18,000 axial orientations retains 541 of 252,000 configurations under all six specified criteria. Every survivor has shape 7|21|7|21. External fit, inner dimensions, path ratio and pivot closure each eliminate the same 13 shape alternatives; their conjunction adds no further shape reduction. The directional criterion supplies the additional restriction, while the binary horizontal/vertical label adds none after it. Giving every control the reference orientation instead leaves one of 14 forms (Supplementary Note 43).

Pythagorean factorisation and quadratic Gram notation

The selected frame is also present in doubled material form. The trilithon channel gives g=10, the compiler gives q=24, and the scaled Aubrey diameter gives p=26. These satisfy $10^2+24^2=26^2$, the doubled 5:12:13 relation. The next register channel follows without a new choice: j=g+q=34.

With N=56 and R=N/2=28, the ordered register has the factorised form Q=(p−g,q,R,g+q,2p,R+g+q,3q,4q). Substitution gives Q=(16,24,28,34,52,62,72,96). Thus the same material system expresses the selected Station geometry and the reversible register in one Pythagorean factorisation.

The same closure also recovers $g=(q^2-r^2)/(2r)=10$ from r=16 and q=24 if p=r+g and $p^2=g^2+q^2$ are imposed. W alone leaves the inventory family (56+t,30,10+t,4+t), so the word by itself does not independently recover all four counts. The Station-anchored route and the joint uniqueness proposition state explicitly which additional material conditions resolve that freedom (Supplementary Notes 27–29).

Quadratic Gram notation provides a compact post-result reexpression of the selected frame. For (a,b,c)=(5,12,13), let X=2ac=130, Y=2a=10, Z=b=12 and J=2(a+b)=34. Then $XY-Z^2-J^2=1300-144-1156=0$ (Supplementary Note 19).

Outer-frame closure

The outer inventories also reproduce the radial index directly. In the ideal integer form, the Aubrey positions minus outer sarsens give A−B=56−30=26=2c, the selected doubled hypotenuse; subtracting this diameter role from the sarsen count returns B−2c=30−26=4 Station positions. Equivalently, B/2+c=15+13=28 and $(B/2)^2-c^2=15^2-13^2=56$. Under the primary continuous branch, the Aubrey diameter is 25.94695u (−0.204% from 26), B−D_Aubrey/u=4.05305 (+1.326% from 4), B/2+R_Aubrey=27.97347 (−0.095% from 28), and $(B/2)^2-R_Aubrey^2=56.68897$ (+1.230% from 56). All disclosed diameter branches retain rounded radius 13. The outer 30:56 ratio also reduces to 15:28 (Supplementary Note 18).

Outer-inventory tangent and Delporte comparison

The two outer circular inventories give theta_AB=arctan(30/56)=28.178590 degrees. Using the retained archival decimal convention, the non-rounded stellar difference descriptor is d*=62.160117−34.077511=28.082606 degrees, giving an absolute residual of 0.095984 degrees. This statement uses the shared astronomical degree convention explicitly. Recomputed primary J2000 descriptors give d*=28.082610° and residual 0.095980°; the descriptive ranking is unchanged (Supplementary Note 24).

Applying the same unrounded ratio-to-angle function to all six inventory pairs ranks the Aubrey-sarsen pair first. The next closest pair, trilithons and Stations, gives arctan(4/10)=21.801409 degrees, 6.281197 degrees from d*. The complete ranking is supplied in Supplementary Note 17.

The remaining relations among 16, 24, 28, 34, 52, 62, 72 and 96 belong to the previously documented register and to the material compiler already reported above. They are not counted as additional tangent results. The continuous bridge is retained because it gives a compact, unit-free material input to one pre-existing directed channel, while leaving the evidence for the full register in the reversible four-count map and its directional ablation.

For modern descriptive context, the IAU/Delporte polygon for Cygnus has declination extrema of 27.73 and 61.36 degrees. The complementary pair generated by the same ratio, 28.178590 and 61.821410 degrees, lies 0.448590 and 0.461410 degrees from those extrema. Delporte’s 1930 polygon partitions the sky in right ascension and declination at epoch B1875.0. The full modern boundary screen is reported in Supplementary Note 17.

Ditch centreline compatibility calculation

Field and Pearson report a circle close to 102 m in diameter between the internal lips, with ditch width generally c. 4 m in the east and c. 6–6.5 m in the west [25]. Defining the test boundary as the enclosure-ditch centreline, the east-west transect gives 102 + 2 + 3.0–3.25 = 107.0–107.25 m, or 32.12–32.19u. Under this explicitly stated convention, the value rounds to 32.

Carrier, internal graph and residual-partner screens

A separate modern-frame carrier screen is reported at the end of Supplementary Note 4. Across the 88 IAU constellation polygons, Cygnus ranks first under the declared area-rank, planar, spherical and interior diagnostics. Its area-rank residual is 0.0329%, versus 12.1895% for the runner-up; the respective planar, spherical and interior margins to the runner-up are 406.23-, 20.45- and 436.44-fold.

The declared modern carrier also has limited internal role freedom. Conditional on each 17-entry historical Cygnus list, a fixed Deneb anchor and the stated J2000 ecliptic convention, only 4 of 3,360 injective ordered assignments (0.119%) recover the rounded typed vector (10,34,62). The g=10 and j=34 roles identify Sadr and Albireo uniquely; four partners round to 62. The frozen continuous value 62.160117° is the Deneb–Fawaris mean latitude, so Fawaris matches that continuous value by construction rather than through an additional selection (Supplementary Note 18).

The existing temporal operator resolves the residual partner class under the archived fixed-base comparison. Fawaris ranks first in both membership lists: its full-window minimum is 0.4180 sidereal minutes at 2964.8 BCE, versus 0.5964 for HIP 99848; at the primary phase, the scores

are 0.4180 and 0.7499. The primary archived stellar input remains the source of the reported 2965.2 BCE phase and 0.4190-minute RMS. A fully homogeneous Hipparcos comparison also selects Fawaris, with minima 0.3893 versus 0.5665. The retrospective floor variant admits both candidates spatially but preserves this temporal ordering. Thus the existing temporal criterion distinguishes the spatial survivors under both astrometric conventions (Supplementary Notes 18 and 33).

A further two-epoch diagnostic selects Sadr–Albireo–Fawaris alone among the 3,360 assignments in each list when the separately rounded descriptors must give (q,d)=(24,28) at both J2000 and the primary ancient phase. Without rounding, the same assignment ranks first under the joint four-residual RMS, 0.2233° versus 0.2426° for the runner-up. Direct-difference rounding admits three assignments, and maximum-error scoring gives a two-way tie (Supplementary Note 27).

The joint census evaluates complete alternative graphs at their own optimized epochs. Under homogeneous Hipparcos inputs, the named graph alone meets the joint inventory and temporal criteria among 2,730 assignments in each list, a conditional frequency of 0.0366%. Inventory recovery alone admits six assignments in the Ptolemaic list and eight in the Ulugh Beg list. Allowing any of the three inventory-estimation rules admits seven and nine spatial assignments, respectively, but the same single graph meets the joint temporal criterion. Its comparison-input minimum is 2965.0 BCE, with RMS 0.389288 sidereal minutes; these values do not replace the primary chronology (Supplementary Note 34).

Free stellar identities concentrate the joint solutions in Cygnus

The broader Hipparcos census supplies no named anchor or constellation. At V≤5, 1,625 eligible stars across 77 regions with at least five entries produce 2,990 ordered candidates after spatial filtering. Seven reach or improve on the nominal full-window temporal RMS, all in Cygnus. Applying the ancient-contrast and Stage 1 filters jointly retains only Deneb–Sadr–Albireo–Aljanah–Fawaris in the declared roles. At V≤6, 1,072,375 spatially eligible quintets yield 903 temporal passes and six joint passes, all in Cygnus and all retaining Deneb and Sadr in their nominal roles. Some alternatives fit time more closely; they remain in the complete census (Fig. 10; Supplementary Note 45).

The nominal quintet has role-ordered catalogue magnitudes (1.25,2.23,3.05,2.48,2.86). Among the joint survivors, no alternative is brighter in any role and each is fainter in at least one. Consequently, the nominal assignment is uniquely retained for every nested magnitude limit from 3.05 inclusive to 5.06 exclusive under the unchanged joint criteria. This retrospective brightness diagnostic adds an observable distinction without assigning weights to the five roles (Supplementary Note 46).

Removing both the latitude target and the two third-channel stars retains Deneb–Sadr–Albireo as the only temporal survivor at V≤4. Its uniqueness holds for magnitude limits from 3.05 inclusive to 4.59 exclusive before applying ancient-contrast or horizon filters. At V≤5 there are five temporal survivors and at V≤6 there are 131. The core alone minimizes near 2848.4 BCE in the uniform catalogue convention; the full nominal graph minimizes near 2965.4 BCE. The third channel therefore helps locate the phase (Supplementary Note 47).

A flat-horizon, annual-night feasibility calculation at latitude 51.18° N admits all five nominal stars simultaneously above 63°, with the solar centre below −18°, at the uniform-catalogue nominal phase. The same rule rules out two V≤5 core competitors containing stars that never rise from the site at their own best-fit epoch. This establishes geometric possibility and some

physical discrimination (Supplementary Note 48).

These expanded tests use uniform Hipparcos astrometry from epoch J1991.25, giving nominal phase 2965.4251 BCE and RMS 0.390126 min. They are comparisons under a common catalogue convention and do not replace the primary mixed-input specification of 2965.2185 BCE and 0.418975 min. All identities, magnitude thresholds, reference conditions and alternative epoch conventions are archived.

Source and model sensitivities

Under the primary Cleal convention, the Aubrey-anchored grid yields index gaps of 8|21|7|20; exact Station–Aubrey registration remains unresolved across the available source conventions. The source alternatives, index-boundary sensitivity and original zero-phase test are reported in Supplementary Note 20.

Changing instead to the mean ecliptic of the ancient date gives (11,35,63). With material r=16, the unchanged inverse then yields (57,30,11,5), while q=24 and d=28, and therefore W, remain unchanged at the tested phase. The continuous coordinates are not invariant, and these agreements are not asserted for every epoch. The fixed-reference module does not establish that prehistoric observers measured the same absolute values relative to their contemporary ecliptic (Supplementary Table S53.1; Supplementary Notes 24 and 27).

The supplementary construction diagnostic did not improve cross-validation over the regular-circle baseline for the specified eight-sector procedure or seven-hole residual model; this concerns construction procedure rather than the Station shape approximation (Supplementary Note 30).

The solar comparison fixes the ideal 7|21|7|21 cyclic construction: at the same diameter role, the exact 5:12:13 long side gives 2784.8 BCE and the published mean-side ratio gives 2713.2 BCE. The near-3000 BCE solar result therefore does not transfer unchanged from the ideal cyclic construction to the continuous Station rectangle (Supplementary Note 25).

Testing the four Station-triangle incentres against all 30 digitized Y symbols, however, gives 2.872 m positional RMS in the primary Cleal branch, with 97.125% of joint rotations matching as well or better. The specific point-to-hole association is therefore unsupported. The digitized Y circle has diameter 53.163 m, also reversing the slight radial preference between the two ideal models. Supplementary Note 37 retains the full positional assignments, source variants and an exploratory outer-ditch diameter comparison.

Under the equal-tension path decoder, the equivalent force line crosses the outline of Stone 1 in the primary branch and clears the entrance outlines only in the indicative-91 branch, so directional agreement does not recover an unambiguous physical passage (Supplementary Note 40).

In the point-triangle census, the selected 52–54–60 triangle has its long side predominantly north–south and therefore does not satisfy the proposed horizontal-long-side assignment. Each comparator fits its own scale, so the shape rankings do not determine a common physical unit (Supplementary Note 42).

The enclosure-ditch centreline estimate is precision-limited. Field and Pearson [25] publish the inner-lip diameter and variable widths, not a directly surveyed centreline diameter; the report also describes local departures of up to 1 m and a flattened north-west sector. It is therefore an

outer-earthwork compatibility calculation, not a high-precision independent diameter or an area-based Cygnus claim. Alternative boundaries, including the directly reported inner-lip diameter, are adverse conventions and do not yield the same integer. Supplementary Note 15 records the arithmetic and failure conditions.

Releasing Deneb within the historical membership lists expands each census from 3,360 to 57,120 ordered assignments. Two Ptolemaic-list and four Ulugh-Beg-list assignments preserve the rounded contrasts at both tested epochs, with two assignments common to the lists. Thus the fixed-anchor uniqueness does not extend to all possible anchors under the contrast-only test. The algebraic normalization of identical contrasts cannot distinguish these origins (Supplementary Note 44).

The Stonehenge-native word result is conditional on its declared material library. Across arbitrary positive integer triples, 179 words attain an equal or smaller full-window RMS; the distinguishing result is therefore the conjunction of material regeneration, score and archaeological interval, rather than the raw sky minimum alone (Supplementary Note 9).

v1.26: Read revised input, execution and reference records in the revision guide and S5 section 8.

Supplementary Note 53 Provenance dependencies and execution scope

Supplementary Table S53.1 Provenance historical portability and directional controls

Route	Typed seeds or outputs	Result	Interpretive role
Published grammar	16; 28; 34H; 62V; 96	Fixed before Stonehenge analysis	Target provenance
Fixed J2000 ecliptic	g=10; j=34; v=62	Same rounded tuple at J2000 and 2965.2 BCE; material r=16	Primary spatial module
Ancient ecliptic of date	g=11; j=35; v=63	Inverse 57,30,11,5; q=24 and d=28 retained	Reference-frame sensitivity
Ulugh Beg	material 16R | 10λ | 34λ | 62β	Exact Q; inverse 56,30,10,4	Historical exact round trip
Ptolemy adverse	material 16R | 11λ | 35λ | 62β	Half-integer non-target inverse	Historical non-target
Directional transpose	16R|10λ|62λ|34β	Station count 4 becomes 32	Allocation sensitivity
Contrasts with Station anchor	q=24; d=28; D=4; r=D^2	Conditional inverse 56,30,10,4 for both tested tuples	Retrospective material conditioning

Retained v1.23 reference numbering: use the v1.26 crosswalk and current S5 interpretation.

Supplementary Table S53.2 Comparative diagnostics and shared inputs

Check	Shared inputs	What it adds	Status
88-constellation carrier screen	Modern IAU polygons and declared catalogue diagnostics	Carrier is first in four descriptive screens	Modern-frame, non-scored
Pythagorean / Gram notation	5:12:13 frame; compiler	Compact discrete and quadratic reexpressions of Q	Algebraic entailment
Outer-frame closure	A=56, B=30, c=13	Connects ring inventory to diameter role and Station count	Algebraic entailment
Tangent and Delporte screen	A=56, B=30; degree convention	Continuous 15:28 angle and non-scored modern context	Conditional / modern-frame, non-scored
Ditch centreline	Published inner lip and widths; u	Compatibility of one derived boundary with 32 units	Material compatibility, precision-limited
Carrier and residual partner	Named carrier, anchor, typed targets and temporal operator	Conditional role and partner resolution	Conditional, non-scored
Free Station circle	Four Station proxies; separate Aubrey fit	Approximate centre and scale compatibility	Retrospective; source dependent
Joint material uniqueness	Primary compiler; $r=D^2$; $d=A/2$; Pythagorean closure; positive integers	Only inventory 56,30,10,4; same frame and W	Retrospective conditional theorem
Station-anchored recovery	Stellar contrasts; D=4; $r=D^2$	Same inventory under the two tested reference conventions	Dependent reconstruction
Construction procedure	56 Aubrey proxies; specified templates	Tested procedures do not improve cross-validation	Retrospective supplementary analysis
Constructive lengths and model separation	Existing frame, ladder and approximate dimensions	Explicit geometric operations; 9 cm model separation; source and inverse sensitivity	Retrospective dependent interpretation
Relative material directions	Three complete trilithons and Station proxies from one plan	All three opening axes favour the long-side family; bounded sensitivity	Retrospective physical diagnostic; Note 35
Pivot and circular constructions	Station frame and specified T	Conditional 5:12:13 to 8:15:17 bridge; inverse exradii	Dependent theorem; Notes 36–37
Physical direction and placement	Same plan proxies; retrospective path rules	Executable axes and placement tests; source-conditioned outcomes	Retrospective; Notes 38–42
Joint geometry census	14 shapes, rotations and six disclosed criteria	Separates redundant shape restrictions from direction	Conditional frequency; Note 43

Check	Shared inputs	What it adds	Status
Free stellar identities and brightness	Fixed grammar; complete eligible catalogue	Joint survivors in Cygnus; nominal brightness advantage	Retrospective; Notes 44–46
Core ablation and night feasibility	Reduced operator; epoch sky and site latitude	Bright-core selection; physical observability; phase dependence	Retrospective; Notes 47–48

Interpretive scope and controls

The inventory-uniqueness theorem is specific to the stated compiler, closures and integer domain. These rules were recognised with the inventories available, so the result is not a blind archaeological prediction. Condition removal, relaxation of integrality and the alternative radial row delimit its scope; full controls are reported in Supplementary Note 29.

The solar comparison concerns the ideal 7|21 construction specifically. It shares the selected diameter role and cyclic geometry with the material model, and numerically identifies a dimensionless chord with an obliquity in degrees. Substituting the exact 5:12:13 ratio moves its central reading by about 232 years. It therefore illustrates a relation within the ideal cyclic model, with substantial shape sensitivity, and supplies neither an independent date nor a robust temporal constraint from the measured Station sides.

The angle labels, primitive identities, exradii and factorisations share the selected frame and its inputs. Their contribution is to specify connected operations, rather than to add independent observations. The compiler and constructive rules were recognized with relevant data available; the condition-removal controls delimit the algebraic uniqueness result. The modern boundary comparisons, including the area rank and Delporte extrema, are descriptive catalogue context and carry no evidential weight for prehistoric knowledge. The earlier Calanais comparison is author-reported context, not a newly verified replication (Supplementary Notes 17–19, 29 and 36).

Coordinate type and terrestrial orientation require separate interpretation. The latitude descriptor is a mean latitude, not the constellation’s vertical extent, and the internal triangle angles do not fix geographic directions. Reference axes, reflections and pair assignments were chosen retrospectively. The path-ratio fit is locally insensitive to shape; direction agreement therefore cannot substitute for line position or clearance. The fixed-J2000 stability does not imply equality with the ancient ecliptic. A geometric construction or a generic architectural axis can explain some of the same structure without a Cygnus cause (Supplementary Notes 24, 33 and 38–42).

The common spatial rotation used for the shape comparison is a fitted parameter and does not replace the original zero-phase test. The 0.0904 m vertex separation is a distance between ideal models; the stipulated coordinate perturbations and their stability bounds are sensitivity assumptions rather than measured archaeological uncertainties. The shared-source circle fits are not independent surveys. Transferring an inradius as a length does not identify a physical incircle at the trilithons, and the restoration history and original settings constrain any proposed construction sequence [1–3,25] (Supplementary Notes 20–23 and 30–42).

The expanded stellar comparisons use the stated magnitude limits, modern regional grouping and uniform catalogue convention. Brightness dominance is a catalogue property; the

flat-horizon night model is an existence calculation that leaves terrain, extinction, weather, lunar conditions and the historical observing occasion unspecified. Alternative assignments and both catalogue-epoch conventions remain available in full. These conditions delimit the identification and observability claims without changing the retained numerical results (Supplementary Notes 45–48).

The spatial analysis relies partly on published summary dimensions, several of which are rounded. The Sarsen channel uses an explicitly declared outer-envelope convention, two Station positions are absent-stone settings, and the buried circuits are irregular. The enclosure-ditch calculation is limited more specifically: it is a centreline derived from published internal-lip and width summaries, not a direct centreline survey. Coordinate-level confirmation therefore requires georeferenced points, uncertainty propagation, robust circuit fits and an algorithmic Sarsen envelope. The ladder and its comparison universe were formulated after pattern recognition, and nearest-integer compression at 2.02% RMS occurs in approximately 7.23% of the declared perturbation ensemble; the ladder is supporting structure, not a p-value.

The complete dependency ledger now includes the constructive bridge, path decoders, positional tests, expanded stellar census and observability model (Supplementary Table S53.2; Supplementary Notes 36–50). Internal consequences explain the model; source comparisons assess sensitivity; free-assignment censuses assess conditional selection; and positional tests confront particular realizations. These functions are complementary but do not supply independent multiplicative probabilities. The Y-incentre test and entrance-line diagnostic, for example, delimit proposed material realizations while leaving the underlying geometric identities intact.

The core Cygnus grammar, temporal operator and W predate this Stonehenge analysis, whereas the seed map, constructive associations and expanded diagnostics were recognized with substantial relevant data already available. Releasing all five stellar identities addresses a wider freedom than the original anchored censuses. It still leaves the grammar, modern IAU partition, magnitude selection and post-fit criteria conditional on the research history. This distinction preserves the substantive result: under the disclosed rules, the selected bright stellar configuration can be recovered among alternatives, rather than merely evaluated after its names are supplied. It does not retrospectively make the research a blind discovery of a prehistoric constellation.

No defensible sampling distribution for “Stonehenge-class monuments” is presently available; consequently, no site-level chance probability is reported. In particular, 179 arbitrary integer words fit the full astronomical window at least as closely as W, so specificity belongs to the Stonehenge-native library and chronological conjunction, not to the raw sky minimum. The primary astrometric input remains the headline specification. Its 0.64-year difference from the six-dimensional variant is not a total uncertainty estimate: hypothetical channel weights move the optimum across 2985.2–2914.7 BCE, and the local interval with RMS no more than 10% above the minimum spans approximately 65 years. These are deterministic sensitivities, not confidence intervals (Supplementary Note 26). Chronological concordance is model-dependent: 2965.2 BCE lies inside Darvill et al.’s Stage 1 interval and Greaney et al.’s 95% ditch interval, but earlier than Greaney et al.’s 68% interval. Radiocarbon-dated cremations in and around Aubrey Holes, including deposits from c. 3000 BC, place their use within Stonehenge’s first construction stage [37]. A common phase does not imply contemporaneous construction, cultural transmission or a universal building date. The original joint-role frequency retains its two fixed anchors; the expanded census releases those anchors but retains the specified grammar and

catalogue grouping. Neither frequency is multiplied by metric, formula, word-census or joint-geometry fractions. The ablated bright core also gives a different temporal optimum, demonstrating why phase agreement belongs to the full operator rather than three independent clocks.

Coordinate tests and the complete execution inventory

The reconstruction specifies observables that further evidence can test directly. Survey-grade coordinates can determine whether the Aubrey, Station, Sarsen, Y-hole and Z-hole structures share a registration within declared uncertainty; incompatible registration would defeat the whole-plan claim. Under the concentric shared-width model, the long Station-side lines are tangent to the Sarsen outer envelope. Testing that consequence requires an independently measured Sarsen centre and boundary, not recentering to obtain contact (Supplementary Note 31). Distinguishing the two ideal Station shapes also requires a positional-error and construction-variation model appropriate to their approximately 9 cm vertex separation. A more specific test of physical reuse would seek shared departures from ideal geometry under a transformation fixed before inspecting the later structure, accounting for terrain, restoration and survey error. The current data do not permit that test (Supplementary Note 30). An algorithmic Sarsen envelope can test the shared-length relation and dimensional ladder. Common Station coordinates and horizon uncertainties permit comparison with orientation-based accounts, while a frozen external corpus can test how often comparable directed closures recur.

The strengthened interpretation is therefore a programme of reconstruction with explicit points of empirical leverage. Original socket and mounting-axis records can test whether the declared directions and position transfers survive a change from drawing proxies to archaeological coordinates. The archived reflection prediction for the original setting of Stone 59 provides a specific unscored target, while the failed Y assignment prevents radial similarity from being mistaken for positional recovery. A frozen application to another site or an independently selected stellar grouping can then test transfer beyond the data used to develop these rules. This is how the proposed connection can gain historical force: by recovering additional structure under a rule fixed before the new comparison, with its source and uncertainty stated.

All numerical inputs, derived outputs, figure data, archived digitized plan proxies and protocols needed to reproduce the reported analyses are supplied in S1 Appendix and S2–S4 Code. The public, timestamped archives that document the pre-existing stellar grammar and temporal operator are available at https://zenodo.org/records/22103786 and https://zenodo.org/records/22691368. The study uses no restricted primary survey coordinates. Confirmatory coordinate-level work will require archive-derived georeferenced data and will preserve their licensing conditions. S3 preserves all later geometric audit inputs and reports; S4 supplies the expanded stellar and ablation results. The shared full Hipparcos input is distributed once in S2 and restored by the stellar runner with a hash check.

Portable Python scripts reproduce the spatial fit, cyclic audit, 600,000-trial Station measurement stress test, 40,960,000-map seed census, exact inversion, the typed three-channel core and its deterministic register expansion, the continuous outer-inventory angle and six-pair comparator, the native Pythagorean factorisation, the outer-frame theorem and its disclosed-diameter sensitivity, the conditional within-Cygnus directional-freedom census, residual-partner resolution under the existing temporal operator, 512-word temporal census, ladder null, historical-coordinate controls and primary plus six-dimensional stellar chronology. Added plan diagnostics reproduce continuous gaps, anchored indices, free circles and all four omissions,

source-convention and coordinate sensitivities, one common spatial rotation for each fixed shape, and the complete 14-template discrete rectangle census with continuous comparators. Reference-frame checks, archived-versus-recomputed descriptors, solar shape sensitivity, temporal channel ablations, conditional algebra and two-epoch membership comparisons are included in the added audit group. The added algebraic group reproduces Station-anchored recovery, the unbounded conditional uniqueness proof and its controls; a construction group reproduces the specified polygon-division and residual-periodicity diagnostics. The constructive-length group reproduces the four geometric operations, all 14 discrete comparators, source sensitivity, model separation and all six inverse pairs. A run-all script, pinned input tables, expected outputs and SHA-256 manifest accompany the submission. This executable form directly addresses documented barriers to reuse of heritage models [38]. Supplementary Notes 33–34 add fixed-plane stability, explicit quantization alternatives, continuous integer-inventory reconstruction, channel-omission diagnostics and the joint role census. Their runner is integrated into run_all.py, with expected outputs and complete assignment records. Supplementary Note 35 adds the physical axial Gram comparison, both Station 91 conventions and deterministic coordinate-sensitivity bounds, reproduced by run_directional_gram_audit.py. Supplementary Notes 36–50 integrate all 25 subsequent audit packages, indexed individually in the coverage ledger. S3 Code contains the geometric and material extensions; S4 Code contains the free-identity catalogue search, brightness analysis, core ablation and geometric night test. Group runners, numerical snapshots, verification logs and manifests distinguish the unchanged primary chronology from uniform-catalogue comparisons. The full primary audit and the new groups can be executed separately; all code paths use local archived inputs except the Note 40 plan raster.

Chronological interval terminology. The archived “Stage 1” filter is the 3000–2920 cal BCE initial-enclosure construction interval listed within Stage 1 in Darvill et al. [3, Table 3]. It is not the duration of the entire stage, whose summary range in that table is 3000–2620 cal BCE. The numerical filter and all census results are unchanged. Greaney et al. [17] report the revised ditch-construction interval as 2980–2720 cal BCE (95%) and 2940–2800 cal BCE (68%). The model phase is inside the former and earlier than the latter. These chronological models use radiocarbon and archaeological context; none is an astronomical fitting prior.

Temporal window coverage. The primary minimum falls in an 80-year initial-enclosure interval and a 260-year revised ditch interval. Their fractions of the 10,000-year search are 80/10,000 = 0.008 (0.8%) and 260/10,000 = 0.026 (2.6%). A single date drawn uniformly from the search window would have these hit probabilities for fixed target intervals. Their overlap is 2980–2920 cal BCE, or 60 years (0.6%); the overlapping targets are not independent and their fractions must not be multiplied.

These analytical benchmarks describe the breadth of the chronological match. They do not establish that optimized dates from the reconstruction follow a uniform distribution. A calibrated chance analysis must specify its candidate-generation and selection rules, including the previously specified word and operator, the retrospective Stonehenge mapping and the archaeological comparisons. Extending the search boundary alone changes the denominator without necessarily changing the optimum. The 1-of-512 material-library conjunction is a separate conditional enumeration, not a probability of historical intention.

Supplementary Note 54. Directional alignments and joint route selection

54.1 Decoder, coordinates and architectural targets

This retrospective synthesis combines the path decoder in Note 40 with the archived Rees/Tim Daw plan proxies used in the preceding material-direction audits. It evaluates an ordered relationship between the outer Station frame, the entrance and three complete inner openings. No plan rotation is fitted. The primary branch uses the labelled Station 91 position; a second branch substitutes its indicative hole position and keeps the other inputs unchanged.

For a path with vertices $x_0,\ldots,x_k$, equal terminal tensions T give the terminal resultant $F/T = (x_1-x_0)/||x_1-x_0|| + (x_{k-1}-x_k)/||x_{k-1}-x_k||$. The tested direction is $u = F/||F||$. This is the sum of the two terminal forces, not the net force on an entire supported cord. Loads at intermediate guides and the archaeological existence of anchors are separate questions. The path length and resultant magnitude are different quantities: 34 and 62 label model lengths, not forces or measured bearings.

For each stone pair (a,b), the opening normal n is the normalized 90° rotation of x_b−x_a. The entrance target is 1–30; the available complete inner targets are 51–52, 53–54 and 57–58. Every target uses this same normal convention. $K(u,n) = (u\cdot n)^2$ compares axes without assigning an arrow: parallel axes give 1 and perpendicular axes give 0. These are squared cross-Gram entries, not independent statistical probabilities. Simultaneously reversing an axis or rotating both coordinate sets leaves K unchanged.

The J route is [(91+92)/2,92,93,(93+94)/2]. The V route is [91,93,94,92]. The alternative J route is [(92+93)/2,93,94,(94+91)/2]. Midpoint notation denotes coordinate averages. The scale conversion uses AE, BE, AN and BN stored in rees_clickplan_extract.json. The input source hash is recorded in results.json.

Let I(u) be the mean of the three inner-opening K values. The assigned score is S = [K(J,entrance)+I(V)]/2. The exchanged score is S_swap = [K(V,entrance)+I(J)]/2. The targets and channel weights remain fixed during exchange; the entrance and inner group each carry one half of the score. The inner group is therefore not counted as three independent votes. Figure 9 displays the compact 2 × 2 matrix and the two assigned alignments in each Station 91 branch.

54.2 Plan alignments and the complement identity

Primary Station 91

Route axis	Entrance 1–30	Inner 51–52	Inner 53–54	Inner 57–58
J (34)	0.999938	0.028244	0.031036	0.145924
V (62)	0.000842	0.982681	0.954911	0.879127
Alternative J	0.001290	0.984439	0.951998	0.883598

The assigned score is 0.969422215; the exchanged score is 0.034621565. The selected J–V axial Gram is 0.001359270; substituting the alternative J gives 0.999952207.

Indicative Station 91

Route axis	Entrance 1–30	Inner 51–52	Inner 53–54	Inner 57–58
J (34)	0.999881	0.022358	0.037876	0.132921
V (62)	0.000567	0.981297	0.957046	0.875713
Alternative J	0.000684	0.981926	0.956092	0.877253

The assigned score is 0.968949705; the exchanged score is 0.032475990. The selected J–V axial Gram is 0.000166333; substituting the alternative J gives 0.999994517.

For the primary branch, J has axial grid azimuth 52.150561° and V 140.037686° (clockwise from grid north, modulo 180°). These are oblique directions. J has the larger east–west component and V the larger north–south component; they are not exact compass axes. Squared Gram values do not establish north-versus-south or east-versus-west polarity. Averaging the three inner scores does not assert that the openings share one identical bearing.

For exactly orthogonal unit axes J and V, their projectors satisfy $JJ^{T}+VV^{T}=I$. Hence $(J\cdot n)^2+(V\cdot n)^2=1$ for every unit target n, and $S_{swap}=1-S$. In the digitized primary and indicative branches, J and V instead make acute angles 87.887125° and 89.261036°; $S+S_{swap}$ is 1.004044 and 1.001426. The contrast therefore restates alignment rather than providing an independent control. Orthogonality alone does not force S to be high: the assigned alignments still depend on the observed target directions.

The primary J–entrance angular discrepancy is 0.450333°. The V discrepancies for 51–52, 53–54 and 57–58 are 7.562135°, 12.259665° and 20.344754°. Gram 0.938906 is their mean squared alignment, not the alignment of a single averaged normal. These are nominal drawing-proxy discrepancies, not archaeological uncertainty estimates.

54.3 Four symmetric route classes

Write a rectangle as corners (0,0),(l,0),(l,s),(0,s), with short side s, long side l and diagonal h. The table gives path lengths and terminal resultants in the local (long,short) basis. The normalization to a unit direction is applied only after these terminal vectors are summed.

Class	Route	Length	F/T
M_short	Opposite short-side midpoints via one long edge	s+l	(0,2)
M_long	Opposite long-side midpoints via one short edge	s+l	(2,0)
D_short	Diagonal–short side–diagonal	2h+s	(2l/h,0)
D_long	Diagonal–long side–diagonal	2h+l	(0,2s/h)

With (s,l,h)=(10,24,26), these lengths are 34,34,62,76. Enumerating all 12 ordered pairs of distinct classes yields the following complete table. A length pass requires the same nearest-integer rule floor(x+0.5) for both positive lengths and the ordered labels (34,62). No evaluated length lies on a rounding tie. An orthogonality pass requires axial Gram zero (numerical tolerance 10^{-12}).

J class	V class	Lengths	Length pass	Orthogonal	Joint pass
M_short	M_long	34,34	No	Yes	No
M_short	D_short	34,62	Yes	Yes	Yes
M_short	D_long	34,76	No	No	No
M_long	M_short	34,34	No	Yes	No
M_long	D_short	34,62	Yes	No	No
M_long	D_long	34,76	No	Yes	No
D_short	M_short	62,34	No	Yes	No
D_short	M_long	62,34	No	No	No
D_short	D_long	62,76	No	Yes	No
D_long	M_short	76,34	No	No	No
D_long	M_long	76,34	No	Yes	No
D_long	D_short	76,62	No	Yes	No

Both midpoint routes recover the J length. Only M_short paired with D_short also has orthogonal outputs. M_long paired with D_short instead gives parallel outputs. The joint rule distinguishes these two candidates without fitting to entrance or inner-opening bearings; the route family and the choice to apply orthogonality jointly remain retrospective.

54.4 Discrete-form and alternative-rectangle checks

The construction can be evaluated in the ideal 7|21|7|21 frame without changing its route definitions. Set s=26 sin(7π/56), l=26 sin(21π/56), h=26. The selected route lengths are 33.970637 and 61.949769; they retain the nearest-integer labels 34 and 62, with orthogonal output axes. This preserves the discrete-form approximation. It does not change the separately reported anchored Station–Aubrey assignment.

Rectangle	J length	V length	Length passes	Joint passes
10:24:26	34.000000	62.000000	2 / 12	1 / 12
Ideal 7|21|7|21	33.970637	61.949769	2 / 12	1 / 12
78:160:178, scaled by 1/7	34.000000	62.000000	2 / 12	1 / 12

The rational 39:80:89 branch also satisfies the joint directional rule at the stated scale. Consequently this rule does not identify the Pythagorean ratio uniquely; the earlier metric and inventory tests perform that discrimination. The 1-of-12 result is a census inside a declared family, not a chance probability for all possible encodings.

54.5 Reproduction, provenance and interpretation

S3 contains STONEHENGE_GRAM_CHANNEL_CLOSURE_v1/audit.py, inputs/rees_clickplan_extract.json, inputs/prior_cord_results.json and results.json. Run python audit.py within that directory, or run the group runner S3_Geometry/run_extensions.py. The latter executes audits in a temporary copy and compares the delivered JSON snapshots. The audit verifies the previous individual path scores, reversal and common-rotation invariance, analytic terminal resultants, all 12 route assignments for each rectangle and the complement identity. Its complement_diagnostic field records the angular discrepancies and exact projector residual. Main Figure 9 is generated by build_directional_figure9.py from these same inputs and results.

The synthesis connects specified outer-frame path lengths to the entrance and inner-opening directions. The path definitions supply the labels 34 and 62; normalizing directions removes magnitude, so Gram scores alone cannot identify those numbers. This matches the earlier directional audit’s warning about numerical relabelling. It does not establish ancient use of the paths, select this decoder from every possible decoder, or identify Cygnus independently of the stellar analyses. Contemporary plan proxies also do not by themselves establish that all compared components belonged to one construction episode. Shared design, inheritance and accidental compatibility require separate archaeological assessment.

The small departure from complementation is accounted for exactly: $S+S_{swap}=1+\mathrm{tr}[(P_J+P_V-I)M]$, where $P_u=uu^T$ and $M=(P_{entrance}+\text{mean } P_{inner})/2$. The two branches give residuals 0.004043780 and 0.001425695. The earlier normal-to-lintel complement check expresses the same planar projection identity under a different 90° rotation. These dependencies supply no additional independent evidence. All previous numerical results and source sensitivities remain archived.